The HONG KONG
POLYTECHNIC UNIVERSITY

Prediction and Abatement of Noise in Long Enclosures

Lam, Pou Man

A thesis submitted in partial fulfillment of the requirements for the Degree of Master of Philosophy

Department of Mechanical Engineering
The Hong Kong Polytechnic University

June 2005

CERTIFICATE OF ORIGINALITY

I hereby declare that this thesis is my own work and that, to the best of my knowledge and belief, it reproduces no material previously published or written, nor material that has been accepted for the award of any other degree or diploma, except where due acknowledgement has been made in the text.

_____(Signed)

Lam, Pou Man (Name of student)

Abstract

The study of noise reduction in long enclosures, such as tunnels, underground stations and long corridors, begins with the examination of sound characteristics in these spaces. In the first part of my study, the ‘coherent’ model, or the complex image model, is extended to predict the reverberation time (RT30 and EDT) and the speech transmission index (STI) in a long enclosure. The approach is different from previous energy-based methods. The interference effects between the direct and reflected waves are included, and the coherent model takes into account the phase information of the sound waves. The sound field is computed in the frequency domain, and the impulse response is generated by applying the inverse Fourier transform. Subsequent calculations are performed on the impulse response to deduce the reverberation time and STI accordingly. The numerical model is validated by comparing the predictions with measured data.

The numerical model is modified to consider the existence of impedance discontinuity on the boundary surfaces in the second part of the thesis. A single change of impedance in a two-dimensional duct is focused as the fundamental study of the problem. The diffraction effect at the impedance discontinuity is proved to be insignificant, and it is ignored in the formulation. With the assumption that the diffraction effect is not important, investigation is moved on to a rectangular long enclosure. A set of equations are developed on the basis of the coherent model to predict the noise reduction and acoustic indices (EDT and STI) in a long enclosure with impedance discontinuities. Experiments are conducted in two scale models, and the predictions are in excellent agreement with the data collected.

Finally, the verified coherent model is used as a tool to investigate the optimal positioning of sound absorption material in a long enclosure. Several cases in an

imaginary long enclosure are presented as examples to show how to determine the location with the numerical model. It is perhaps not surprising to find that an increase in the amount of absorption material does not always result in a remarkably higher degree of noise reduction. Moreover, when the absorption material is meant to be installed on two surfaces, perpendicular boundaries are preferred to parallel planes. The prediction scheme can be used to evaluate the optimal arrangement of sound absorption material. It facilitates the goals of noise reduction and improvement of speech intelligibility in a long enclosure.

Publications arising from the thesis

Refereed journal articles:

1. LI, K. M. and LAM, P. M. Prediction of reverberation time and speech transmission in long enclosures. Journal of the Acoustical Society of America, vol. 117, no. 6, pp. 3716-3726 (2005).
2. LAM, P. M. and LI, K. M. A coherent model for predicting noise reduction in long enclosures with impedance discontinuities. Submitted to Journal of Sound and Vibration.

Conference presentation:

1. LAM, P. M. and LI, K. M. The predicted reverberation time in a rectangular long enclosure. InterNoise 2004, Prague, Czech Republic, 22-25 August 2004.

Acknowledgements

I would like to express my thanks to Prof. K. M. Li, the supervisor of this project, for his professional guidance and continual support. I am indebted to the technical staff and the colleagues of the acoustics team for their kind assistance with the experiments carried out in the Hong Kong Polytechnic University, the Western Harbour Tunnel and the Chaiwan Depot. Financial support from the Research Grants Council of the HKSAR and the Research Committee of the Hong Kong Polytechnic University Research Grants is very much appreciated. Thanks to Samantha Lei for her time and effort in proofreading. I wish to thank my family and friends for their understanding and encouragement throughout the course of my research study. Finally, I would like to dedicate this thesis to my Heavenly Father, who has made it possible.

Table of contents

Chapter 1

Introduction

1.1 Background of research

The main objectives of this study are the prediction and reduction of noise in long enclosures. An enclosure is identified as ‘long’ when one dimension is much greater than the other two, while the two are still relatively large compared to the acoustical wavelength of interest. The ideal model of a long enclosure has an infinite length, which means there is no reflection of sound waves from the end walls. Examples of long enclosures are underground train stations, tunnels, subways, corridors and trains. A street canyon can also be regarded as a long enclosure with an anechoic ceiling. Different types of acoustic problems exist in long enclosures in urban areas.

A tunnel for the passing of vehicles is an example of a long enclosure in the large scale. There is a problem that the emergency announcements being broadcasted in a tunnel can be misinterpreted by drivers. Both the drivers and passengers are insulated by the vehicle. The concrete walls of many road tunnels are good reflectors of sound: the message from the loudspeakers will be echoed through the tunnel, making the announcements from the loud speakers unrecognizable. Furthermore, when the vehicles are moving, the noise produced will be enhanced by the tunnel surfaces. The speech intelligibility will be even worse.

The broadcast of public announcements in an underground train station faces a similar problem. The sound level of the loud speakers must be high enough so that the

announcements can be perceived in spite of the train noise. However, too loud a volume will bring discomfort to the passengers. It is necessary to optimize the volume of the speakers. Another example of a long enclosure is the corridor in a building. It can be the corridor in an office building, which demands quietness, or even masking; it can also be an exhibition corridor in an art gallery, in which background music is required. On the other hand, the attenuation of dissipative duct silencers is an acoustic problem of long enclosures in the small scale.

The abatement of noise in a long enclosure serves not only for mere comfort or hearing protection, but also an enhancement in speech intelligibility. Before any design or installation of acoustic treatment for noise reduction in a long enclosure, the investigation of the properties of sound propagation is essential. The characteristics of sound such as propagation and reverberation in a long enclosure are different from those in a rectangular room. Kang [1] has pointed out that the sound field in a long enclosure is not diffuse, and hence the classic theory of room acoustics is not applicable. In the first part of this study, a theoretical model has been developed for the prediction of acoustic indices in a long enclosure. It is then extended to account for the case of inhomogeneous boundaries. Finally the efficiency of the arrangement of absorption materials in a long enclosure will be studied.

1.2 Literature review

1.2.1 Sound propagation in a long enclosure

The investigation of sound propagation in long enclosures dated back to the 1960’s, when Yamamoto [2] developed a formula based on the image source method to predict the sound distribution in a corridor. In the 1970’s, Davies [3] presented an estimation of the attenuation of high-frequency noise in corridors

with a similar approach. However, these formulations did not consider the interference effects due to the multiple reflections from the four boundary walls. The models were limited to high frequency sound propagation and to either very high or very low absorption coefficient of the boundaries.

In the late 1970's, Sergeev [4] derived a series of formulae based on the image source method for the sound energy density of an incoherent point source in city streets and long tunnels. The absorption of sound in air was considered, and the reflection coefficient was angle-dependent. However, no measurement result was presented to support this model. In the 1980's, Redmore [5] developed the acoustic ray theory to predict the relative sound levels along a corridor or in adjacent rooms caused by a sound source in the corridor. The formulation gave satisfactory prediction for corridors with relatively hard boundaries, but it overestimated the sound levels when the boundaries were more absorbent and the source and receiver were farther apart.

In 1996, Kang analysed the unsuitability of classic theory in long enclosures [1]. It was concluded that the sound field in long enclosures, whether with geometrically or diffusely reflective boundaries, was not diffuse as assumed in the classic theory. Meanwhile, he presented a formulation for the prediction of sound pressure level in rectangular long enclosures with geometrically reflecting boundaries [6] based the image source method. The steady-state sound pressure level is given by

$$SPL_d = 10\log\sum_{\Delta t} 10^{SPL_d(t)/10} - SPL_{ref} \tag{1.1}$$

and

$$SPL_d(t) = 10\log\sum_{m=-\infty}^{\infty}\sum_{n=-\infty}^{\infty} e^{-ad_{m,n}}\left[\frac{K}{d_{m,n}^2}(1-\alpha)^{|m|+|n|}\right] \tag{1.2}$$

where $d_{m,n}$ is the path length from the image source *(m,n)* to the receiver, *K* is a constant relating to the sound power of the source, α is the absorption coefficient of the boundaries, *a* is the air absorption coefficient, and SPL_{ref} is the reference sound pressure level. Eqs. (1.1) and (1.2) were also employed to predict the reverberation time in long enclosures, which will be discussed in the next section. This prediction model is referred to as the 'incoherent' model in this report, since an incoherent summation of the intensities of image sources is involved.

Yang and Shield [7] developed a computer model based on the ray-tracing technique, for the investigation of sound field in a long enclosure. The model was also based on the summation of sound intensities from the direct source and its reflected rays. The predictions were compared with the experimental results in a later publication [8]. Significant discrepancies, especially at low frequency, between the predicted and measured noise levels were reported, because the interference effects were not included in their models. Moreover, the surface absorption was assumed as angle independent, which was not the case in practice.

Picaut *et al.* [9] used a diffusion equation to predict the sound propagation in long enclosures with diffusely reflecting boundaries. Kang developed another model for the prediction of acoustic indices in rectangular enclosures with diffusely reflecting boundaries using the technique of radiosity [10]. The Prediction Model 1998 for Road Traffic Noise by the Acoustical Society of Japan [11] for the prediction of noise radiated from a tunnel opening was adopted by Kobayashi *et al.* [12] to predict the noise propagation in a road tunnel.

The interference effects of the direct and reflected sound waves and the change of phase on reflection were ignored in all the numerical models mentioned above. Dance *et al.* [13] pointed out the importance of interference effects in an

enclosed space. They developed an interference model for calculating the total sound fields in an industrial space. However, the change of phase on reflection was ignored in their predictions. Zeng *et al.* [14] also included the phase information in their numerical model, but it was limited to enclosures with perfectly hard boundaries.

Gensane and Santon [15] proposed the use of a complex image-source method to evaluate the sound field of bounded spaces. Lemire and Nicolas [16] further improved the method to simulate spherical sound-wave propagation in enclosures. In the light of these previous works, Li and Iu presented a ‘coherent’ model, or the complex image source model, for the prediction of sound propagation in street canyons [17] and tunnels [18]. The model was based on an analytic Green’s function, which allowed a variation of the reflection factors with the angle of incidence. The total sound pressure was obtained by summing up the contribution from each image source. The mutual interference effects of the direct and reflected sound waves were considered. It was shown that the coherent model [19] gave a more accurate prediction than the incoherent model. Unlike Li and Iu’s model, the plane wave reflection coefficient was used instead of the spherical wave reflection coefficient in Suh and Nelson’s model [20]. They pointed out that their formulation could give a good approximation, except for the prediction of sound fields of near grazing incidence. When the propagation distance increases, it becomes more and more likely the propagation of near-grazing waves in long enclosures. Consequently, the spherical wave reflection coefficient is preferred to the plane wave reflection coefficient.

1.2.2 Reverberation and speech intelligibility in long enclosures

Among various acoustic indices used in room acoustics, reverberation time plays an important role in the design of a room for speech or music, while the speech transmission index has been widely accepted as an indicator of speech intelligibility. The reverberation time is inversely proportional to speech intelligibility. In other words, a higher reverberation time means a longer period of time for the reverberation to settle, making the consecutive words in a speech unrecognizable. These two parameters (Reverberation Time and STI) are crucial, for example, in the design of public address systems in long enclosures like underground stations and building corridors.

1.2.2.1 Reverberation time

A number of classic formulae have been derived for the prediction of reverberation time in rectangular enclosures [21,22,23]. These formulae assume that the sound field in a room is diffuse, and the reverberation time is a single value. However, this assumption does not hold in a long enclosure, as pointed out by Kang [1].

The investigation of reverberation in long enclosures started with the study of reverberation in street canyons in the 1970's by Schröder [24], Kuttruff [25], and Steenackers *et al.* [26]. It was noticed that the decay curves were not straight. Hirata [27] and Barnett [28] deduced approximate theoretical formulae for calculating the reverberation time in rectangular tunnels and tube stations respectively, but the variation in reverberation along the length was not taken into account.

Kang [6] derived a numerical model based on the image source method to predict the reverberation time in rectangular long enclosures with geometrically reflecting boundaries. The reverberation time was obtained from the reverse-time integration of Eq. (1.2). The directivity of source and the effect of end walls were also considered. Again this was referred to as the 'incoherent' model, because it was based an energy approach. Along with the prediction of sound propagation in long enclosures, the calculation of reverberation time was also given in the theoretical models [7, 8, 9, 10] mentioned in the previous section. Similar to the 'incoherent' model, they were energy-based and the phase information was ignored. Suh and Nelson [20] agreed that when the phase information of the waves was included, the model gave a more accurate prediction. António *et al.* [29] and Dance *et al.* [13] also highlighted the importance of interference effects in an enclosed space.

António *et al.* [29] derived a set of analytical solutions to evaluate the pressure response inside an empty parallelepiped closed space subjected to a harmonic point source. The computations were performed in the frequency domain and Inverse Fourier Transforms were subsequently applied to obtain impulse responses, from which the reverberation time was deduced. The time signals were a sequence of pulses that corresponded to the incident pulse and a train of pulses which had been successively reflected on the wall surfaces during the time period. At lower frequencies, two successive pulses might not arrive at the receiver with a sufficient time lapse to avoid being overlapped. Consequently, the resulting pulse was smaller when the two pulses experienced a phase change of 180°. At higher frequencies the pulses were narrower in the time domain, and the overlapping phenomenon was less possible to occur. Therefore, the phase information should

be included in the prediction model, especially in low frequency range. In their numerical model, the absorption coefficients were still band-averaged values and independent of incidence angle. Furthermore, only the cases of 0^o and 180^o phase shift upon reflection were studied.

1.2.2.2 Speech Transmission Index

Different acoustical measures have been used as predictors of speech intelligibility, such as the signal-to-noise method, the speech transmission index (STI), and useful/detrimental sound ratios [30]. Amongst the various indices, the STI has been widely accepted as an indicator of speech intelligibility in an enclosure [31]. Based on the modulation transfer function (MTF) introduced by Houtgast and Steeneken [32], it was a scheme of assessing the effect of a room on intelligibility. The MTF was able to combine the effects of reverberation, ambient noise and the contribution of direct field, which are usually treated individually, into a single function. In order to evaluate the effect of a room on speech intelligibility in a simple manner, the MTF was then converted to a single index, the STI [33]. The index was obtained by simple addition of the contributions from individual frequency bands. Redundancy-correction factors for adjacent frequency bands were introduced in a later literature [34] to consider the mutual dependence of the octave-band weights in predicting speech intelligibility. The rapid speech transmission index (RASTI) was a simplified version of the STI. It provided a fast evaluation of speech intelligibility [35], as it was dependent on two octave bands (500 Hz and 2000 Hz) only. Based on a series of articulation tests, it has been demonstrated that the STI and RASTI were highly correlated with the articulation scores. It has also been shown that the early decay of a room governed the MTF and STI.

The mirror image source method [36] and the ray-tracing method [37] were used to determine the STI in rectangular rooms. The image source method was limited to geometrically reflective boundaries, whereas diffusion was included in the ray-tracing method. However, both methods were restricted to absorption coefficients that were independent of frequency and angle of incidence.

The preceding prediction scheme was limited to the presence of a single point source. It is more common to deal with a series of loud speakers in a long enclosure, such as an underground station or a tunnel. Basically it is a summation of the contribution from every single source. Kang [38] carried out a series of scale model measurements for improving the STI of multiple loudspeakers in long enclosures by architectural treatments. Wu and Zhao [39] has developed a numerical model for the prediction of STI by considering the traffic volume in a tunnel.

1.2.3 Sound propagation over impedance discontinuity

1.2.3.1 Diffraction at impedance discontinuity

Regarding the existing prediction models described in Section 1.2.1, much attention has been devoted to the sound propagation in long enclosures with homogeneous boundaries. The acoustical properties of the four boundaries remain unchanged along the length of the enclosure. These numerical models provide a fundamental ground for the study of acoustic properties in real life situation. A common practice of acoustic treatment is the lining of sound absorption material.

In outdoor sound propagation, a number of formulations have been developed for mixed impedance ground based on different theories. Nyberg [40] presented a solution of the Helmholtz equation for multiple discontinuities using the technique of Fourier transform. The model presented by Koers [41] was based on Kirchhoff

diffraction theory where the diffraction at an impedance transition was calculated by taking it as a wedge with a top angle of 180°. Another numerical model developed by Rasmussen [42] involved the joining the two parts of the sound field calculated, respectively, over the two infinite half-planes at the impedance discontinuity. It was adopted by Chan [43] to predict the sound propagation in a 2-D duct with single impedance discontinuity. De Jong *et al.* [44] presented a semi-empirical model for the transmission of sound over ground with a wedge shaped barrier. The propagation over an impedance discontinuity was treated as the special case of a rigid half-plane. The total sound field was composed of the direct wave, the reflected wave, and the diffracted wave terms. The diffracted field was found to be significant at near-grazing incidence.

Hothersall and Harriott [45] compared three numerical models in their paper. The first was a numerical solution based on a boundary integral equation formulation [46]. Although involving some approximation, this approach provided accurate results for a wide range of propagation conditions in a still homogeneous atmosphere but suffered from the need for large computing resources. The second one was the Fresnel-zone model [47], in which the sound field at the receiver was assumed to be governed by the surface conditions in a region around the specular reflection point. The region was defined by a Fresnel-zone condition. The computational time for the boundary integral equation calculations was several orders of magnitude greater than the computational time required for the other two methods. The theoretical model by De Jong was also studied. This approach proved flexible in application to all the boundary conditions considered and agreed well with the boundary integral equation and the experimental resulted in most cases.

1.2.3.2 Existence of inhomogeneous boundaries in an enclosure

The computation of sound field in a room with mixed impedance surfaces can be traced back to the classical theory. The Sabine absorption coefficient [48] was an area-weighted value of the surfaces in a room. It was used to deduce the reverberation time with the assumption of a diffuse sound field. Kang [10] presented a radiosity model for the prediction of sound field and acoustic indices in a long enclosure. It was an energy approach, and the boundaries in the enclosure were modelled as diffusely reflective. In the calculation procedure, each boundary was divided into a certain amount of patches. The absorption coefficients of the patches could be different to simulate inhomogeneous boundaries. Since the model was energy-based, the phase information of all reflected waves was ignored in the calculation.

The attenuation of noise by duct silencers is a similar problem to that of a tunnel. Although the dimension and boundary conditions are different, some of the theoretical principles for ducts are also useful for long spaces. The mode-matching technique was adopted by Mechel [49] and Somraz et al. [50] to account for diffraction at the duct silencer's terminations. Astley and Eversman presented a finite element formulation [51] and the weighted residual method [52] for finite length silencers with mean gas flow. These prediction schemes required considerable computational effort, and it was difficult to track the modes in the mode-matching method.

Tester [53] compared ray theory and modal predictions of the sound field from a line source in a two-dimensional duct with zero flow and locally reacting walls. He concluded that the ray models were "surprisingly" accurate. The advantages of ray models were simplicity and versatility. Cummings [54] developed a hybrid mode/ray model for a two-dimensional duct with a length of soft walls and rigid inlet and outlet

sections. He suggested that the diffraction effect was not important when the frequency was sufficiently high. The formulation did not account for the diffraction at the inlet and outlet sections of the silencer. On the other hand, Chan [43] adopted the Rasmussen model [42] to account for the diffraction at a single impedance jump in a two-dimensional duct. It was an integral method based on the approximation of the Boundary Element formulation. However, it would be a far more complicated problem to extend this theoretical model to the case of a rectangular long enclosure due to the multiple reflections and diffractions at the impedance discontinuity.

An alternative measure was adopted by researchers to investigate the absorption effect of periodic absorptive strips [55,56,57,58,59]. Both scattering and absorption effects were expressed by a single absorption coefficient when strips of absorbent material were arranged periodically on a surface. This type of material was treated as homogeneous surface in this research.

1.3 Organization of thesis

The thesis is arranged as follows. Chapter 1 contains a literature review of the prediction models of sound propagation and acoustic indices in a long enclosure. The theories of the different approaches are described.

In the first part of this study, the ‘coherent’ model is extended to predict the reverberation time (RT30 and EDT) and speech transmission index (STI) in a long enclosure with a rectangular cross-section. The theoretical model is presented in Chapter 2. It takes into account the interference effects of the direct and reflected waves, and the angle-dependence of the reflection coefficients. It is called the ‘coherent’ model because the contributions from the sound waves are summed up coherently. The difference between the use of spherical and plane wave reflection

coefficients in the computation will be studied with computer simulations. Measurements have been carried out in a road traffic tunnel, a corridor in a building and a model corridor to validate the proposed theoretical formulation. Experimental results and their comparisons with the numerical models are given.

In Chapter 3, the prediction model is extended to include a single impedance discontinuity in a long enclosure. De Jong's formulation has been incorporated into the coherent model to account for the diffracted sound field due to the impedance change. In this way, the phase information of the images is retained, and the interference effects between the direct and reflected waves are included. The significance of the diffracted field in this model is studied. Measurements have been conducted in model tunnels to validate the proposed formulation.

Applications of the theoretical model are discussed in Chapter 4. Case studies are explored in an imaginary long enclosure. A demonstration of how the coherent model can contribute in the arrangement and installation of sound absorption materials to achieve the goal of noise reduction and improvement in speech intelligibility in a long enclosure is given.

Conclusions of the whole study will be given in Chapter 5, followed by some recommendations for future work.

References

1. J. Kang, “The unsuitability of the classic room acoustical theory in long enclosures,” Architectural Science Review **39**, 89-94 (1996).
2. T. Yamamoto, “On the distribution of sound in a corridor,” J. Acoust. Soc. Jpn. **17**, 286-292 (1961).
3. H. G. Davies, “Noise propagation in corridors,” J. Acoust. Soc. Am. **53**, 1253-1262 (1973).
4. M. V. Sergeev, “Scattered sound and reverberation on city streets and in tunnels,” Sov. Phys. Acoust. **25** (3), 248-252 (1979).
5. T. L. Redmore, “A theoretical analysis and experimental study of the behaviour of sound in corridors,” Appl. Acoust. **15**, 161-170 (1982).
6. J. Kang, “Reverberation in rectangular long enclosures with geometrically reflecting boundaries,” Acustica - Acta Acustica **82**, 509-516 (1996).
7 . L. N. Yang and B. M. Shield, “Development of a ray tracing computer model for the prediction of the sound field in long enclosures,” J. Sound Vib. **229**, 133-146 (2000).
8. L. Yang and B. M. Shield, “The prediction of speech intelligibility in underground stations of rectangular cross section,” J. Acoust. Soc. Am. **109**(1), 266-273 (2001).
9. J. Picaut, L. Simon, J.-D. Polack, “Sound field in long rooms with diffusely reflecting boundaries,” Appl. Acoust. **56**, 217-240 (1999).
10. J. Kang, “Reverberation in rectangular long enclosures with diffusely reflecting boundaries,” Acustica - Acta Acustica **88**, 77-87 (2002).

11. Research Committee of Road Traffic Noise in Acoustical Society of Japan, "ASJ Prediction Model 1998 for Road Traffic Noise," J. Acoust. Soc. Jpn. (J), **55**(4), 281-324 (1999).
12. Y. Kobayashi, S. Seki, T. Kitamura, K. Mitsui and S. Yamada, "Study on the characteristics of noise propagation in tunnel and noise control with absorbing material of ceramics," Proc. Internoise **99**, 517-522.
13. S. M. Dance, J. P. Roberts and B. M. Shield, "Computer prediction of sound distribution in enclosed spaces using an interference pressure model," Appl. Acoust. **44**, 53-65 (1995).
14. X. Zeng, K. Chan and J. Sun, "Modeling the sound fields in rooms with multiple sources using a hybrid image method including phase," Acustica – Acta Acustica **88**, 88-92 (2002).
15. M. Gensane and F. Santon, "Prediction of sound fields in rooms of arbitrary shape: the validity of the image sources method," J. Sound Vib. **63**, 97-108 (1979).
16. G. Lemire and J. Nicolas, "Aerial propagation of spherical sound waves in bounded spaces," J. Acoust. Soc. Am. **86**, 1845-1953 (1989).
17. K. K. Iu and K. M. Li, "The propagation of sound in narrow street canyons," J. Acoust. Soc Am. **112** (2), 537-550 (2002).
18. K. M. Li and K. K. Iu, "Propagation of sound in long enclosures," J. Acoust. Soc. Am. **116**, 2759-2770 (2004).
19. K. M. Li and K. K. Iu, "Full-scale measurements for noise transmission in tunnels," J. Acoust. Soc. Am. **117**, 1138-1145 (2005).

20. J. S. Suh and P. A. Nelson, “Measurement of transient response of rooms and comparison with geometrical acoustic models,” J. Acoust. Soc. Am. **105**(4), 2304-2317 (1999).
21. W. C. Sabine, Collected papers on acoustics, Dover, New York (1964).
22. C. F. Eyring, “Reverberation time in dead rooms,” J. Acoust. Soc Am. **1**, 217-241 (1930).
23. G. Millington, “A modified formula for reverberation,” J. Acoust. Soc Am. **4**, 69-82 (1932).
24. E. Schröder, “Nachhall in geschlossenen bebauten Straßen,” Lärmbekämpfung **17**, 11 (1973).
25. H. Kuttruff, “Zur berechnung von Pegelmittelwerten und Schwankungsgrößen bei Strabenlärm,” Acustica **32**, 57 (1975).
26. P. Steenackers, H. Myncke and A. Cops, “Reverberation in town streets,” Acustica **40**, 115-119 (1978).
27. H. Hirata, “Geometrical acoustics for rectangular rooms,” Acustica **43**, 247-252 (1979).
28. P. W. Barnett, “Acoustics of underground platforms,” Proceedings of the Institute of Acoustics **16**, Part 2, UK, 433 (1994).
29. J. António, L. Godinho and A. Tadeu, “Reverberation times obtained using a numerical model versus those given by simplified formulas and measurements,” Acustica – Acta Acustica **88**, 252-261 (2002).
30. J. S. Bradley, “Predictors of speech intelligibility in rooms,” J. Acoust. Soc. Am. **80** (3), 837-845 (1986).
31. J. Kang, “A method for predicting acoustic indices in long enclosures,” Appl. Acoust. **51** (2), 169-180 (1997).

32. T. Houtgast and H. J. M. Steeneken, “The modulation transfer function in room acoustics as a predictor of speech intelligibility,” Acustica **28**, 66-73 (1973).

33. T. Houtgast, H. J. M. Steeneken and R. Plomp, “Predicting speech intelligibility in rooms from the modulation transfer function I. General room acoustics,” Acustica **46**, 60-72 (1980).

34. H. J. M. Steeneken, T. Houtgast, “Mutual dependence of the octave-band weights in prdicting speech intelligibility,” Speech Communication **28**, 109-123 (1999).

35. H. J. M. Steeneken, T. Houtgast, “RASTI: a tool for evaluating auditoria,” Brüel & Kjær Technical Review **3**, 13-39 (1985).

36. R. Plomp, H. J. M. Steeneken and T. Houtgast, “Predicting speech intelligibility in rooms from the modulation transfer function. II: Mirror image computer model applied to rectangular rooms,” Acustica **46**, 73-81 (1980).

37. H. F. van Rietschote, T. Houtgast and H. J. M. Steeneken, “Predicting speech intelligibility in rooms from the modulation transfer function IV: a ray-tracing computer model,” Acustica **49**, 245-252 (1981).

38. J. Kang, “Improvement of the STI of multiple loudspeakers in long enclosures by architectural treatments,” Appl. Acoust. **47** (2), 129-148 (1996).

39. S. Wu and Y. Zhao, “Predicting STI in a tunnel in case of emergency with the image wall method,” Internoise **33** (2004).

40. C. Nyberg, “The sound field from a point source above a striped impedance boundary,” Acta Acust. (China) **3**, 315-322 (1995).

41. P. Koers, “Diffraction by an absorbing barrier or by an impedance transition,” Proc. Internoise **1**, 311-314 (1983).

42. K. B. Rasmussen, “A note on the calculation of sound propagation over impedance jumps and screens,” J. Sound Vib. **84**(4), 598-602 (1982).
43. C. L. Chan, “Numerical models for predicting sound propagation in ducts,” MPhil Thesis, Dept. of Mechanical Engineering, Hong Kong Polytechnic Univ., Hong Kong (2002).
44. B. A. De Jong, A. Moerkerken, and J. D. Van Der Toorn, “Propagation of sound over grassland and over an earth barrier,” J. Sound Vib. **86**, 23-46 (1983).
45. D. C. Hothersall and J. N. B. Harriott, “Approximate models for sound propagation above multi-impedance plane boundaries,” J. Acoust. Soc Am. **97**, 918-926 (1995).
46. S. N. Chandler-Wilde and D. C. Hothersall, “Sound propagation above an inhomogeneous plane,” J. Sound Vib. **98**, 475-491 (1985).
47. D. C. Hothersall and J. N. B. Harriott, “A Fresnel zone approach to the prediction of sound propagation above a multi-impedance plane,” Proc. Inst. Acoust. **16**, 83-90 (1994).
48. K. S. Sum, “Some comments on Sabine absorption coefficient,” J. Acoust. Soc. Am. **117**, 486-489 (2005).
49. F. P. Mechel, “Theory of baffle-type silencers,” Acustica **70**, 93-111 (1990).
50. N. Sormaz, A. Cummings and B. Nilsson, “Sound attenuation in finite-length splitter silencers,” Proceedings of the Euronise 1992 meeting.
51. R. J. Astley and W. Eversman, “Acoustic transmission in non-uniform ducts with mean flow, part II: the finite element method,” J. Sound Vib. **74**, 103-121 (1981).
52. W. Eversman and R. J. Astley, “Acoustic transmission in non-uniform ducts with mean flow, part I: the method of weighted residuals,” J. Sound Vib. **74**, 89-101 (1981).

53. B. J. Tester, “Ray models for sound propagation and attenuation in ducts, in the absence of mean flow,” J. Sound Vib. **27**, 515-531 (1973).

54. A. Cummings, “High frequency ray acoustics models for duct silencers,” J. Sound Vib. **221**(4), 618-708 (1999).

55. L. G. Ramer, “The absorption of strips, effects of width and location,” J. Acoust. Soc. Am. **12**, 323-326 (1941).

56. R. K Cook, “Absorption of sound by patches of absorbent materials,” J. Acoust. Soc. Am. **29**, 324-329 (1951).

57. J. R. Pellam, “Sound diffraction and absorption by a strip of absorbing material,” J. Acoust. Soc. Am. **11**, 396-400 (1940).

58. J-B Park, K Grosh and Y-H Kim, “The effect of a periodic absorptive strip arrangement on an interior sound field in a room,” J. Acoust. Soc. Am. **117**, 763-770 (2005).

59. D. Takahashi, “Excess sound absorption due to periodically arranged absorptive materials,” J. Acoust. Soc. Am. **86**, 2215-2222 (1989).

Chapter 2

Prediction of Reverberation Time and Speech Transmission Index in long enclosures

2.1 Introduction

It was mentioned in the previous chapter that the sound field in a long space is not diffuse, and hence the classic theory of room acoustics is not applicable. A theoretical model will be presented in this chapter for the prediction of reverberation time and speech transmission index in rectangular long enclosures. The model is based on an image-source method, and both acoustically hard and impedance boundaries are investigated. An approximate analytical solution is used to predict the frequency response of the sound field. The reverberation time is determined from the decay curve which is computed by a reverse-time integration of the squared impulse response. The angle-dependence of reflection coefficients of the boundaries and the change of phase upon reflection are incorporated in this model. Due to relatively long distance of sound propagation, the effect of atmospheric absorption is also considered. Measurements of reverberation time and speech transmission index taken from a real tunnel, a corridor, and a model tunnel are presented. Theoretical predictions are found to agree well with the experimental data.

2.2 Theory

2.2.1 Computation of the impulse response

A rectangular long enclosure is modelled as two parallel vertical walls and two parallel horizontal planes (i.e., the ground and the ceiling). The enclosure is assumed to be infinitely long, and the reflection from the end walls is ignored. Based on the image source method, the boundaries are assumed to be geometrically reflective, and the effect of diffusion is ignored. The width of the enclosure is *W*, with the left vertical wall located at plane $x = 0$. The height of the enclosure is *H*, with the ground situated on plane $z = 0$. The y-axis represents the direction along length of the enclosure. A point source S_0 is located inside the enclosure, with coordinates $(x_s, 0, z_s)$, and a receiver *R* is positioned at (x_R, , y_R , z_R), as shown in Fig. 2.1.

When the sound source is turned on in a long enclosure, an infinite number of images are discretely located on plane $y = 0$ (Fig. 2.2). The reflection order of an image source $S_{m,n}$ is $|m|+|n|$, where $m, n = -\infty \ldots \infty$. The value $|m|$ is the total number of times the image reflects from the vertical walls, and $|n|$ is that from the horizontal planes. The distance of an image $S_{m,n}$ from the receiver can be determined by simple geometry as

$$d_{m,n} = \sqrt{(x_R - x_m)^2 + y_R{}^2 + (z_R - z_n)^2}\,, \qquad (2.1)$$

where

$$x_m = \begin{cases} (m+1)W - x_S & \text{for odd m} \\ mW + x_S & \text{for even m,} \end{cases} \qquad (2.2a)$$

and

$$z_n = \begin{cases} (n+1)H - z_S & \text{for odd n} \\ nH + z_S & \text{for even n.} \end{cases} \qquad (2.2b)$$

The incident angles at which the sound wave from image $S_{m,n}$ reflects from the vertical and horizontal boundaries are given respectively by

$$\cos\theta_{m,n} = \frac{\left|x_R - x_{m,n}\right|}{d_{m,n}}, \tag{2.3a}$$

and

$$\cos\varphi_{m,n} = \frac{\left|z_R - z_{m,n}\right|}{d_{m,n}}. \tag{2.3b}$$

Assume that the four boundaries have different acoustic impedance. The contribution of the image $S_{m,n}$ to the total pressure can be written as

$$P_{m,n} = Q_L Q_R Q_G Q_C \frac{e^{ikd_{m,n}}}{4\pi d_{m,n}}, \qquad \text{for } m, n = -\infty \ldots \infty, \tag{2.4}$$

where $k(\equiv \omega / c)$ is the wave number. The time-dependent factor, $e^{-i\omega t}$, is understood and suppressed. The terms Q_L, Q_R, Q_G and Q_C are the spherical wave reflection coefficients of the left and right walls, the ground and the ceiling respectively. They are expressed by

$$Q_L = \begin{cases} \left[Q\left(d_{m,n}, \theta_{m,n}, \beta_L\right)\right]^{\frac{|m-1|}{2}}, & \text{for odd m,} \\ \left[Q\left(d_{m,n}, \theta_{m,n}, \beta_L\right)\right]^{\frac{|m|}{2}}, & \text{for even m,} \end{cases} \tag{2.5a}$$

$$Q_R = \begin{cases} \left[Q\left(d_{m,n}, \theta_{m,n}, \beta_R\right)\right]^{\frac{|m+1|}{2}}, & \text{for odd m,} \\ \left[Q\left(d_{m,n}, \theta_{m,n}, \beta_R\right)\right]^{\frac{|m|}{2}}, & \text{for even m,} \end{cases} \tag{2.5b}$$

$$Q_G = \begin{cases} \left[Q\left(d_{m,n}, \varphi_{m,n}, \beta_G\right)\right]^{\frac{|n-1|}{2}}, & \text{for odd n,} \\ \left[Q\left(d_{m,n}, \varphi_{m,n}, \beta_G\right)\right]^{\frac{|n|}{2}}, & \text{for even n,} \end{cases} \tag{2.5c}$$

$$Q_C = \begin{cases} \left[Q\left(d_{m,n}, \varphi_{m,n}, \beta_C\right)\right]^{\frac{|n+1|}{2}}, & \text{for odd n,} \\ \left[Q\left(d_{m,n}, \varphi_{m,n}, \beta_C\right)\right]^{\frac{|n|}{2}}, & \text{for even n,} \end{cases} \tag{2.5d}$$

where, according to Ref.1 ,

$$Q = R_p + (1 - R_p)F(w) \tag{2.6}$$

and

$$R_p = \frac{\cos\theta - \beta}{\cos\theta + \beta}. \tag{2.7}$$

R_p is the plane wave reflection coefficient. The function *F(w)* is the boundary loss factor given by

$$F(w) = 1 + i\sqrt{\pi}we^{-w^2}\,\mathrm{erfc}(-iw), \tag{2.8}$$

where efrc(*w*) is the complementary error function. The parameter *w* is called the numerical distance, which is determined by

$$w = +\sqrt{\tfrac{1}{2}ikd}\,(\cos\theta + \beta). \tag{2.9}$$

The normalized admittance of the left and right walls, the ground, and the ceiling are denoted by β_L , β_R , β_G and β_C respectively. They can be obtained from the one-parameter model by Delany and Bazley [2], or the two-parameter model by Attenborough [3]. For acoustically hard boundaries, $\beta = 0$, and consequently $Q_L=Q_R=Q_G=Q_C = 1$.

The wave number *k* can be modified to take air absorption effect into consideration. According to the standard published by the Acoustical Society of America [4], the attenuation coefficients for pure-tone sounds are calculated by means of equations over ranges of frequency and atmospheric humidity, pressure and temperature. When a pure-tone sound wave propagates through the atmosphere over a distance *d*, the pressure amplitude P_t decreases exponentially, as a result of the atmospheric absorption effect, from its initial value P_i as given by

$$P_t = P_i \exp(-0.115ad), \tag{2.10}$$

where *a* is the pure-tone sound-attenuation coefficient for atmospheric absorption in dB/m. Eq. (2.4) can be modified to include the effect of air absorption by multiplying the term "exp(-0.115*ad*)", where *d* is the corresponding path length of each term as determined by Eq. (2.1), and *a* is calculated according to the Standard [4]. Alternatively, the atmospheric absorption coefficient can be included as the complex part of the wave number:

$$k = 2\pi f / c + i0.115a \quad . \tag{2.11}$$

The total sound field in the long enclosure is then obtained by the summation of the contribution from the direct and reflected image sources:

$$P_{total}(\omega) = \sum_{m=-\infty}^{\infty} \sum_{n=-\infty}^{\infty} P_{m,n} \quad . \tag{2.12}$$

The impulse response of sound pressure is computed by taking the inverse Fourier transform of the frequency response:

$$p(t) = IFFT(P_{total}(\omega)) \quad . \tag{2.13}$$

The time interval and the length of the FFT depend on the frequency of interest. For octave band analysis, the frequency response is first filtered before applying the inverse Fourier transform. Alternately, if the source generates a known band limited time signal instead of white noise, the frequency response will be multiplied by the Fourier transform of the source strength signal. The impulse response is then obtained by taking the inverse Fourier transform of the product.

The number of reflections used in the computation is estimated by considering the required duration (T_D) for the impulse response in the time domain. The duration is determined by the inverse of the frequency increment ($T_D = 1/\Delta f$) used in the numerical analysis. These two parameters are chosen according to the configuration of the practical experimental set-up.

The critical frequency where the coherent model should be used instead of the incoherent model was introduced by Li and Iu [5]. Assuming the source-receiver distance $L >> 0$, the critical frequency is determined by

$$f_c \sim 2c\left(L^2 + A\right)/\, AL, \tag{2.14}$$

where c is the speed of sound in air, and A is the cross-sectional area of the long enclosure.

2.2.2 Computation of Reverberation Time and Speech Transmission Index

A curve showing the decay of sound energy after the cessation of the source can be generated by a reverse-time integration of the squared impulse response, known as the Schroeder approach [6]:

$$E(t) = 10\log\left\{\int_t^\infty [p(\tau)]^2 d\tau \Big/ \int_0^\infty [p(\tau)]^2 d\tau\right\}. \tag{2.15}$$

Fig. 2.3 shows an example of the predicted impulse response. The corresponding decay curve computed with Eq. (2.15) is demonstrated in Fig. 2.4. The RT30 is determined using the rate of decay given by the linear regression of the decay curve from a level of 5 dB below the initial level to 35 dB below, while the early decay time (EDT) is obtained from the initial 10 dB of the decay. Other indices related to speech intelligibility, such as Clarity and Definition, can also be derived from the impulse response.

The speech transmission index (STI) is widely accepted as an indicator of speech intelligibility. It is based on the modulation transfer function as described by Houtgast and Steeneken [7]. When both the effect of reverberation and ambient background noise are taken into account, the modulation transfer function *m(F)* is

written in a general form as:

$$m(F) = \frac{\int_0^{\infty} e^{2\pi j F\tau} [p(\tau)]^2 d\tau}{\int_0^{\infty} [p(\tau)]^2 d\tau} \left[1 + 10^{(-S/N)/10}\right]^{-1} \quad (2.16)$$

,

where *S/N* is the signal-to-noise ratio in dB at the receiver's position and *F* is the modulation frequency. It can be seen from Eq. (2.16) that the contribution of ambient background noise to the transfer function is inversely proportional to the signal-to-noise ratio. When the signal-to-noise ratio is sufficiently high, the contribution of the term in squared brackets of Eq. (2.16) is negligible, and the formulation becomes:

$$m(F) = \frac{\int_0^{\infty} e^{2\pi j F\tau} [p(\tau)]^2 d\tau}{\int_0^{\infty} [p(\tau)]^2 d\tau} \quad (2.17)$$

.

The modulation transfer function is computed with 14 modulation frequencies, from 0.63 Hz to 12.5 Hz, in one-third octave intervals. These are then converted into a single index, the STI, which is defined by [8]

$$STI = \sum_{f=125Hz}^{8kHz} w_f STI_f \quad (2.18)$$

,

where w_f is the frequency weighting factor. From the octave bands of 125 Hz to 8 kHz, w_f equals to 0.13, 0.14, 0.11, 0.12, 0.19, 0.17 and 0.14, respectively. STI_f is the speech transmission index at each of the seven octave bands. It can be calculated by[9]

$$STI_f = \frac{\left\lfloor \left(S/\overline{N}\right)_{app} + 15 \right\rfloor}{30} \quad (2.19\ a)$$

,

$$(S/\overline{N})_{app} = \frac{1}{14}\sum_{F=0.63}^{12.5}(S/N)_{app,F}, \qquad (2.19\text{ b})$$

$$(S/N)_{app,F} = 10\log\frac{m(F)}{1-m(F)}, \qquad (2.19\text{ c})$$

where $(S/N)_{app}$ is the apparent *S/N* ratio. $(S/N)_{app,F}$ is clipped between ±15 dB, i.e., $(S/N)_{app,F}$ = 15 dB if $(S/N)_{app,F}$ > 15 dB, and $(S/N)_{app,F}$ = -15 dB if $(S/N)_{app,F}$ < -15 dB. In the experimental validation of the proposed model in the Section 2.3, the measured and predicted STI_f at different octave bands, together with the overall STI, will be compared.

2.2.3 Analysis of the reflection coefficient

The purpose of this section is to examine and gain more understanding toward the effect of the replacement of the spherical wave reflection coefficient with the plane wave coefficient on the numerical prediction of EDT, RT30 and STI. It is analysed with an imaginary long rectangular enclosure of width 6 m and height 4 m. The enclosure is assumed to be infinitely long, meaning there is no reflection from the walls at either end. The vertical walls of the enclosure are perfectly hard. The horizontal planes are impedance boundaries. They share the same level of absorptiveness as characterized by the one-parameter model [2] based on the effective resistivity, σ_e, of the boundary surfaces. Four values of σ_e are used in the computation: 100 kPa s m^{-2}, 500 kPa s m^{-2}, 1000 kPa s m^{-2} and 10,000 kPa s m^{-2}. They are chosen to simulate different levels of absorptiveness of the horizontal boundaries.

The different locations of the point source and the receiver are listed in Table 2.1. In case 1, both source and receiver are placed at the centre of the cross-section,

with source-receiver distance of 5 m, 20 m and 50 m respectively. The source is then moved to a higher position, which is 3.8 m from the lower boundary, in case 2. In the third case, the receiver is also moved to a height of 3.8 m, at the same level as the source. The source and receiver are separated by 5 m, 20 m and 50 m in each case. Computations of EDT, RT30 and STI are made at each source-receiver combination, with the four different values of effective flow resistivity as mentioned before. In order to illustrate the difference in computation of the two reflection coefficients, data are presented in relative error, Δ, which is given by:

$$\Delta_{RT30} = \frac{\left|RT30(Q) - RT30(R_p)\right|}{RT30(Q)} \times 100\% \quad \text{(2.20 a)}$$

$$\Delta_{EDT} = \frac{\left|EDT(Q) - EDT(R_p)\right|}{EDT(Q)} \times 100\% \quad \text{(2.20 b)}$$

$$\Delta_{STI} = \frac{\left|STI(Q) - STI(R_p)\right|}{STI(Q)} \times 100\% \quad \text{(2.20 c)}$$

where EDT(Q), RT30(Q) and STI(Q) are the corresponding parameters computed with the spherical wave reflection coefficient, Q, and EDT(R_p), RT30(R_p) and STI(R_p) are those with the plane wave reflection coefficient, R_p. Comparisons are made in relative 'error' so that the effect of the use of Q and R_p on the predicted parametric values of EDT, RT30 and STI can be assessed.

Fig. 2.5 shows the relative error of EDT, RT30 and STI. The results are computed at different frequency bands, source-receiver positions and absorptiveness of the boundaries. These three factors are believed to be associated with the effect of the spherical wave reflection coefficient (*c.f.* Eq. (2.6)) on the prediction of reverberation time and speech transmission index. The results of Δ_{EDT} and Δ_{RT30} are presented in one-third octave bands, and those of Δ_{STI} are presented in octave bands.

In Fig. 2.5(a), for the Δ_{EDT} bars that extend to the upper boundary line, the actual values are over 50% and marked beside the bars.

It is obvious that the relative error decreases with the increase of frequency. As mentioned before, four different values of effective flow resistivity are used in the calculation to simulate different impedance of the horizontal boundaries. The relative error is higher when the boundaries are more absorptive in most of the cases. Its largest value occurs when the effective flow resistivity changes from 100 kPa s m^{-2} to 500 kPa s m^{-2}. There are exceptions, for example, in the prediction of EDT at 500 Hz in case 3. A combined effect of the interference phenomenon and the positions of the source and receiver could have an influence on the initial stage of the decay process.

It is remarkable that the existence of the ground wave term has long been identified in the propagation of sound above a ground surface at long ranges [10]. Each of the 4 boundary surfaces of the rectangular enclosure has its own ‘ground’ wave term. Due to the existence and significance of these ground wave components, the relative error is expected to increase with the source-receiver distance, and especially when the source and receiver are placed near a boundary surface. This can be observed, for example, in the prediction of Δ_{EDT} and Δ_{RT30} at 125 Hz in case 1, Δ_{RT30} at 250 Hz in case 1 and 2, and that of Δ_{STI} at 500 Hz in case 3. However, the trend is not consistent in other cases. It may be caused by a combined effect of the source-receiver distance and the reflection order of contributing images. When the source-receiver distance increases, the contribution of the direct wave becomes smaller. The sound field is then dominated by the reverberant field. The incident angle of an image increases with its reflection order, and the sound propagation is not near-grazing anymore.

It is noticed that the effect on the prediction of reverberation time is bigger than that of speech transmission index. Although there does not seem to be an exact rule to identify the trend of the overall effect, the data in Fig. 2.5 show that the use of plane wave reflection coefficients to approximate the spherical one does alter the prediction of the reverberation time and speech transmission index. The difference can be over 100 % at certain frequency and boundary conditions. The spherical wave reflection coefficient is, therefore, preferred in the prediction model, especially in the case of sound propagation in a long enclosure.

2.3 Experimental Validation

Measurements of reverberation time and speech transmission index taken from a real tunnel, a corridor and a model tunnel are presented to validate the proposed prediction model. The data are compared with predictions from the coherent and incoherent models in this section.

2.3.1 Long enclosure with perfectly hard boundaries

The Western Harbour Tunnel is a two-kilometre three-lane road tunnel in Hong Kong's Victoria Harbour. It has a rectangular cross-section with nominal width of 12.5 m and height of 5.8 m. The walls and the ground are made of concrete with relatively flat and smooth surfaces. Raised walkways in adjacent to the vertical walls and other scattering surfaces on the ceiling are found. A photograph of the tunnel is shown in Fig. 2.6.

A Tannoy Superdual B475 loudspeaker and a Tannoy T300 loudspeaker were used together as a single sound source generating white noise, with the T300 placed on top of the B475. They could be treated as a single point source due to the

long-distance sound propagation in the measurements. There were other maintenance activities in the tunnel throughout the period of our measurements. This led to a typical background noise level of about 70 dB(A). In our preliminary measurement, we found that the measured sound pressure level due to the loudspeakers reached a level of about 105 dB(A) at a distance of 150 m in the tunnel. Hence, the maximum source-receiver distance was restricted to 150 m in the present set of measurements. The limit on the maximum source/receiver separation can guarantee that the lowest equilibrium sound level at measuring positions was at least 20 dB above the background noise level, which was required for the measurement of STI and EDT. A PC-based maximum length sequence system analyser (MLSSA) [11] was used both as the signal generator for the source and as the analyser for subsequent data processing. Its post-processing functions calculate most of the acoustical parameters, including the reverberation time and speech transmission index, from the measured impulse response. The same technique was used by Kang [12] and Li [5] to carry out site measurements in Hong Kong. The receiver used in the measurement was a B&K pre-polarized diffuse field ½-inch condenser microphone of type 4942, fitted with a B&K Deltatron Pre-amplifier of type 2671. The experimental set-up is illustrated in Fig. 2.7. Data are collected in one-third octave bands.

The source was located at the centre of the width of the cross-section, i.e. 6.25 m from both vertical walls. The receiver was placed at different positions along the centreline (x = 6.25 m) and the offset line (x = 9.85 m), as marked in Fig. 2.8. The height of the receiver was 1.2 m. The source-receiver distance refers to the horizontal distance along the y-axis hereafter, unless otherwise stated. It ranged from 5 m to 150 m. The average background noise during the measurement was about 70 dB(A) as mentioned above. In order to ensure sufficient rooms for the sound level to

decay and that the results would not be affected by the background noise, only the Early Decay Time was measured. With the same level of sound power being used in the measurement of STI, the signal-to-noise ratio was sufficiently high in each octave band, and its contribution to the STI was ignored in the computation.

Separate measurements were conducted to characterize the impedance of the wall surfaces and the ground. It was found that they can essentially be treated as perfectly hard surfaces in the numerical models. This was in consistency with previous works performed by Li and Iu in the same tunnel. The ceiling was assumed to be perfectly hard as well. For the incoherent model, the absorption coefficients (α) were set to 0 in order to simulate the ideal case of perfectly reflecting boundaries. A clear comparison between the coherent and incoherent models could then be made. Decay curves were generated by setting $\alpha = 0$ in Eq. (2.2), and from which the corresponding EDT and STI were obtained. The effect of atmospheric absorption was included in the computation. The absorption coefficients for atmospheric absorption were determined according to the formulation given in Ref. 4.

For the coherent model, the sound field is first computed in the frequency domain with Eq. (2.12). Since the boundaries are assumed to be perfectly hard, the spherical wave reflection coefficients in Eq. (2.4) equal to 1. The results are then digitally filtered by Butterworth IIR band pass filter. The same type of filter is used in the MLSSA system. The impulse response in the corresponding one-third octave band is obtained by applying the inverse Fourier transform on the filtered results. A decay curve can be generated by a reverse-time integration of the squared impulse response, as in Eq. (2.15). The EDT is obtained from the first 10 dB of the decay of sound level, and the STI is determined from the impulse response as given in the previous section.

Both the EDT and STI were measured at different positions as marked in Fig. 2.8. It was found that the predictions with the coherent model agreed well with the experimental data, whether the receiver was located on the centreline or the offset line. For the brevity in the illustration, only the comparison of measured and predicted EDT on the centreline, and that of the STI on the offset line, are presented. Fig. 2.9(a) shows the comparison of EDT spectra at source-receiver separations of 15 m, 50 m, 75 m and 150 m on the centreline. It can be seen that the incoherent model gives a general trend of the EDT only, while the coherent model provides a better prediction. For example, when the source and receiver are separated by 75 m, there are dips at 200 Hz and 630 Hz, and a peak at 400 Hz. The coherent model is able to predict the fluctuations in different frequency bands. The incoherent model overestimates by more than 1.5 s at 200 Hz, and 1 s at 630 Hz. At higher frequencies, e.g. over 2000 Hz, the difference between predictions by the two models becomes smaller.

Fig. 2.9(b) demonstrates how the EDT varies along the length of the tunnel at two typical frequencies of 200 and 2500 Hz. At 200 Hz, the EDT fluctuates along the length of the tunnel due to the interference effect of the contributory sound rays. On the other hand, the incoherent model is unable to predict the reduction in EDT at a distance over 50 m at 200 Hz. In fact, it overestimates the EDT for over 1 s at distances beyond 75 m from the source. The coherent and incoherent models give similar predictions in the one-third octave band centred at 2500 Hz, within a difference of 0.5 s. This is in accordance with the findings by António *et al.* [13], who suggested that the interference effects were significant in low frequency bands. The coherent predictions generally match the measurements better than the incoherent predictions, especially in the low frequency range. For the prediction of

the EDT, the average error of the coherent model was 0.3 s, and that of the incoherent model was 0.6 s. It is noted that the prediction results might match the measurements better at some positions by changing the parametric values of the absorption coefficients in the incoherent model. However, it is not able to predict the fluctuations due to interference effects as offered by the coherent model.

In the next set of measurements, the receiver was located along the offset line. Observations from the comparisons of the measured and predicted EDT are similar to the case when the receiver was located at the centreline. In order to show that the coherent model is also valid in this receiver location, the comparisons of measured and predicted STI are shown in Fig. 2.10. The interference effects are observed in the lower frequency bands, where the coherent model gives a better prediction than the incoherent model. For the overall value of STI, both models give similar predictions. The reason is that the overall STI, defined in Eq. (2.18), is a weighted average of the values at seven octave bands. The incoherent model over-estimates the STI at 8000 Hz, but under-estimates at other frequency bands, as shown in Fig. 2.10. The average errors in predicting the STI were 0.02 and 0.04 for the coherent and incoherent models, respectively. By a numerical weighted average of the values at different octave bands, the incoherent model seems to give a reasonably good prediction of the overall STI, as the corresponding discrepancies are cancelled out mathematically. In this way, the overall STI values can only give a general idea of the speech intelligibility in an enclosure. In order to have a better understanding of the enclosure on the performance of speech, the STI at different octave bands, of which the coherent model can give a satisfactory prediction, should be examined as well. Corresponding acoustic treatments can then be applied to improve the speech intelligibility.

It can be seen from Figs. 2.9 and 2.10 that the predictions by the coherent model agree reasonably well with the field measurements in most cases. However, some discrepancies between the experimental data and theoretical predictions have been found. This is probably due to the scattering of sound from the raised walkways adjacent to the vertical walls and other scattering subjects hung from the ceiling. The fact that the tunnel cross-section is not a true rectangular shape also affects the results. Other factors include the use of loudspeakers as a point source, and the assumption of a perfectly hard ceiling. It is important to show that the numerical model also works in enclosures with impedance boundaries, which will be discussed in the next section.

2.3.2 Long enclosure with two impedance boundaries

Measurements of RT30 and STI were conducted in a corridor in the Department of Mechanical Engineering, the Hong Kong Polytechnic University. The length and width of the corridor were 35.6 m and 1.53 m respectively. The height of the corridor, which was measured from the floor to the false ceiling, was 2.45 m. We found from subsequent measurements that the false ceiling could be treated as perfectly hard. Therefore, 2.45 m is used as the height of the corridor hereafter. The Tannoy T300 loudspeaker was again used as the sound source to generate white noise. The same set of equipment mentioned in the previous section was used, except for the loudspeaker. The ground of the corridor was covered with a carpet. The ceiling was made up of perforated metallic panels and embedded with fibre glass (see Fig. 2.11).

Separate measurements of excess attenuation (EA) were made for the characterization of the impedance of the corridor surfaces. A Tannoy driver fitted with a tube of length 1 m was used as a point source. The excess attenuation is

defined as the ratio of the total sound field of sound propagation along an impedance surface, P_T, to the direct sound field, P_d:

$$EA = 20\log(P_T / P_d) \quad (2.21)$$

The source and receiver were located 0.5 m from each other and at a distance of 0.2 m from the surface of interest. The measured data are compared with predictions with the one-parameter model in the excess attenuation spectra shown in Fig. 2.12. They are also compared with predictions with the assumption of perfectly hard surfaces. The best-fit values for the effective flow resistivity (σ) of the ceiling and the ground surfaces are found to be 5,000 kPa s m^{-2} and 400 kPa s m^{-2} respectively. Based on the measurements of excess attenuation, the vertical walls along the length of the corridors and the end walls are perfectly hard. The scattering effects that might occur from the edge between the wall and the doors can also be ignored. It is noted that a high flow resistivity of 5,000 kPa s m^{-2} is deduced for the ceiling. It may essentially be treated as a hard boundary. However, it is found from subsequent calculations that the use of this parameter for the flow resistivity leads to better agreement with experimental data.

The loudspeaker was located 4 m from one end of the corridor, equidistant from the vertical walls (i.e. along the centreline), and 0.95 m above ground. The receiver was placed along the centreline at a height of 1.2 m. Atmospheric absorption is included in the predictions. The absorption coefficient (α) used in the incoherent model is deduced from the plane wave reflection coefficient (R_p) with the assumption of normal incidence:

$$\alpha = 1 - R_p^2 \quad (2.22)$$

The absorption coefficients of the ground and ceiling surfaces from 100 Hz to 4000 Hz in one-third octave bands are listed in Table 2.2. It is noted from the absorption

coefficients that the ceiling is relatively hard.

Both RT30 and STI were measured in one-third octave bands, with the source-receiver distance ranging from 1 m to 28 m. This can be perceived as a long-distance sound propagation with respect to the cross-sectional area. Fig. 2.13(a) shows the RT30 spectra when the receiver was located at separations of 16 m, 24 m and 28 m from the source. The coherent model can give a satisfactory prediction up to the maximum distance at 28 m, following the pattern of the fluctuations of the measured values in most cases. On the other hand, the incoherent model can only give a general trend of the RT30. When the source and receiver are located 16 m apart, the incoherent model gives an over-estimation of 0.2 s at 160 Hz, and under-estimation of about 0.2 s at 1600 Hz. At source-receiver distance of 24 m, discrepancies between the incoherent predictions and measurements are found in lower frequency region, while the predictions above 1000 Hz seem agreeable. However, at a distance of 28 m, it is noticed that the coherent model generally gives a much more accurate prediction than the incoherent one. One of the main objectives of the current study is the prediction of sound propagation at larger distances in a long enclosure. Although experimental measurements are also conducted at shorter distances, these measured spectra are not presented here for brevity. Nevertheless, some of the measured results at shorter distances are displayed in Fig. 2.13(b) for the source frequency of 250, 500 and 2500 Hz.

The variations of RT30 along the length of the corridor at frequency bands of 250 Hz, 500 Hz and 1000 Hz are shown in Fig. 2.13(b). Similar to Fig. 2.13(a), the coherent model gives a satisfactory prediction in most cases. The coherent model is more preferable to the incoherent model, especially in lower frequency region, where the interference effects are believed to be more significant. For the incoherent

predictions, the shape of the curve does not seem to change much at the three different frequency bands, since its amplitude depends on the value of the absorption coefficients. The selection of absorption coefficients, or the determination of the impedance of the boundaries, plays an important role in the incoherent model. However, the absorption coefficients cannot represent the true physical properties of the boundary surfaces because normal incidence is assumed in the incoherent model. This is even more obvious when a receiver is set farther apart from the source in a long enclosure. In the coherent model, the spherical wave reflection coefficient is dependent on frequency and angle of incidence, which is more reasonable in practice.

Results similar to those shown in Fig. 2.13 are obtained at other source-receiver separations and frequency bands. They are not included here for brevity. For the prediction of RT30, the average error of the coherent model is 0.05 s, with a maximum of 0.06 s at 630 Hz. On the other hand, the predicted RT30 according to the incoherent model has a higher average error of 0.07 s. Though the coherent model gives a reasonably good approximation in most cases, some discrepancies between the experimental data and the coherent predictions can still be found. Possible factors include the scattering of sound from the edges between the vertical side walls and the doors, and from the perforated metallic panels of the ceiling, the use of a loudspeaker as a point source, and the assumption of perfectly hard vertical boundaries and end walls.

Similar to the case in the Western Harbour Tunnel, the coherent model is able to predict the STI more accurately than the incoherent model, as shown in Fig. 2.14. The average errors of the coherent and incoherent models are 0.03 and 0.06 respectively. There are under-estimations by the incoherent model at frequency

bands of 250 Hz, 500 Hz, 100 Hz and 2000 Hz, and over-estimations at some distances at 4000 Hz. Dips and peaks are observed at 250 Hz, and the coherent model can predict the pattern well. The incoherent model is not capable of showing this interference effects. Comparing the results in Figs. 2.10 and 2.14, the advantage of the coherent model is more obvious here than in the case of the real tunnel. As mentioned before, the impedance of the boundaries are characterized by the one-parameter model for the coherent model. It can simulate the reflection properties of the boundaries better than simply giving a nominal value as the absorption coefficient used in the incoherent model.

2.3.3 Long enclosure with an acoustically soft surface

In the previous section, two impedance boundaries were introduced into the model. The approximation of the coherent model is found to be satisfactory. However, the two boundaries are relatively hard. A third experiment has been conducted to study the performance of the coherent model in long enclosures with an acoustically soft boundary. A 4.8-metre-long model corridor made of hard plywood was set up in the anechoic chamber (Fig. 2.15). The cross-sectional area was 0.8 x 1.2 m^2. The lower horizontal plane was covered with a layer of 3-cm-thick fibreglass. When the model was viewed upside-down, it simulated the situation in which absorptive material was placed on the ceiling in a long enclosure where sound absorption treatment was usually made. The impedance of this boundary was calculated according to the one-parameter model with a hard-back layer [14]. This impedance model has led to a good prediction of the excess attenuation, as shown in Fig. 2.16(a). In the acoustic characterization of the boundary, the source and receiver were separated by a horizontal distance of 0.8 m and placed at a height of 0.13 m. The best-fit parametric

value for the effective flow resistivity was 40 kPa s m^{-2}. The absorption coefficient of the fibre-glass used in the incoherent model was also measured with the impedance tube. The results are presented in Fig. 2.16(b).

The cross-section of the model tunnel was relatively smaller than those in the previous experiments; hence a Tannoy driver fitted with a tube of length 1 m was used as a point source. The same microphone as mentioned before was used. The source and receiver were placed at several different positions to measure the corresponding EDT and STI. Comparisons between some of the measured data and the coherent predictions were presented in Fig. 2.17. The source was placed 0.2 m from one of the vertical planes, and 0.13 m above the lower horizontal surface. The receiver was placed in alignment with the source along the length of the enclosure, but at a height of 0.7 m. In the same way, when the model was viewed upside down and properly scaled, it simulated the scenario of a loud-speaker being fixed near the ceiling and the wall, and a listener standing on the ground.

Fig. 2.17(a) shows the measured and predicted EDT spectrum at four different source-receiver separations, namely 1.5 m, 2 m, 2.5 m and 3 m. Fluctuations caused by interference effects are again observed. For example, at a distance of 1.5 m, there is a significant peak at 800 Hz, and a dip at 500 Hz. The coherent model can give a satisfactory prediction, especially between 200 Hz to 400 Hz. The predictions at other distances are also reasonably good. At a distance of 3 m, a downward slope is found from 630 Hz to 1250 Hz, which is predicted precisely by the coherent model. However, the trend is not observed in the incoherent prediction. Similar results have been obtained in other source-receiver configurations. The average error of the coherent prediction is 0.09 s, with a maximum of 0.19 s at 200 Hz.

Fig. 2.17(b) shows the measured and predicted STI at 500 Hz and 2000 Hz octave bands. It seems that both the coherent and incoherent models give good approximations of the STI. The prediction also matches the experiment data well at other octave bands, but they are not presented here for brevity. The advantage of the coherent model over the incoherent one cannot be observed clearly here. It may be due to the length of the model corridor being limited by the size of the anechoic chamber, and the source-receiver distance being relatively small. There is an over-prediction at 3.5 m source-receiver separation at 2000 Hz. This is probably caused by the scattering effects which occur at the edges of the model. This is also believed to be the major reason for discrepancies between the measurement results and the predictions both in EDT and STI.

2.5 Conclusions

The coherent model has been extended to evaluate the impulse response of sound in a long enclosure, from which the reverberation time and speech transmission index can be obtained. The model was validated by comparing the theoretical predictions with the experimental data in a real tunnel with hard boundaries, a long corridor with two impedance boundaries, and a model corridor with an acoustically soft boundary. It was shown that the coherent model could give a more accurate prediction than the incoherent model, because the interference effects between contributory rays were included. The coherent model gave satisfactory predictions of both the reverberation time and the speech transmission index, at different receiver positions as shown in the figures.

It was described in the theory section that the impulse response was obtained by the inverse Fourier transform of the predicted sound field. The number of

predicted data in single frequency will increase from low to high frequency bands, which means the computational time will also increase. The advantage of the coherent model can also be observed better in narrow band analysis, since the number of frequencies included in each band increases with the width of the band, and the interference effects may be averaged out and become less significant. Considering the computational time and the significance of the interference effects, the coherent model is therefore preferable in narrow band analysis, and in low frequency regions. It has also been demonstrated that the spherical wave reflection coefficient should not be replaced by the plane wave reflection coefficient, especially in cases of long source-receiver distance and enclosures with relatively soft boundaries, and in low frequency ranges. The propagation of sound in a long enclosure with an impedance discontinuity will be discussed in the next chapter.

References

1. T. F. W. Embleton, “Tutorial on sound propagation outdoors,” J. Acoust. Soc. Am. **100**, 31-48 (1996).
2. M. E. Delany and E. N. Bazley, “Acoustical properties of fibrous absorbent materials,” Appl. Acoust. **3**, 105-116 (1970).
3. K. Attenborough, “Ground parameter information for propagation modelling,” J. Acoust. Soc. Am. **92** (1), 418-427 (1992).
4. ANSI S1.26, “Method for calculation of the absorption of sound by the atmosphere,” (1995).
5. K. M. Li and K. K. Iu, “Full-scale measurements for noise transmission in tunnels,” J. Acoust. Soc. Am. **117**, 1138-1145 (2005).
6. M. R. Schroeder, “New method of measuring reverberation time,” J. Acoust. Soc. Am. **37**, 409-412 (1965).
7. T. Houtgast and H. J. M. Steeneken, “The modulation transfer function in room acoustics as a predictor of speech intelligibility,” Acustica **28**, 66-73 (1973).
8. H. J. M. Steeneken and T. Houtgast, “A physical method for measuring speech-transmission quality,” J. Acoust. Soc. Am. **67**(1), 318-326 (1980).
9. J Kang, Acoustics of long spaces, Thomas Telford, London : Thomas Telford, (2002).
10. K. Attenborough, “Review of ground effects on outdoor sound propagation from continuous broadband sources,” Appl. Acoust. **24**, 289-319 (1988).
11. D. D. Rife and J. Van der Kooy, “Transfer-function measurement with Maximum-Length sequences,” J. Audio Eng. Soc. **37**, 419-443 (1989).
12. J. Kang , “Reverberation in rectangular long enclosures with geometrically reflecting boundaries,” Acustica – Acta Acustica **82**, 509-516 (1996).

13. J. Antonio, L. Godinho and A. Tadeu, “Reverberation times obtained using a numerical model versus those given by simplified formulas and measurements,” Acta - Acta Acustica **88**, 252-261 (2002).
14. K. M. Li, T. Waters-Fuller and K. Attenborough, “Sound propagation from a point source over extended-reaction ground,” J. Acoust. Soc. Am. **104**, 679-685 (1998).

Tables

Case	Source Height	Receiver Height	Source-receiver distance
1a	2m	2m	5m
1b	2m	2m	20m
1c	2m	2m	50m
2a	3.8m	2m	5m
2b	3.8m	2m	20m
2c	3.8m	2m	50m
3a	3.8m	3.8m	5m
3b	3.8m	3.8m	20m
3c	3.8m	3.8m	50m

Table 2.1: Location of source and receiver in the rectangular enclosure.

Frequency (Hz)	**100**	**125**	**160**	**200**	**250**	**315**	**400**	**500**	**630**
Absorption coefficient (Ceiling)	0.009	0.011	0.013	0.016	0.018	0.022	0.026	0.030	0.036
Absorption coefficient (Ground)	0.058	0.068	0.081	0.094	0.110	0.130	0.152	0.177	0.206
Frequency (Hz)	**800**	**1000**	**1250**	**1600**	**2000**	**2500**	**3150**	**4000**	
Absorption coefficient (Ceiling)	0.042	0.050	0.058	0.069	0.081	0.094	0.111	0.131	
Absorption coefficient (Ground)	0.240	0.277	0.317	0.367	0.415	0.467	0.522	0.581	

Table 2.2: Absorption coefficients of the ground and ceiling surfaces in the corridor (in 1/3 octave bands).

Figures

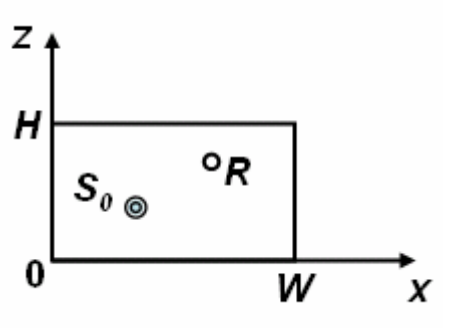

(a)

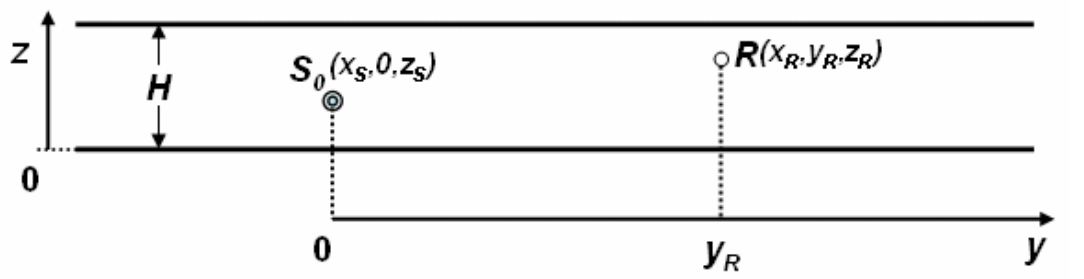

(b)

FIG. 2.1: Position of source and receiver in a long enclosure.

(a) Cross-section;

(b) Side view.

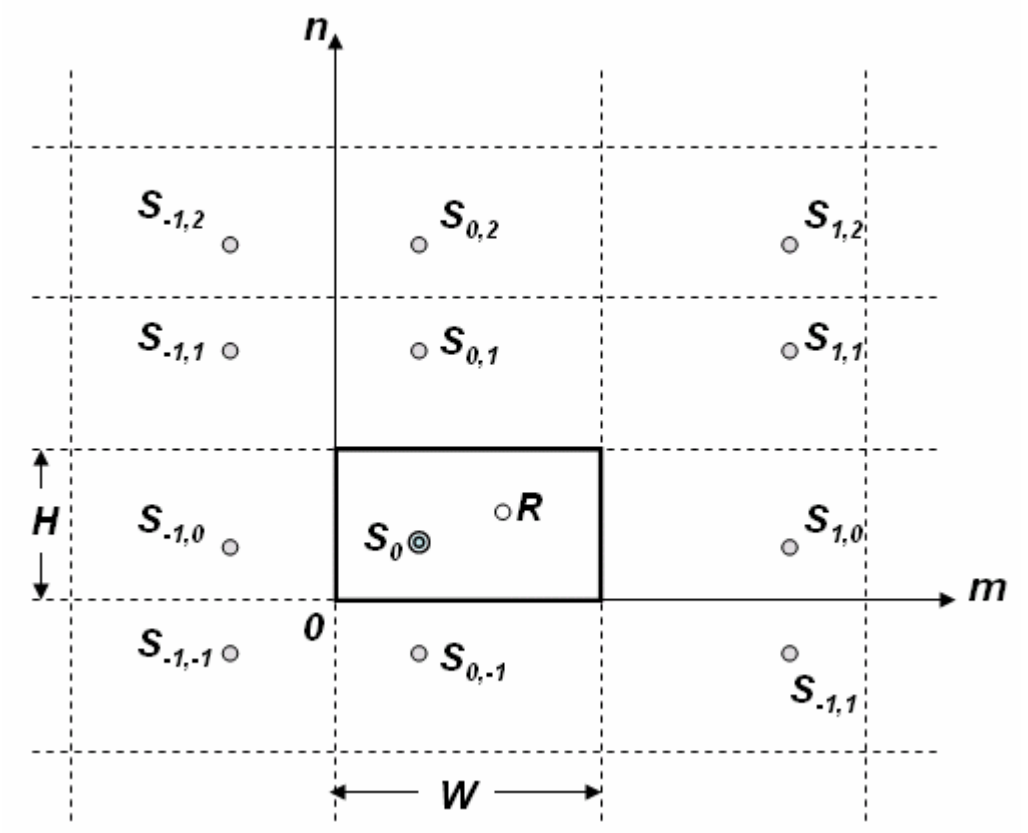

FIG. 2.2: Formation of image sources.

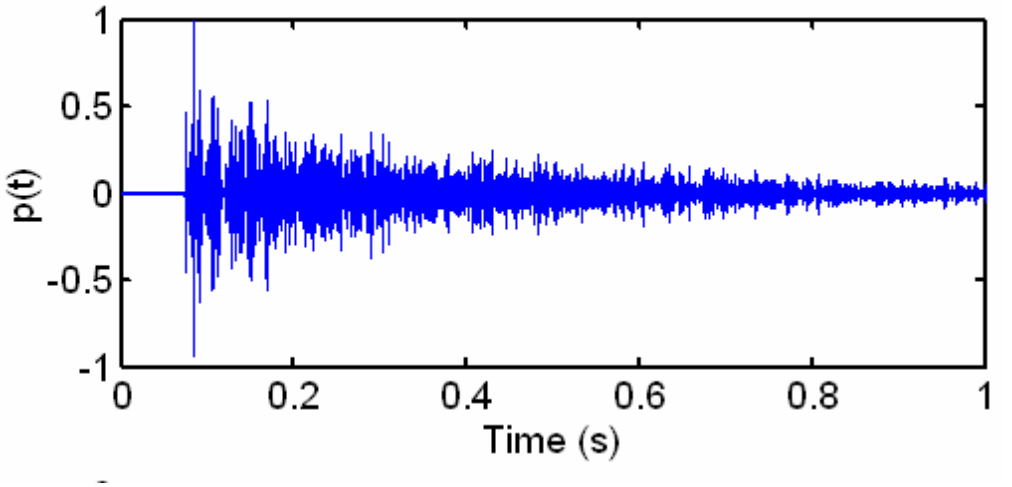

FIG. 2.3: Impulse response.

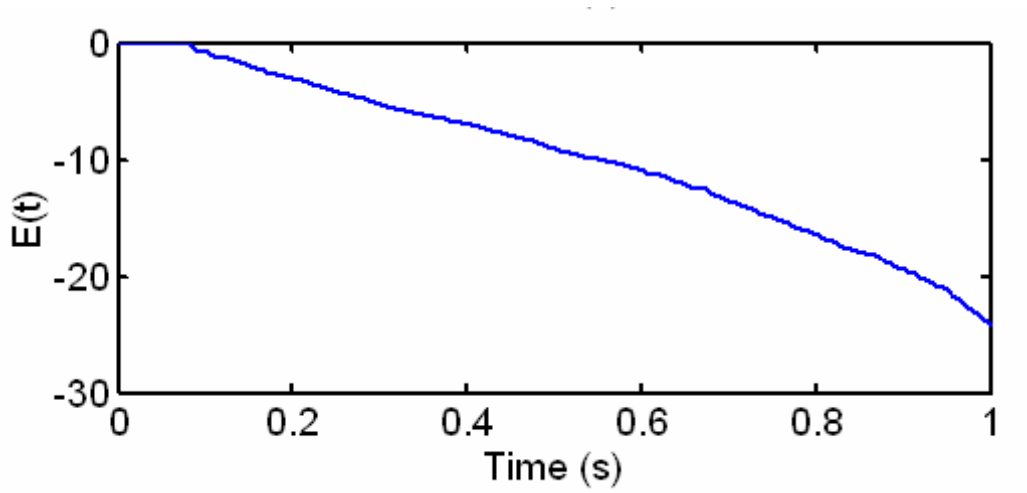

FIG. 2.4: Decay curve.

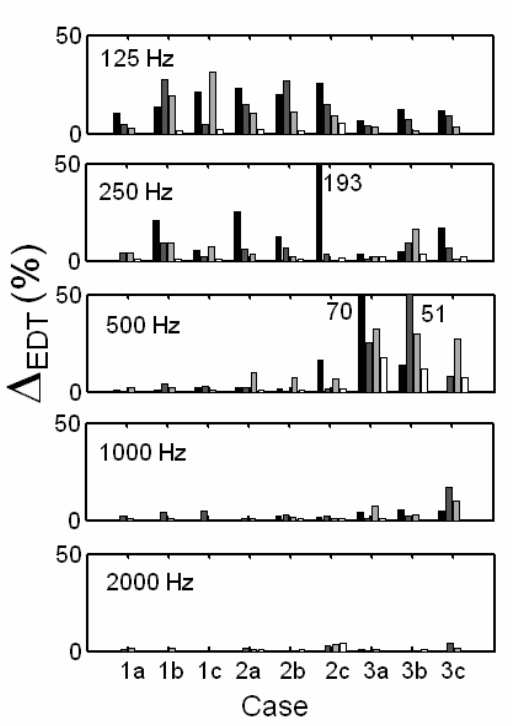

(a)

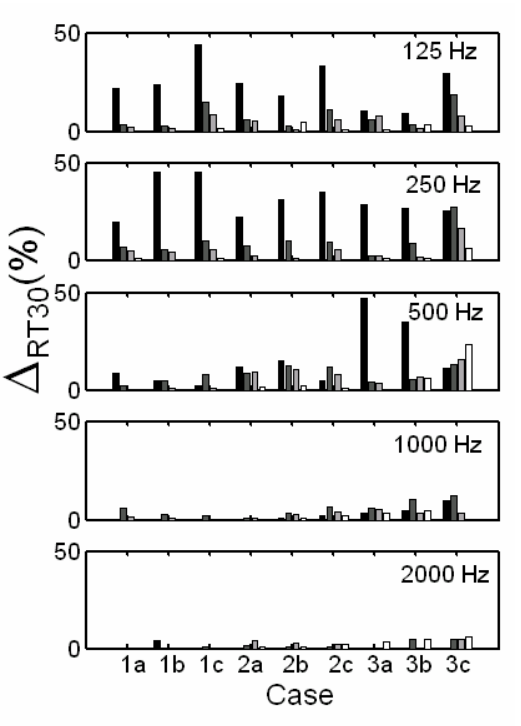

(b)

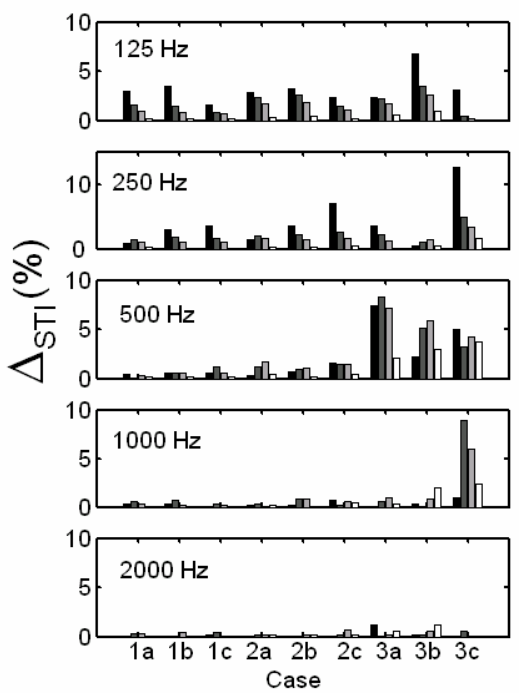

(c)

FIG. 2.5: Relative error in the use of plane wave reflection coefficients to predict (a) EDT, (b) RT30 and (c) STI at different source-receiver geometry. Results computed with effective flow resistivities of:

100 kPa s m^{-2}: ,

500 kPa s m^{-2}: ,

1,000 kPa s m^{-2} : , and

10,000 kPa s m^{-2}: .

FIG. 2.6: The Western Harbour Tunnel.

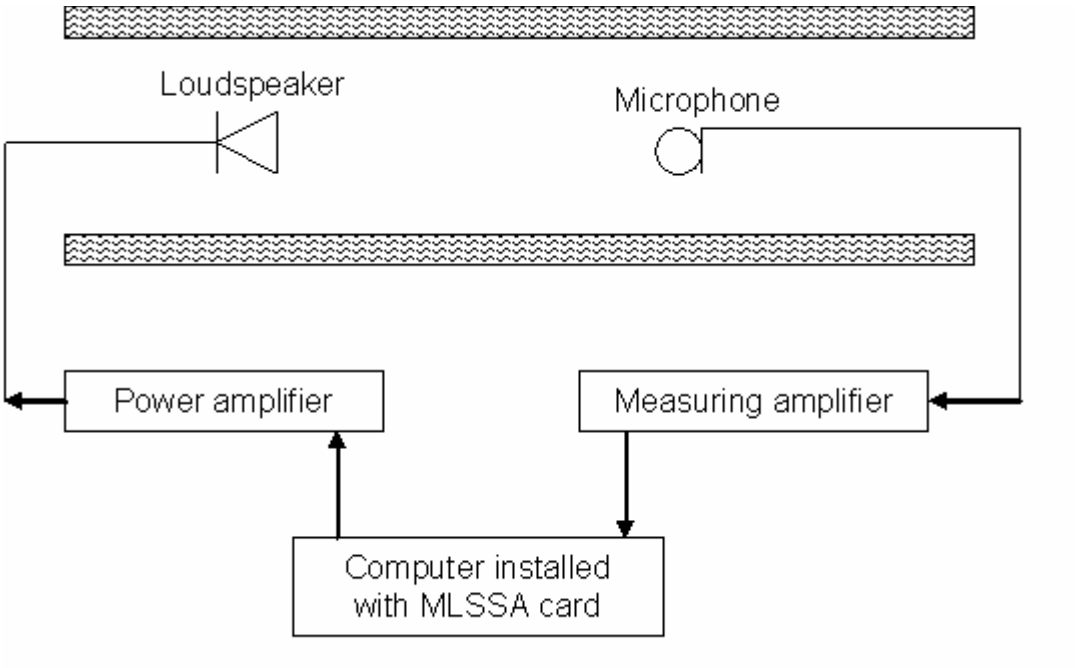

FIG. 2.7: Experimental set-up.

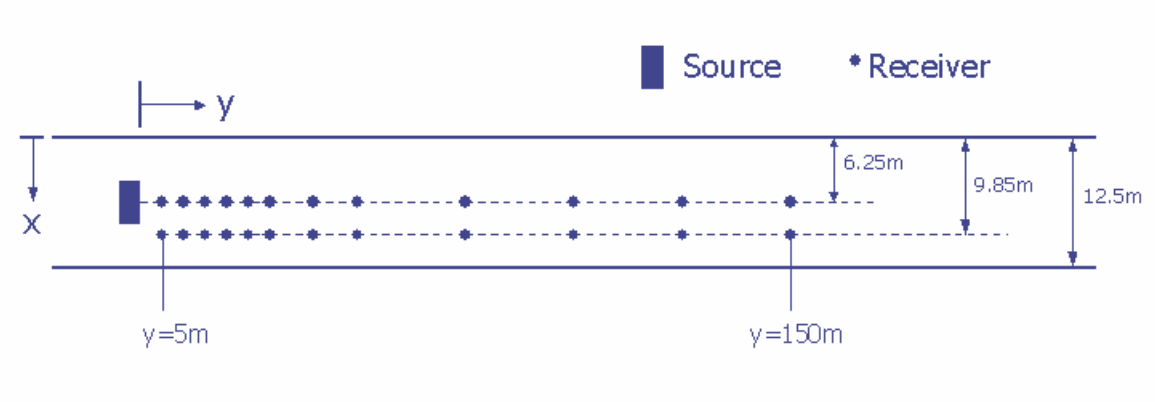

FIG. 2.8: Arrangement of source and receiver in the tunnel (plan view).

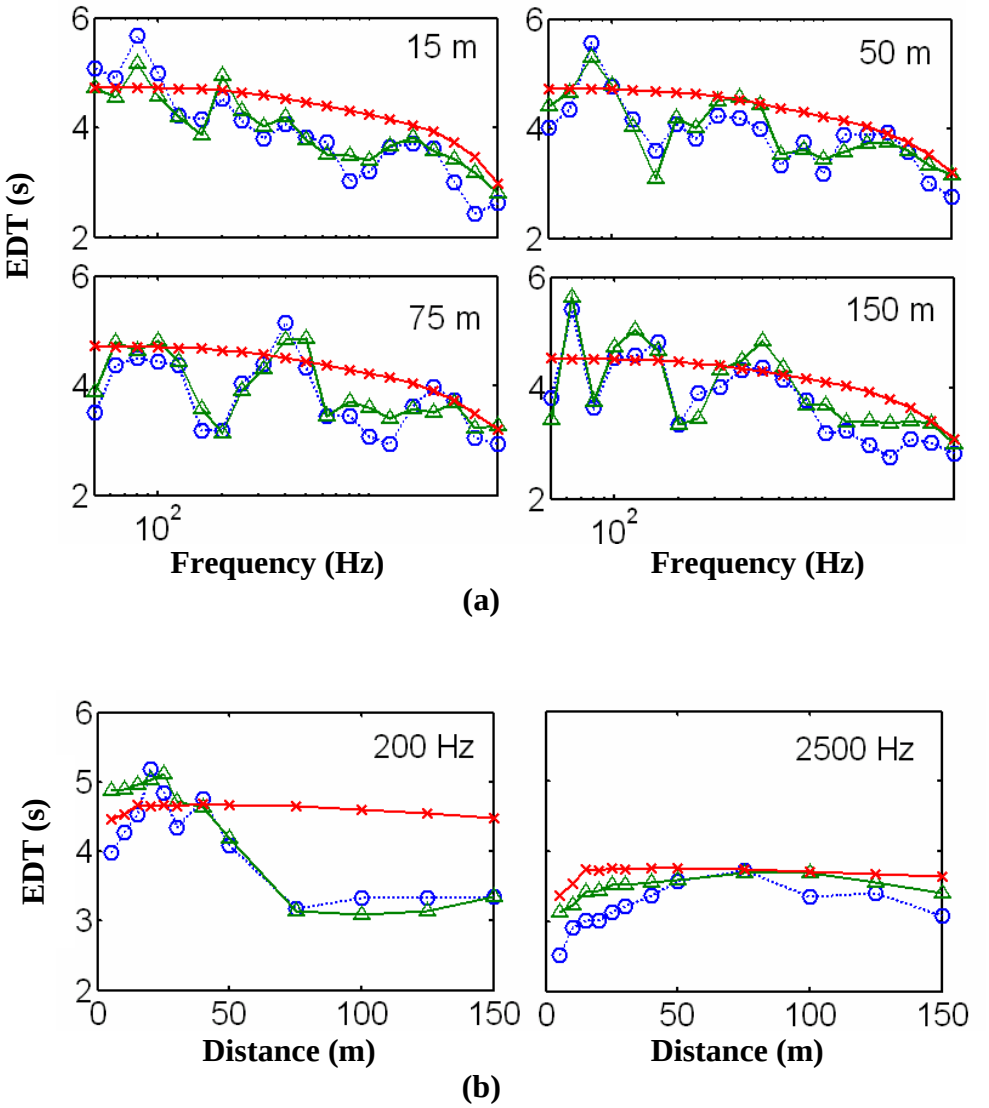

FIG. 2.9: Comparison of measured and predicted EDT in the tunnel.

Measurement: ; Coherent prediction: ; Incoherent prediction:

(a) EDT spectra at different source-receiver distance;

(b) EDT along the length of the tunnel at different frequency bands.

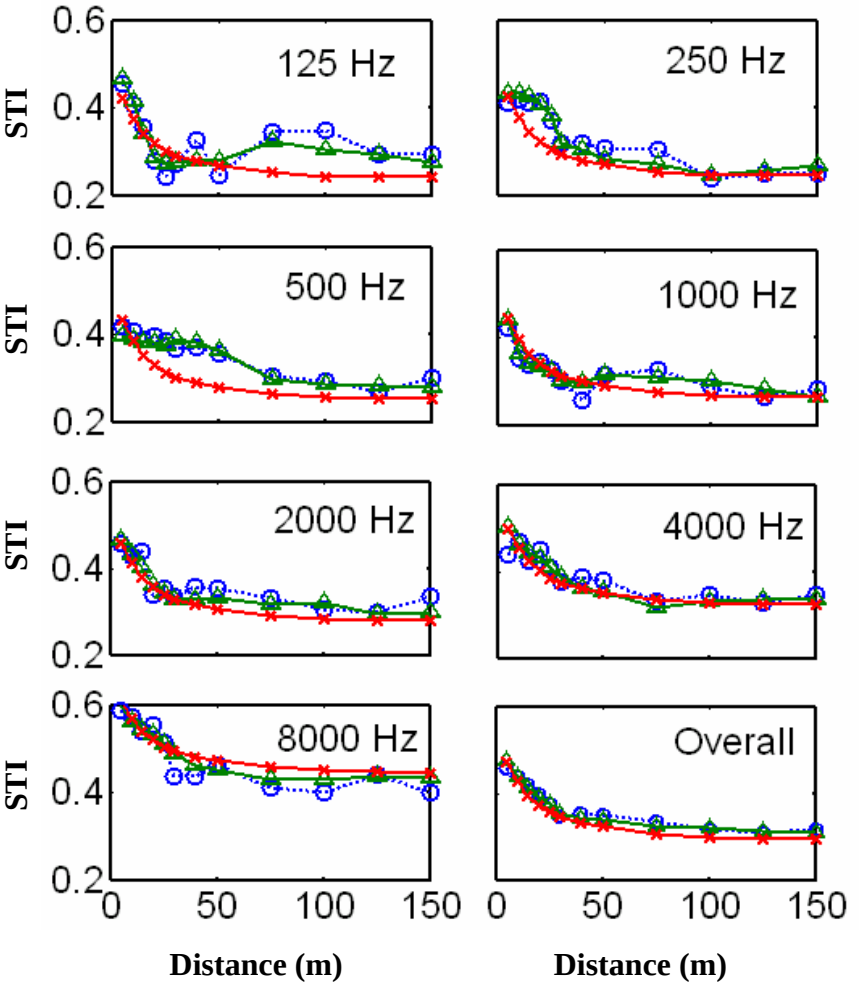

FIG. 2.10: Comparison of measured and predicted STI, receiver located along the offset line. Measurement: ; Coherent prediction: ; Incoherent prediction:

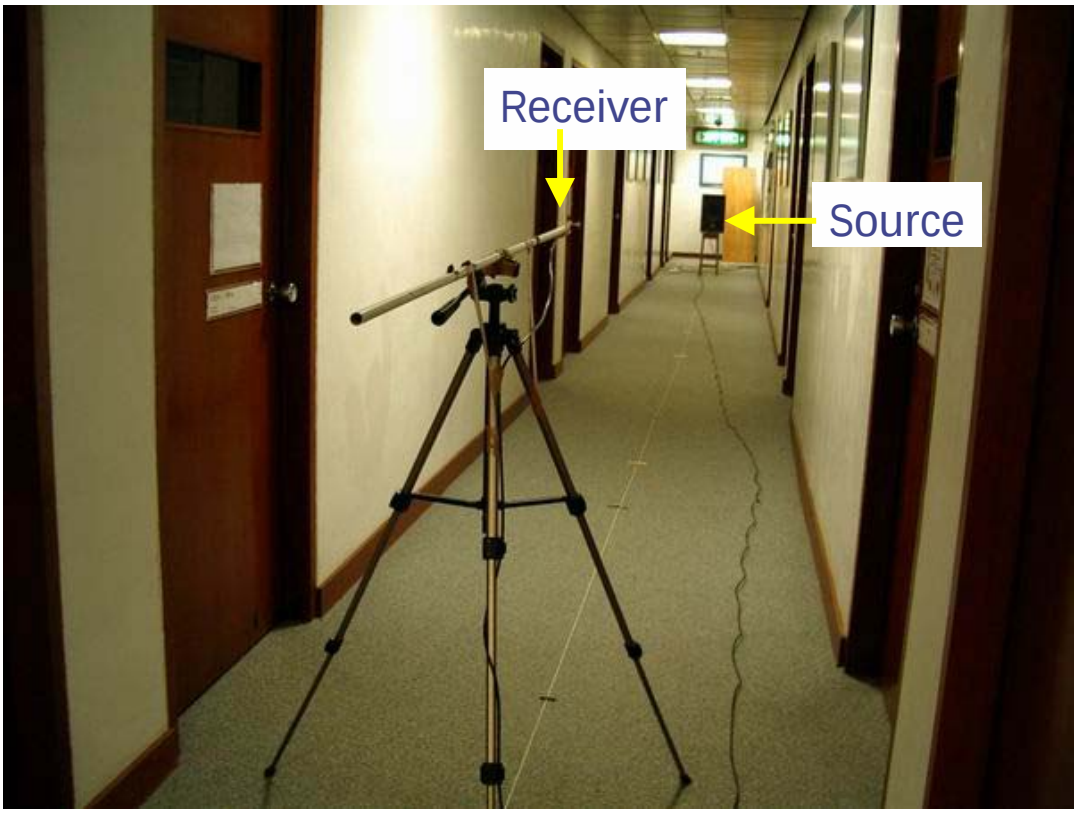

FIG. 2.11: Arrangement of the source and receiver in the corridor

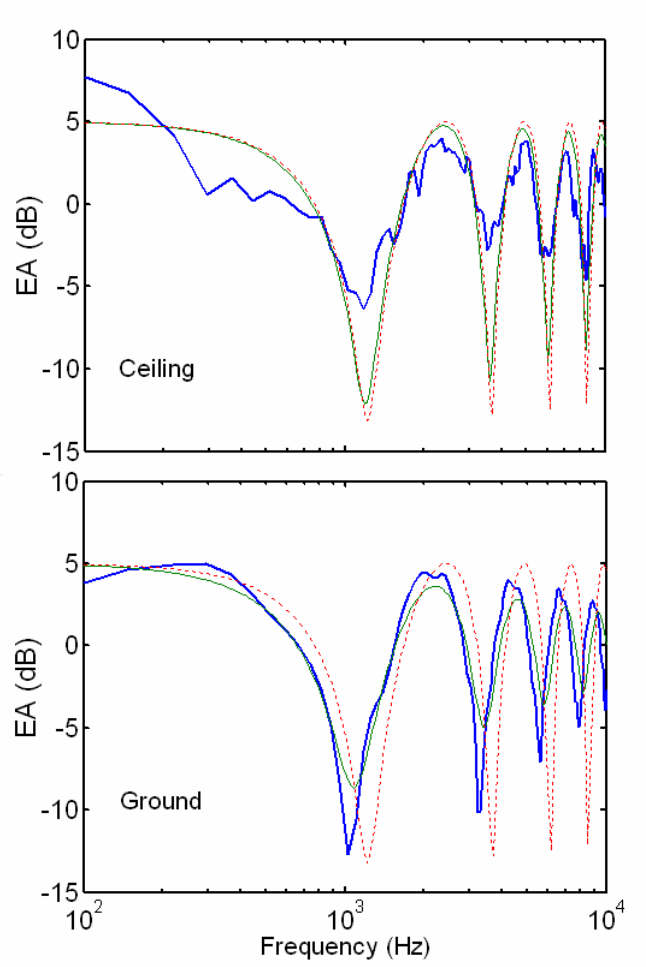

FIG. 2.12: Plot of excess attenuation against frequency for the characterization of surfaces in corridor. Measurement: ——, prediction with one-parameter model:——, and prediction with the assumption of perfectly hard surface:·····.

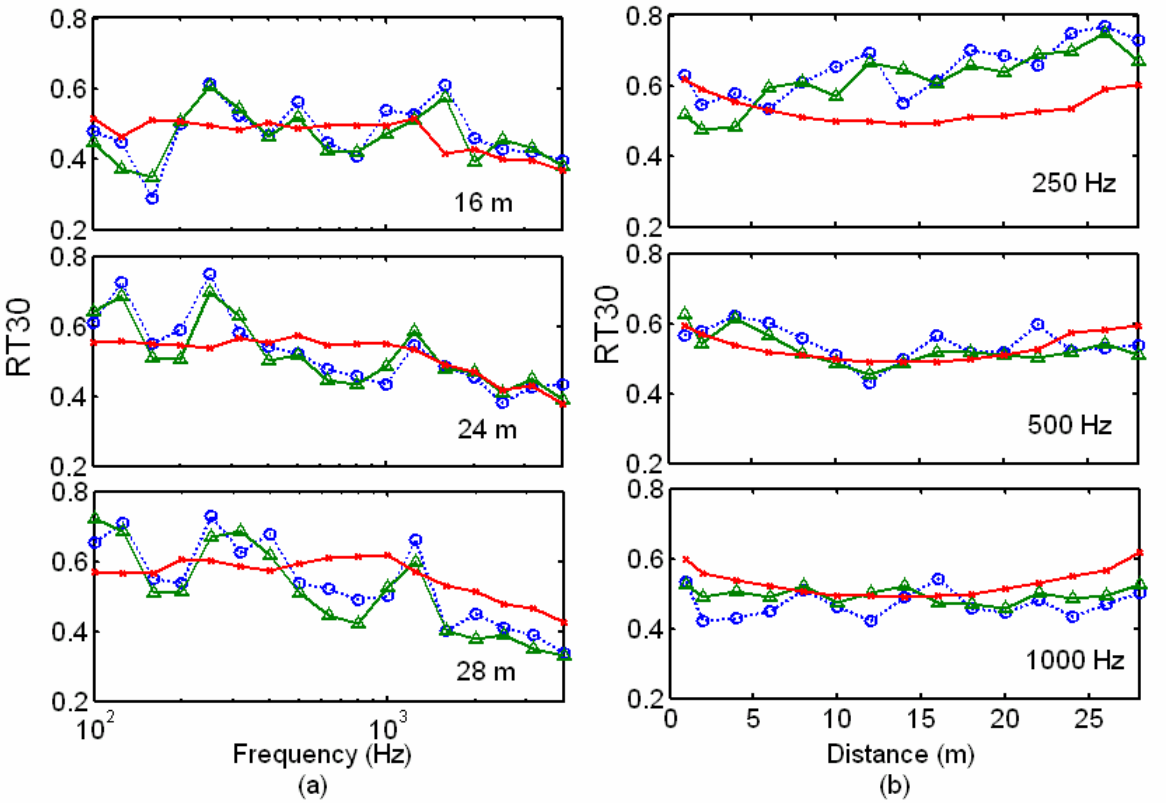

FIG. 2.13: Comparison of measured and predicted RT30 in corridor.

Measurement: ; Coherent prediction: ; Incoherent prediction:

(a) RT30 spectra at different source-receiver distances;

(b) RT30 along the length of the tunnel at different frequency bands.

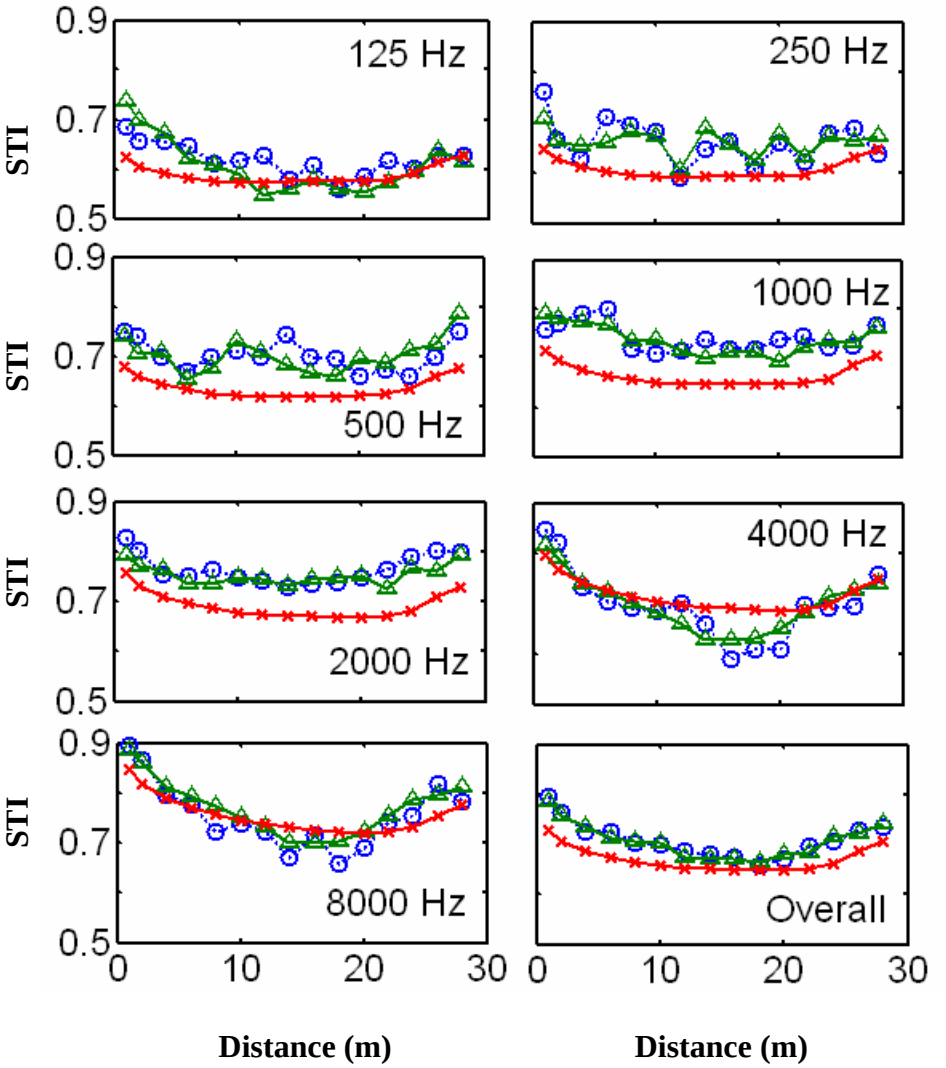

FIG. 2.14: Comparison of measured and predicted STI in corridor.

Measurement: ; Coherent prediction: ; Incoherent prediction:

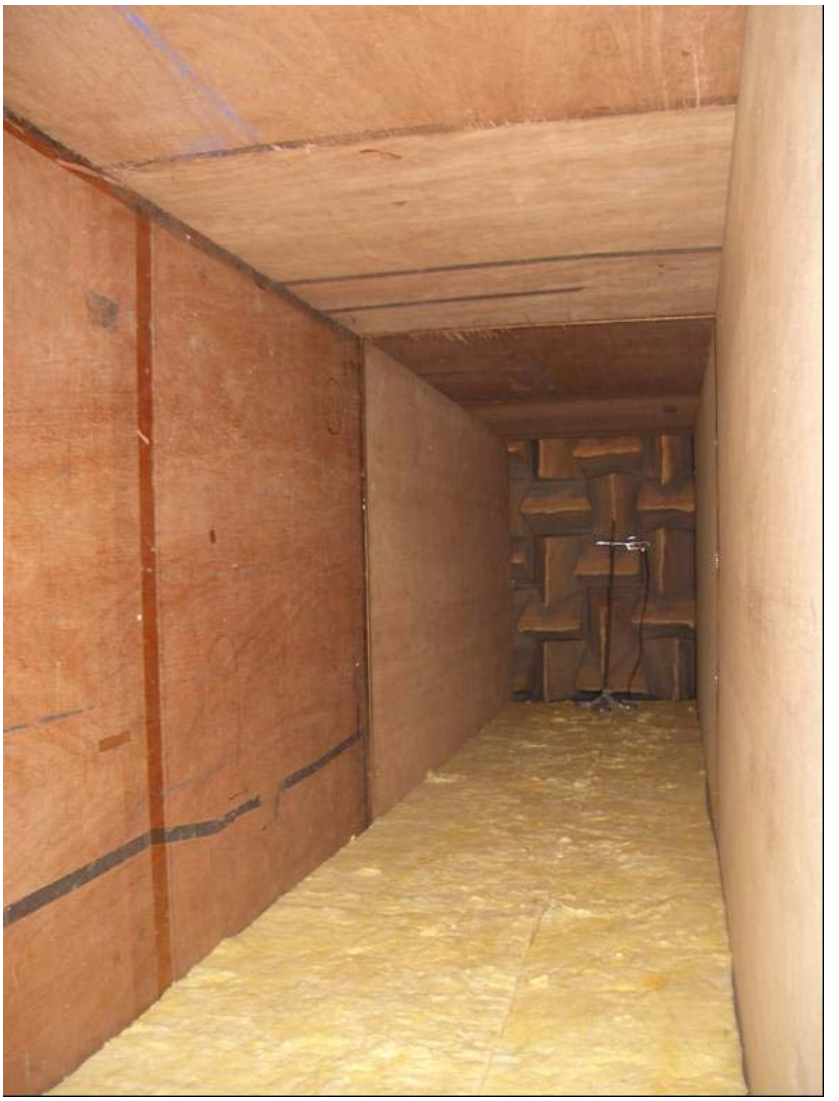

FIG. 2.15: Model corridor in the anechoic chamber.

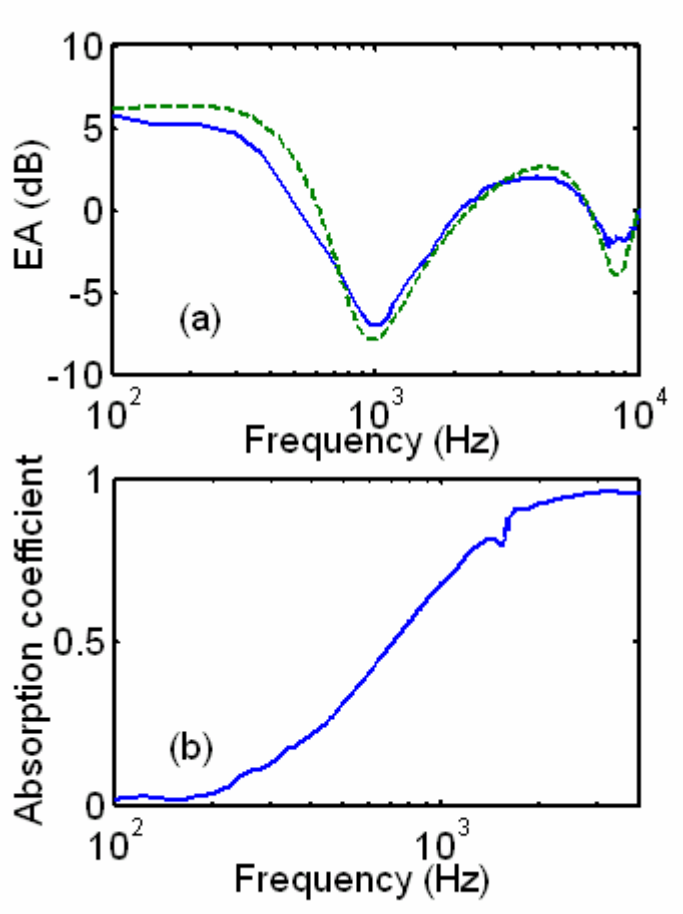

FIG. 2.16: Characterization of the impedance of fiberglass.

(a) Plot of excess attenuation against frequency.

Measurement: ——; Prediction: - - - - .

(b) Plot of absorption coefficient against frequency.

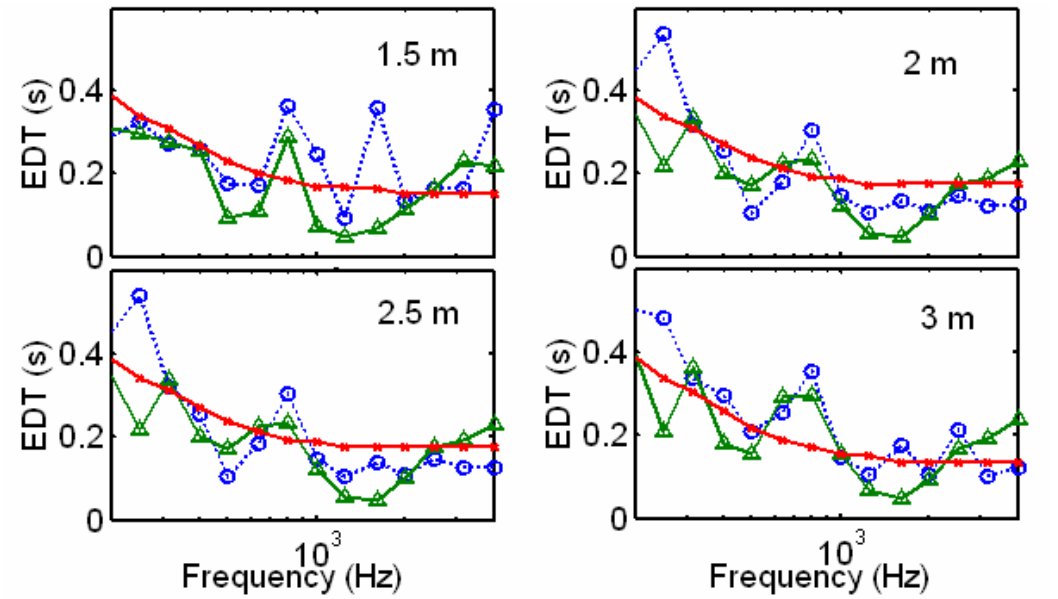

(a)

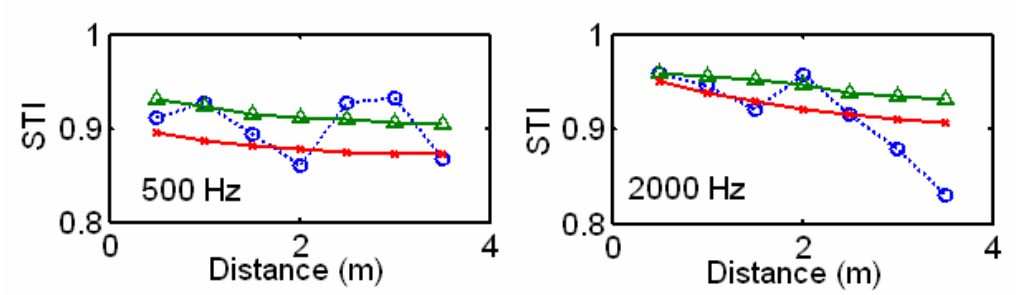

(b)

FIG. 2.17: Comparison of measured and predicted results in model corridor.

Measurement: ; Coherent prediction: ; Incoherent prediction: .

(a) EDT spectra at different source-receiver distance;

(b) STI at 500 Hz and 2000 Hz octave bands.

Chapter 3

Sound propagation in a long enclosure with an impedance discontinuity

3.1 Introduction

The research described in Chapter 2 concentrated on long enclosures with homogeneous surfaces. The acoustic properties of the four boundaries remain the same along the length of the enclosure. A common practice of acoustic treatment is the lining of sound absorption materials along the enclosure walls. However, it will not be economical, nor can it achieve maximum efficiency, if the sound absorption materials are installed on the entire length of an enclosure. It is necessary to optimize the pattern, the amount, and the location of the absorption materials. For example, patches of absorption material can be placed on the ceiling at certain intervals. A theoretical model can assist the design of such an arrangement of absorption materials.

As the first attempt to investigate the problem, the basic theory of sound propagation over a half-rigid half-soft plane will be reviewed. It is then incorporated into the coherent model and applied to a two-dimensional duct. The diffraction effect will be examined. In the second part of this chapter, the coherent model will be extended to a three-dimensional long enclosure. Experimental validation of the coherent model will be presented in the last section.

3.2 Theory

3.2.1 Sound propagation over ground with an impedance discontinuity

The formulation for the prediction of outdoor sound propagation over an impedance discontinuity proposed by De Jong *et al.* [1] will be reviewed first. The geometry of the problem is shown in Fig. 3.1. The change of impedance occurs at $y = y_D$. The source is placed at (0,0, z_S), and the receiver R at (x_R, , y_R , z_R), where $y_R > y_D$. The image of the source is located at (0,0,-z_S). There are three ray paths leading from the source to the receiver: the direct path (r_1), the reflected path (r_2) and the diffracted path (r_3). The total sound field is expressed as:

$$p_t = p_i(1-D_i) + p_r - \frac{D_r}{Q_{G1}} p_r , \tag{3.1a}$$

if the reflection point *M* falls on the region $y < y_D$, and

$$p_t = p_i(1-D_i) + p_r + \frac{D_r}{Q_{G2}} p_r , \tag{3.1b}$$

if the reflection point *M* falls on the region $y > y_D$. The direct and reflected sound fields are denoted by p_i and p_r respectively. Here, the spherical wave reflection coefficients Q_{G1} and Q_{G2} are calculated according to Eq. (2.6) with the impedances of the two regions, Z_{G1} and Z_{G2} of the corresponding ground surfaces. The diffraction coefficients D_i and D_r are given respectively by:

$$D_i = \frac{r_1 e^{-i\pi/4}}{r_3\sqrt{\pi}} (Q_{G1} - Q_{G2}) F\left(\sqrt{k(r_3 - r_1)}\right), \tag{3.2a}$$

$$D_r = \frac{r_2 e^{-i\pi/4}}{r_3\sqrt{\pi}} (Q_{G1} - Q_{G2}) F\left(\sqrt{k(r_3 - r_2)}\right), \tag{3.2b}$$

where

$$F(\chi) = \int_{\chi}^{\infty} e^{it^2} dt \tag{3.3}$$

is the Fresnel integral function [2].

3.2.2 Single impedance discontinuity in two parallel horizontal planes

The formulation for the prediction of outdoor sound propagation over an impedance discontinuity proposed by De Jong *et al.* [1] is incorporated into the coherent model to account for the case of a two-dimensional duct, i.e. calculation of sound fields between two parallel horizontal planes. The geometry of the 2-d enclosure is shown in Fig. 3.2. There is an impedance change from Z_{G1} to Z_{G2} at $y = y_D$ on the lower horizontal surface. It means the region $y < y_D$ on the lower plane has a specific normalized impedance of Z_{G1}, and that of the region $y > y_D$ is Z_{G2}. The upper horizontal plane has a specific normalized impedance of Z_C. The source S_0 is placed at (0,0, z_S), and the receiver R at (x_R, y_R , z_R) where $y_R > y_D$.

In the image-source method, the boundaries of an enclosure are imagined to be removed, leaving an infinite number of images behind. Fig. 3.2 demonstrates the formation of image sources. The coordinates of the image sources are (0, 0, z_n) where $n = -\infty \ldots \infty$. The images are conveniently grouped into matching pairs. A typical pair of images is shown in Fig. 3.3. It contains two image sources: S_j and S_{-j-1}, where $j = 0, 1, \ldots, \infty$. The contribution of sound pressure of each pair of images is composed of 3 parts, represented by waves traveled through the three paths: the direct path (r_1), the reflected path (r_2), and the diffracted path (r_3). The lengths of the paths are determined by:

$$r_1 = d_j, \tag{3.4a}$$

$$r_2 = d_{-j-1}, \tag{3.4b}$$

and

$$r_3 = \sqrt{x_D{}^2 + y_D{}^2 + z_j{}^2} + \sqrt{(x_R - x_D)^2 + (y_R - y_D)^2 + z_R{}^2}\,. \tag{3.4c}$$

The calculation of d_j and d_{-j-1} is given in Eq. 2.1 with $n = j$ and $n = -j - 1$ respectively, and $m = 0$. The diffracted path is the shortest distance traveled from the image source S_j to the edge of the impedance step, and then to the receiver. The point at which it hits the impedance step is called the diffraction point D_j. It has the coordinates of $(x_D, y_D, 0)$, where

$$x_D = \frac{x_R\sqrt{y_D{}^2 + z_j{}^2}}{\sqrt{y_D{}^2 + z_j{}^2} + \sqrt{(y_R - y_D)^2 + z_R{}^2}}\,. \tag{3.5}$$

The reflection point M_j is the position at which the image S_j reflects from the ground surface. It has the coordinates of $(x_M, y_M, 0)$, where

$$y_M = \frac{y_R z_j}{z_R + z_j}, \tag{3.6}$$

The sound field contributed by the image source can be written as:

$$P_D(j) = P_j(1 - D_i) + P_{-j-1} - \frac{D_r}{Q_{G1}} P_{-j-1}, \quad \text{if } y_M < y_D, \tag{3.7a}$$

and

$$P_D(j) = P_j(1 - D_i) + P_{-j-1} + \frac{D_r}{Q_{G2}} P_{-j-1}, \quad \text{if } y_M > y_D. \tag{3.7b}$$

It is noted that the expression $P_D(0)$ is the total sound field in outdoor sound propagation with an impedance discontinuity, as given in Eq. (3.1). The diffraction coefficients D_i and D_r can be obtained from Eq. (3.2). The respective spherical wave reflection coefficients Q_{G1} and Q_{G2} are determined by:

$$Q_{G1} = Q\left(d_{-j-1}, \varphi_{-j-1}, \beta_{G1}\right), \tag{3.8a}$$

and

$$Q_{G2} = Q\left(d_{-j-1}, \varphi_{-j-1}, \beta_{G2}\right), \tag{3.8b}$$

in which $Q(d, \varphi, \beta)$ is defined in Eq. (2.6). β_{G1} and β_{G2} are the respective specific normalized admittances of the lower horizontal surface with impedance Z_{G1} and Z_{G2}.

The sound field of an image source S_n is given by:

$$P_n = Q_G Q_C \frac{e^{ikd_n}}{4\pi d_n}, \qquad \text{for } n = -\infty \ldots \infty, \tag{3.9}$$

where Q_C is the spherical wave reflection coefficient of the upper plane. It can be calculated according to Eq. (2.5d) by substituting 0 into m. The values of P_j and P_{-j-1} can be obtained from Eq. (3.9) with $n = j$ and $n = -j - 1$ respectively. The expression of Q_G is the respective spherical wave reflection coefficient of the lower horizontal plane which can be determined by:

$$Q_G = Q\left(d_n, \varphi_n, \beta_{G1}\right)^{n_{G1}} \times Q\left(d_n, \varphi_n, \beta_{G2}\right)^{n_{G2}}. \tag{3.10}$$

The index n_{G1} is the number of times the image S_n reflects on the region with impedance Z_{G1}, while n_{G2} is that on the region with impedance Z_{G2}. They can be calculated according to:

$$n_{G1} = \text{int}\left[\frac{y_D + z_S \tan\Phi_n}{2H \tan\Phi_n}\right], \tag{3.11a}$$

for positive odd n and negative even n,

$$n_{G1} = \text{int}\left[\frac{y_D - z_S \tan\Phi_n}{2H \tan\Phi_n} + 1\right], \tag{3.11b}$$

for positive even n and negative odd n, and

$$n_{G2} = \begin{cases} \dfrac{|n-1|}{2} - n_{G1} & \text{for odd n,} \\ \dfrac{|n|}{2} - n_{G1} & \text{for even n,} \end{cases} \tag{3.12}$$

where

$$\tan \Phi_n = \frac{y_R}{|z_R - z_n|}. \tag{3.13}$$

Finally, the total sound field can be obtained by the summation of the contribution from every image pair, as:

$$P_{total} = \sum_{j=0}^{\infty} P_D(j). \tag{3.14}$$

3.3 Diffraction effect

The diffraction of sound at an impedance discontinuity in outdoor sound propagation has been studied widely (see for example Ref. [1]). It was found that the diffraction effect was very pronounced at near-grazing incidence if there was only a single boundary surface with an impedance discontinuity. In the presence of another boundary surface parallel to the first one, Cummings [3] suggested that the diffraction effect was not important when the frequency was sufficiently high. Indeed, Cumming used this configuration to model the attenuation of sound in a duct silencer. In this section, the diffraction effect on the prediction of sound field in a two-dimensional duct with an impedance discontinuity was explored by extending the De Jong model.

3.3.1 The Effects of Diffraction between Two Parallel Planes

The diffraction effect is first studied by comparing the predicted sound fields with

and without the diffraction coefficients (D_i and D_r) respectively. The geometry is the same as the one shown in Fig. 3.2. The distance between the two horizontal planes is 4 m. The upper horizontal plane and the region $y < y_D$ of the ground are perfectly hard, i.e. Z_{G1}=1. The remaining area of the ground ($y > y_D$) has an impedance of Z_{G2}. It is assumed from the definition of the diffraction coefficients that the amount of change of impedance and the ratio of the area in the two regions are the major factors determining their contribution to the prediction results. Therefore, different values of effective resistivity are used in the one-parameter model [4] to simulate the normalized impedance Z_{G2}. The proportion of the ground with impedance Z_{G1} and Z_{G2} is also varied in the analysis.

The source and the receiver, which are separated by a horizontal distance of 50 m, are placed at equidistance from the lower and upper horizontal planes (i.e. 2 m from the surfaces). This propagation distance is considered long with respect to the height of the duct. The geometrical configuration can simulate a 'near-grazing' sound propagation, since the diffraction effect is known to be significant in the outdoor situation of similar source/receiver geometry. Comparisons are made on the prediction of excess attenuation to investigate the diffraction effect. The excess attenuation is defined as the ratio of the total sound field to the direct field. It is already defined in Eq. (2.21). The predictions are made with the set of equations that are listed in the previous section. When the diffraction effect is ignored, the diffraction coefficients, D_i and D_r, equal to 0. Eq. (3.7) can be reduced to:

$$P_D(j) = P_j + P_{-j-1}. \tag{3.15}$$

Fig. 3.4 compares the excess attenuation when the diffraction effect is included (solid line) and excluded (dotted line) correspondingly. The impedance Z_{G2} is calculated with an effective flow resistivity of 100 kPa s m^{-2}, 500 kPa s m^{-2} and

1000 kPa s m^{-2} in the one-parameter model. Generally speaking, a lower value of flow resistivity represents a more absorptive surface. The impedance of the ground changes at y = 35 m. The diffraction effect is better observed in Fig. 3.4(a) than in Figs. 3.4(b) and 3.4(c), but the difference is not significant. The shapes of the two curves in Fig. 3.4 are rather similar, except for some differences in the amplitudes at certain frequencies. For example, there is a difference of 6 dB at 235 Hz in Fig. 3.4(a), 10 dB at 390 Hz in Fig. 3.4(b). However, this mismatch in amplitude will be averaged out when an octave or a third octave frequency band is concerned. The overall differences for the three cases are 0.12 dB, 0.01 dB and 0.02 dB respectively.

The percentage of the harder ground is varied in the predictions shown in Fig. 3.5. The impedance change occurs at y = 10 m, 20 m and 40 m in Figs. 3.5(a), 3.5(b) and 3.5(c) respectively. The numerical results represent three different ratios of hard/soft ground surfaces, but the effective flow resistivity remains unchanged at 100 kPa s m^{-2}. The maximum difference is 11.8 dB at 580 Hz in Fig. 3.5(a), 7.5 dB at 580 Hz and 2220 Hz, 3870 Hz in Fig. 3.5(b), and 16.34 dB at 390 Hz in Fig. 3.5(c). The differences are not obvious at other frequencies. The overall differences for the three cases are 0.12 dB, 0.17 dB and 0.22 dB respectively.

It is demonstrated that the diffraction coefficients do not have a notable influence on the computation of the total sound field in a two-dimensional duct. The diffraction effect is small and smoothed out after multiple reflections in a long enclosure. Though the effect is more pronounced in near-grazing propagation over ground, it is not observed in two parallel planes. The sound field has been dominated by the multiple reflected waves. As the reflection order of an image increases, it is no longer near-grazing incidence. The diffraction effect is not significant in the above analysis. Therefore, Eq. (3.7) will be replaced by Eq. (3.15) in subsequent

calculations of the total sound field.

3.3.2 Comparison with another numerical model

In this section, numerical results from the coherent model are compared with those computed by the modified Rasmussen integral model [5]. These comparisons serve to prove that the ray model can give a reasonable prediction when the diffraction effect is ignored.

The source and receiver are placed in two parallel horizontal planes, as shown in Fig. 3.6 (Fig. 4.6 in Ref. 3). The heights of the source and receiver are 1 m and 0.5 m respectively. They are separated horizontally by a distance of 2 m. In Fig. 3.6(a), the enclosure has impedance boundaries at the first 1 meter, and hard boundaries at the next meter. The positions of the boundaries are reversed in Fig. 3.6(b): the two-dimensional duct has hard boundaries at the first 1 meter, and impedance boundaries in the next meter. The impedance of the surface is characterized by Attenborough's two-parameter model [6]. The effective flow resistivity and the effective rate of change of porosity with depth are 120 kPa s m^{-2} and 100 m^{-1} respectively.

Fig. 3.7 shows the comparison of the predicted excess attenuation corresponding to the geometry in Fig. 3.6(a). The prediction with the modified Rasmussen integral model is given in Fig. 3.7(a) (Fig. 4.5c in Ref. 3), and that with the proposed coherent model is given in Fig. 3.7(b). The results calculated with the two models are very similar. Another set of data regarding the duct geometry in Fig. 3.6(b) is shown in Fig. 3.8. The predictions from the two models are very much alike, except for some mismatch at 750 Hz and 3100 Hz.

A major reason for the difference in prediction is the choice of parameters in

the corresponding formulation, since the two models are based on different approaches. However, it is enlightening to find that the results are similar, even when diffraction effect has been ignored in the coherent model. This has reduced the complication of computation, while the essential phase information is retained.

3.4 Single impedance discontinuity in a long enclosure

3.4.1 Theory

The coherent model will be extended to the case of a long enclosure with a rectangular cross-section. The diffraction effect is assumed to be unimportant, and is ignored in the computation. The geometry of the long enclosure is shown in Fig. 3.9. It is similar to the one in Fig. 2.1, except for an impedance change from Z_{G1} to Z_{G2} at $y = y_D$ on the lower horizontal surface. It means that the region $y < y_D$ on the lower plane has an acoustic impedance of Z_{G1}, and that of the region $y > y_D$ is Z_{G2}. The left and right vertical planes and the upper horizontal planes have impedance of Z_L, Z_R, Z_C respectively. The source S_0 is placed at (x_S,0, z_S), and the receiver R at (x_R, , y_R , z_R), where $y_R > y_D$.

In the image-source method, the walls of an enclosure are assumed to be removed, leaving an infinite number of images behind. The cross-section of the plane of virtual images can be found in Fig. 2.2. The coordinates of the image sources are (x_m, 0,z_n) where m, n = -∞ … ∞. The contribution of sound field from the image $S_{m,n}$ can be written as:

$$P_{m,n} = Q_L Q_R Q_G Q_C \frac{e^{ikd_{m,n}}}{4\pi d_{m,n}}, \qquad \text{for } m, n = -\infty \ldots \infty, \qquad (3.16)$$

where $Q(d, \varphi, \beta)$ is defined in Eq. (2.6). β_{G1} and β_{G2} are the normalized

admittances of the lower horizontal surface with impedance Z_{G1} and Z_{G2} respectively.

The expression of the spherical wave reflection coefficients for the four boundaries can be found in Eq. (2.5), except for Q_G which is now changed to:

$$Q_G = Q\left(d_{m,n}, \varphi_{m,n}, \beta_{G1}\right)^{n_{G1}} \times Q\left(d_{m,n}, \varphi_{m,n}, \beta_{G2}\right)^{n_{G2}} . \tag{3.17}$$

The index n_{G1} is the number of times the image $S_{m,n}$ reflects on the region with impedance Z_{G1}, while n_{G2} is that on the region with impedance Z_{G2}. They have been defined in Eq. (3.12) and Eq. (3.13) respectively. Finally, the total sound field can be obtained by the summation of the contribution from every image pair, as:

$$P_{total} = \sum_{m=-\infty}^{\infty} \sum_{n=-\infty}^{\infty} P_{m,n} . \tag{3.18}$$

For the case of sound propagation in two parallel planes, the above formulation can be employed by substituting 0 into *m*.

The impulse response of sound pressure is computed by taking the inverse Fourier transform of the frequency response. The decay curve is then generated by a reverse-time integration of the squared impulse response. Reverberation time and speech transmission index can be obtained according to the procedures described in Chapter 2.

3.4.2 Experimental validation

Since the diffraction effect is excluded, the incoherent model can also be used straightforwardly. One of the major tasks is to determine the number of times an image hits the boundaries with different absorption coefficients. In this section, experimental results are presented to validate the proposed coherent model. The predictions from the incoherent model are also displayed to make a comparison of the two approaches. Data were collected from experiments in two model tunnels.

3.4.2.1 Model corridor in anechoic chamber

Measurements were made in a 4.8-metre-long model corridor in the anechoic chamber. The corridor was made up of hard plywood. The boundaries were assumed to be rigid, or perfectly hard. The cross-sectional area was 0.8 ×1.2 m^2. Another set of experiment was conducted in the same model corridor, and the results were presented in Section 2.3.3. A Tannoy driver fitted with a tube of length 1 m was used as a point source. The receiver used in the measurement was a B&K prepolarized diffuse field ½ in. condenser microphone of type 4942, fitted with a B&K Deltatron Pre-amplifier of type 2671. The PC-based maximum length sequence system analyzer (MLSSA) was again used as the signal generator for the source and as the analyzer for subsequent data processing. The source and receiver were set at 0.13 m and 0.67 m above ground respectively.

At the beginning of the experiment, the entire lower horizontal plane was covered with a 3-cm thick layer of fiberglass. The impedance of the fiberglass had been characterized in Chapter 2 (Fig. 2.16(a)). The excess attenuation was calculated according to the one-parameter model with a hard-backed layer [7]. The best-fit parametric value for the effective flow resistivity was 40 kPa s m^{-2}. The absorption coefficient of the fiberglass used in the incoherent model was measured with the impedance tube. The results were shown in Fig. 2.16(b). The sound pressure levels at different positions of the source and receiver were measured. Afterwards, only part of the surface was covered with fiberglass, so that y_D = 1.8 m. The geometric configuration of the corridor could be referred to Fig. 3.9. The impedance of the fiberglass was represented by Z_{G2}. A photograph of the model corridor was shown in Fig. 3.10. The rest of the boundary surfaces were acoustically hard. The sound pressure levels at the same positions were measured again. The relative SPL was

defined as the SPL when the plane was entirely covered with fiberglass, with reference to the SPL when only part of the surface was covered with fiberglass.

Fig. 3.11 showed the relative SPL when the source and receiver were separated by 2 m, 2.5 m, 3 m and 3.5 m respectively. The source was placed 0.2 m from one of the vertical walls, and the receiver was placed equidistant to both walls. Predictions from the coherent model are compared with those from the incoherent model, and with the measurements. It is found that the coherent prediction can give an accurate approximation of the measurements. There is an obvious dip at 630 Hz in Fig. 3.11(b), and one at 800 Hz in Fig. 3.11(d). The coherent model can predict the positions of the dips accurately. The figure shows that when the entire plane is covered with fiberglass, it gives an extra noise reduction up to 10 dB, in a particular frequency range. The idea of noise reduction will be discussed in more detail in the next section. The average error of the coherent model is 1.19 dB, and that of the incoherent model is 3.17 dB.

Fig. 3.12 shows the measured and predicted EDT spectra at two other source-receiver locations. Fluctuations of EDT due to interference effect are observed. In Fig. 3.12(b), the model can predict the down slope between 250 Hz and 500 Hz, followed by a peak at 630 Hz as well. The average error of the coherent model is 0.1 s. On the other hand, the incoherent prediction is simply a straight line. Interference effects can not be approximated by the incoherent model.

Some discrepancies between the measurements and predictions are found in Fig. 3.11 and 3.12. One major factor is the insufficient length of the corridor. The edge of both ends may have diffraction and scattering effects on the sound field in the corridor. Another factor is the unleveled junction between the fiberglass and the plywood. Slight difference in the height of the two materials at the meeting junction

is inevitable in the experiment. This can bring extra scattering which affects the sound field. Results obtained at other source-receiver combinations are similar to those in Figs. 3.11 and 3.12. They are not shown here for concision. In the next section, a model tunnel of greater length is used to investigate the proposed theoretical model.

3.4.2.2 Model tunnel

Experiments were conducted in another model tunnel with an internal cross-sectional area of 1.16 × 1.46 m^2. Its length was about 27 m, with an anechoic termination at one end. The inner surfaces were made of gypsum board. By comparing the measured and predicted excess attenuation as mentioned before, it was found that the gypsum board could be treated as perfectly hard. The same set of equipment as before was used, except for the source. Here a Renkus-Heinz PN61 loudspeaker was used as the source. The heights of the source and receiver were 0.2 m and 0.5 m respectively. Fig. 3.13 shows the inside of the model tunnel near the place of impedance discontinuity.

The source and receiver were placed at different positions, and the sound pressure level, EDT and STI were measured. The measured and predicted EDT spectra are compared in Fig. 3.14. For the data shown in Fig. 3.14(a), the source and receiver are placed at the centerline, i.e., 0.58 m from both vertical walls. They are separated by 16 m, and the impedance discontinuity occurs at 10 m. The downward slop between 250 Hz and 500 Hz, and also the trend between 500 Hz and 1000 Hz, are predicted by the coherent model. The coherent predictions are also close to the measurements at other frequency bands.

In Fig. 3.14(b), the source-receiver distance is 10 m, and the impedance

changes at y = 7 m. The coherent model gives an accurate prediction of the shape from 250 Hz to 2000 Hz. The predictions from the incoherent model cannot predict the trend of the EDT spectra. It only gives an average value of the EDT. The results from the two models are close at frequency bands above 2000 Hz. The average error of the coherent model is 0.15 s.

In another set of measurements, the separation between the source and receiver is fixed at 10 m. Both of them are placed at a distance of 0.2 m from one of the vertical boundaries. The portion of the ground covered with fiberglass is altered. The discontinuity position y_D ranges from 1 m to 9 m. Fig. 3.15 shows the relative SPL when the lower horizontal plane between the source and receiver are covered with different portions of fiberglass. Note that 10 % of harder surface means y_D = 1 m. Relative SPL is defined in this case as the SPL taken when the ground was partly covered with fiberglass, with reference to the SPL taken at the same positions with rigid ground. The results at frequency bands of 200 Hz, 400 Hz, 1250 Hz and 1600 Hz are shown. In Fig. 3.15(a), there is a good fit of data by the coherent model from 10 to 50 % of hard ground. In Figs. 3.15(b), 3.15(c) and 3.15(d), the coherent predictions follow the trend of how the relative SPL varies with the change of percentage of hard ground. The relative SPL is directly proportional to the percentage of hard ground. When the coverage of fiberglass increases, the relative SPL decreases, indicating the sound attenuation caused by the absorption material. This phenomenon is also shown in the incoherent prediction, but it is not as close to the measurement data as the coherent model. The average errors of the coherent and incoherent models are 1.83 dB and 3.14 dB respectively.

The STI was also measured in the experiments. The source and receiver were moved to the centerline, i.e., 0.58 m from the vertical walls. The distance between

them remained to be 10 m. The STI was measured while varying the portion of fiberglass placed between the source and receiver. Since the power of the source was sufficient, the signal-to-noise ratio was high enough that its effect on the STI was ignored. The measured STI at 500 Hz and 2000 Hz are compared with predictions in Figs. 3.16(a) and 3.16(b) respectively. The predictions by the coherent model match reasonably well with the measured data. In Fig. 3.16(a), the STI decreases slightly with the increase of the percentage of hard ground. It means that the speech intelligibility has become better when more absorption material is introduced. The predictions by the two models are close to each other in Fig. 3.16(b). The average error of the coherent model is 0.07. The predictions can also give a good approximation at other frequency bands, but they are not shown here for brevity.

3.5 Conclusions

A theoretical model for the prediction of sound field in two parallel horizontal planes with an impedance discontinuity has been introduced. The diffraction term described in the De Jong model was incorporated into the coherent model. Analysis was to study the diffraction effect on the computation. Comparisons were made with predictions from another theoretical model. It was shown that diffraction at the point of impedance change was not important in the prediction of the sound field. When the diffraction coefficients were ignored, the formulation was simplified and the computational time was greatly shortened.

The coherent model was then extended to account for the case of sound propagation in a long enclosure with a single impedance discontinuity. It had been validated by experiments. It was demonstrated that the coherent model yielded results that were in excellent agreement with the experimental data collected, even

when the diffraction at the impedance discontinuity was ignored. The accuracy of the coherent model was shown to be greater than that of the incoherent model, because the mutual interference between the source and the receiver had been included. Applications of the coherent model will be presented in the next chapter.

References

1. B. A. De Jong, A. Moerkerken and J. D. Van der Toorn, “Propagation of sound over grassland and over an earth barrier,” J. Sound Vib. **86**(1), 23-46 (1983).

2. M. Abramowitz and I. A. Stegun (Eds.), Handbook of Mathematical Functions with Formulas, Graphs, and Mathematical Tables, 9th printing, New York: Dover, 231-233 (1972).

3. A. Cummings, “High frequency ray acoustics models for duct silencers,” J. Sound Vib. **221**(4), 618-708 (1999).

4. M. E. Delany and E. N. Bazley, “Acoustical properties of fibrous absorbent materials, ” Appl. Acoust. **3**, 105-116 (1970).

5. C. L. Chan, “Numerical models for predicting sound propagation in ducts,” MPhil Thesis, Dept. of Mechanical Engineering, Hong Kong Polytechnic Univ., Hong Kong (2002).

6. K. Attenborough, “Ground parameter information for propagation modeling,” J. Acoust. Soc. Am. **92**, 418-427 (1992).

7. K. M. Li, T. Waters-Fuller and K. Attenborough, “Sound propagation from point source over extended-reaction ground,” J. Acoust. Soc. Am., **104**, 679-685 (1998).

Figures

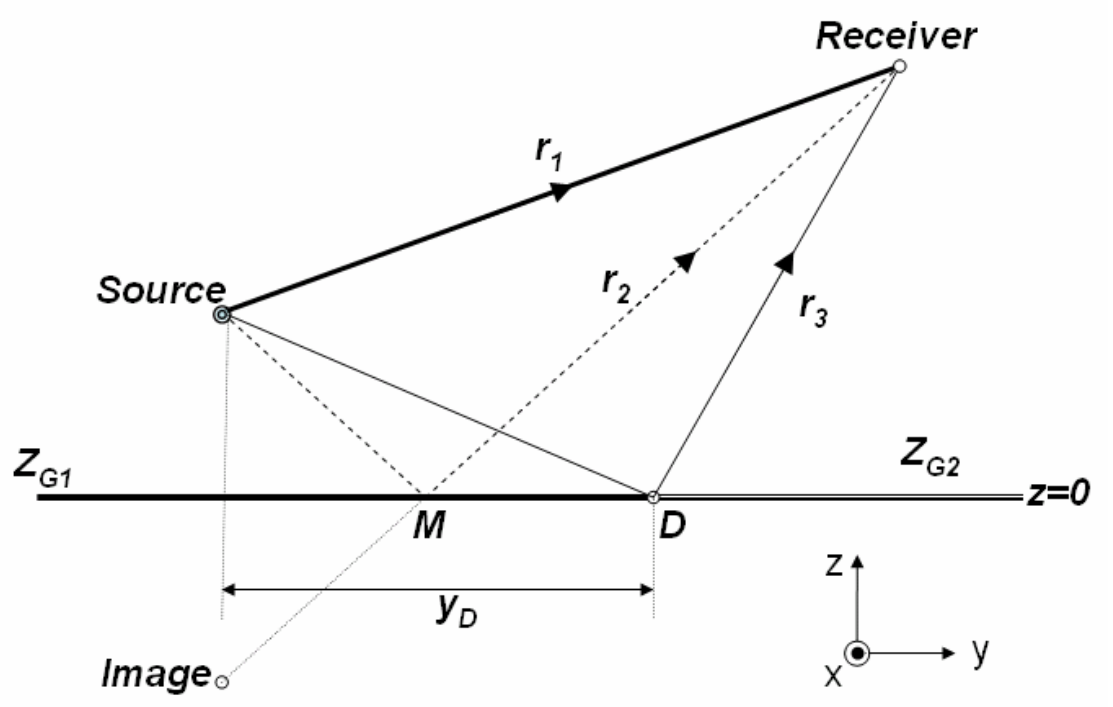

FIG. 3.1: Diffraction at impedance discontinuity.

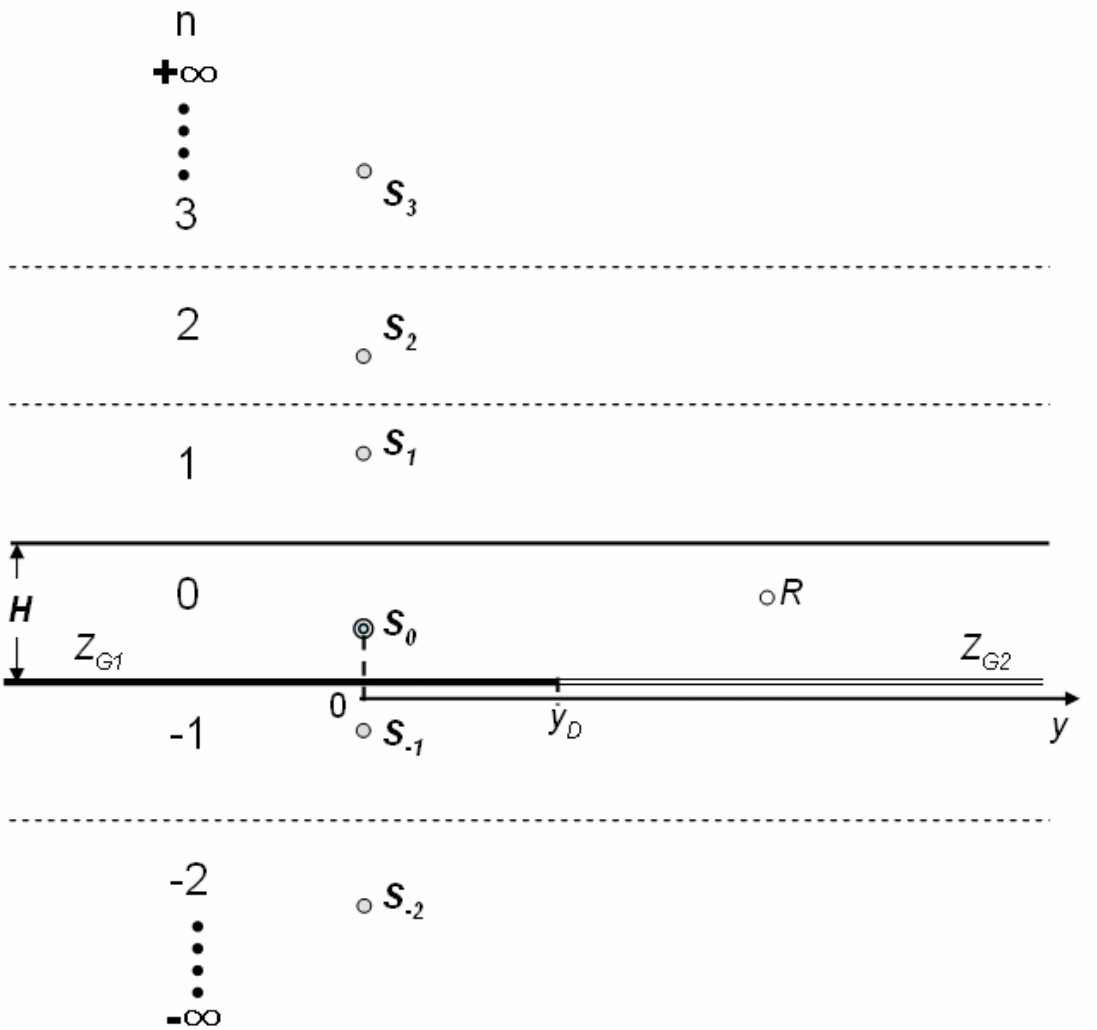

FIG. 3.2: Formation of images in two parallel horizontal planes.

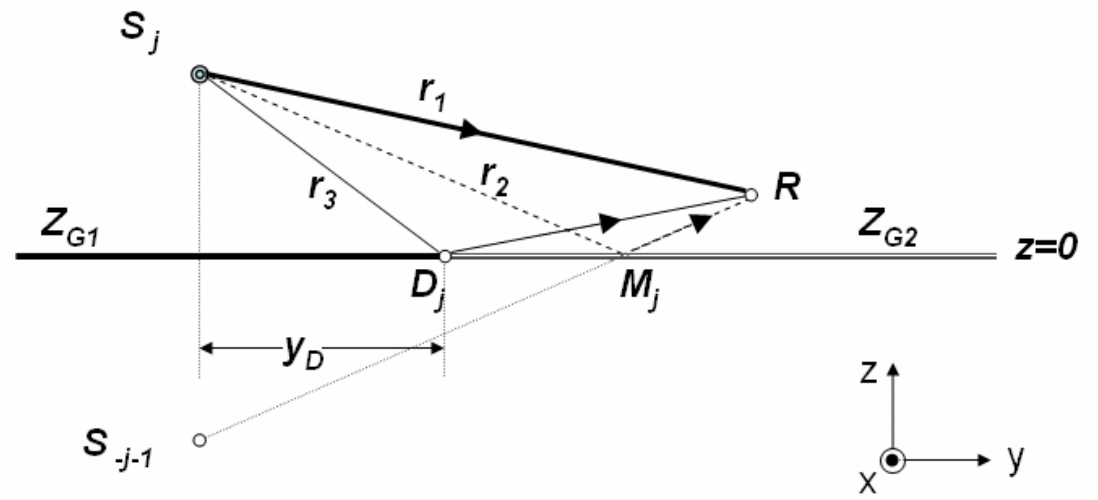

FIG. 3.3: An image pair.

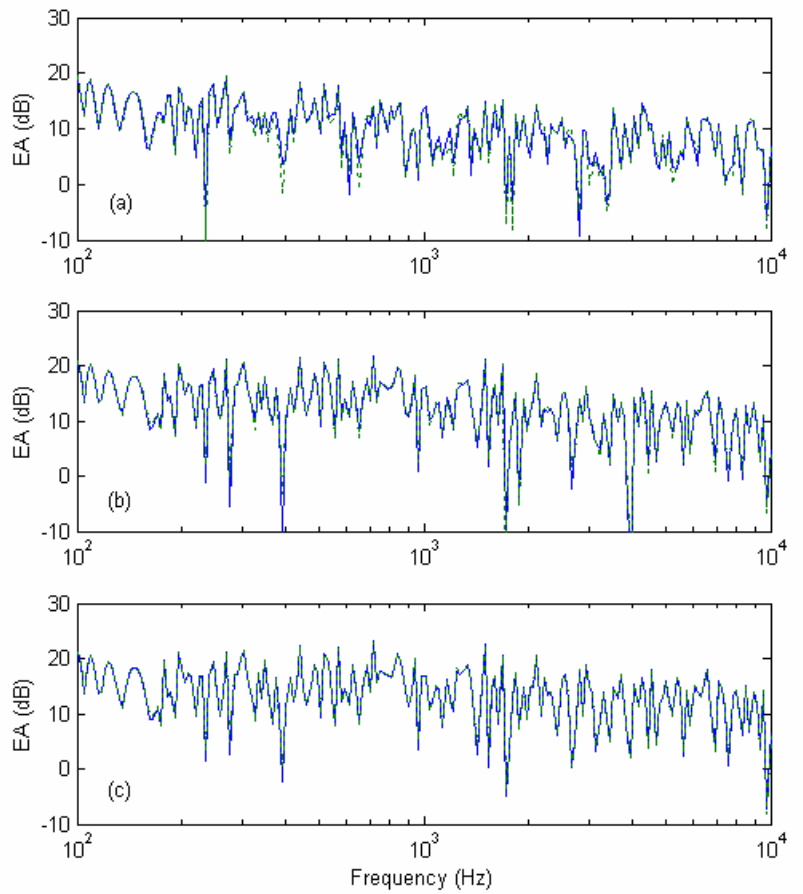

FIG. 3.4: Comparison of excess attenuation. Solid line: prediction with diffraction term; Dotted line: prediction without diffraction term.

Source at (0, 0, 2), receiver at (0, 50, 2), $y_D = 35$ m.

(a) $\sigma_e = 100$ kPa s m^{-2}

(b) $\sigma_e = 500$ kPa s m^{-2}

(c) $\sigma_e = 1000$ kPa s m^{-2}

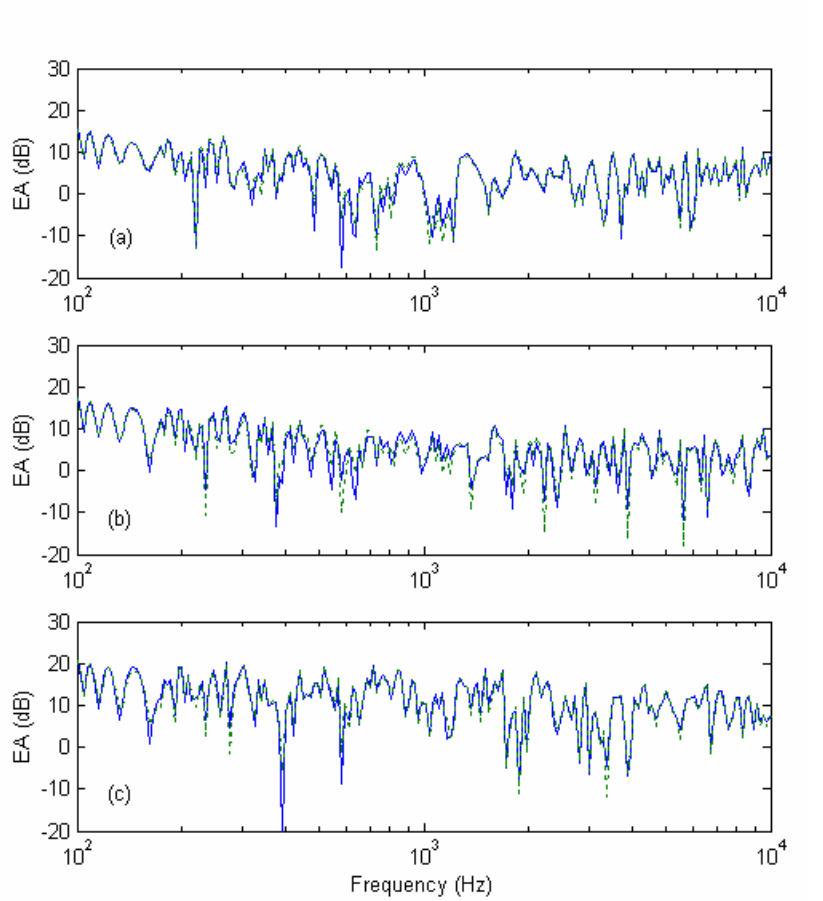

FIG. 3.5: Comparison of excess attenuation. Solid line: prediction with diffraction term; dotted line: prediction without diffraction term.

Source at (0,0,2), receiver at (0, 50, 2), σ_e = 100 kPa s m^{-2}.

(a) y_D = 10 m;

(b) y_D = 20 m;

(c) y_D = 40 m.

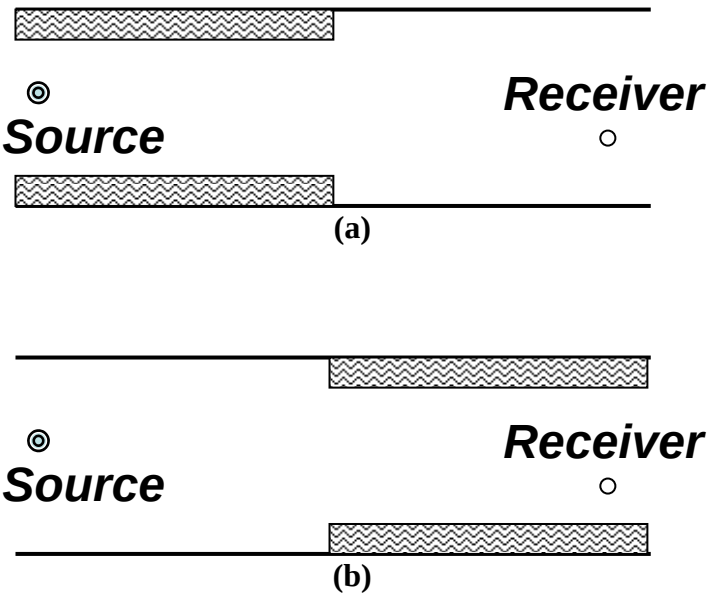

FIG. 3.6: Different duct geometries.

(a) Impedance boundaries at first 1 m and hard boundaries at next 1 m.

(b) Hard boundaries at first 1 m and impedance boundaries at next 1 m.

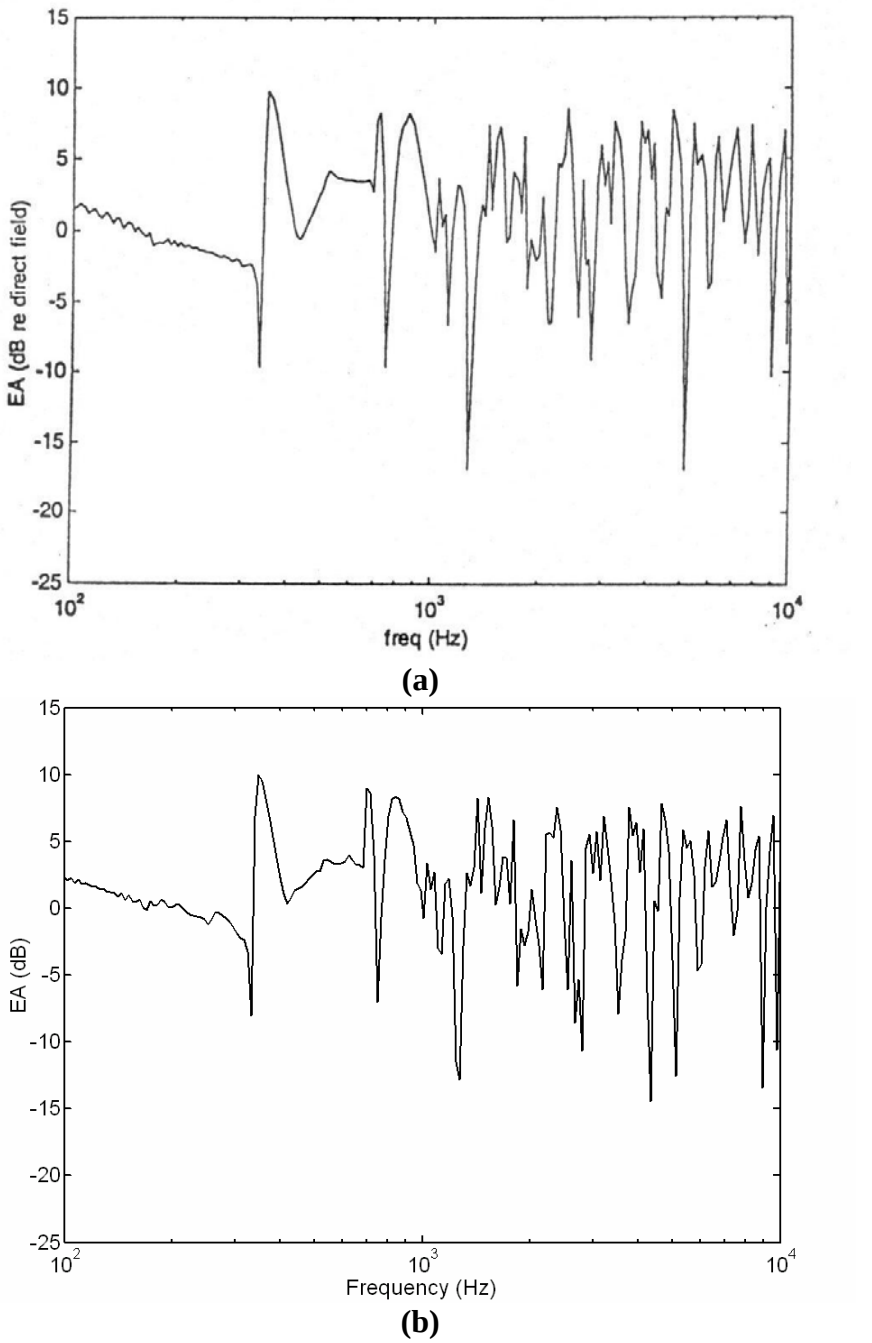

FIG. 3.7: Plot of excess attenuation for the duct geometry in FIG. 3.6(a).

(a) Prediction from Chan's model (FIG. 4.5c in Ref. 3);

(b) Prediction from the coherent model.

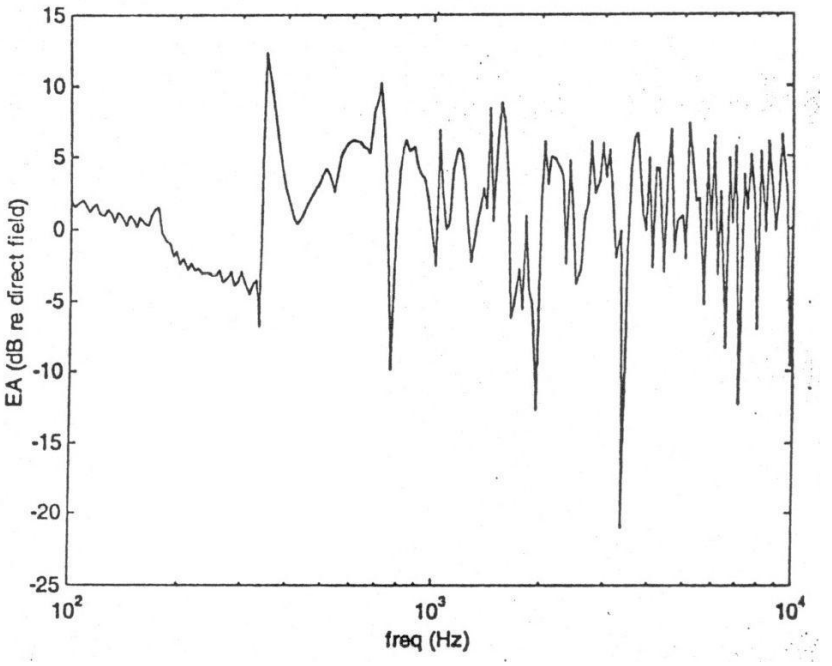

(a)

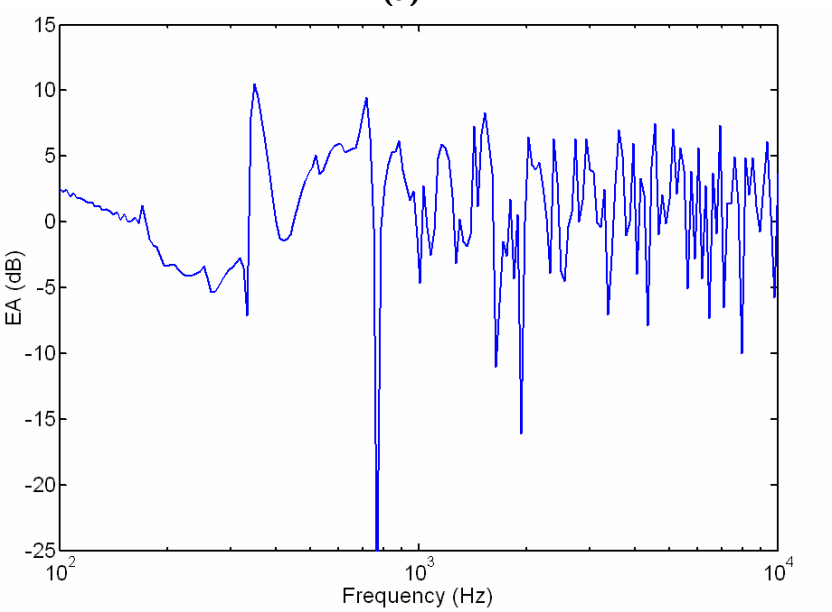

(b)

FIG. 3.8: Plot of excess attenuation for duct geometry in FIG. 3.6(b).

(a) Prediction from Chan's model (FIG. 4.5d in Ref. 3)

(b) Prediction from the coherent model.

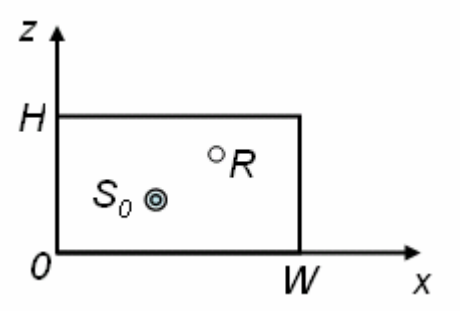

(a)

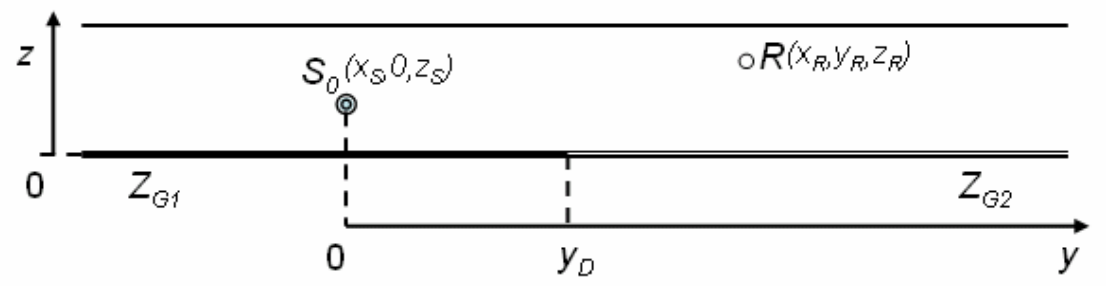

(b)

FIG. 3.9: Long enclosure with single impedance discontinuity.

(a) Cross-section;

(b) Side view.

FIG. 3.10 The model corridor with a single impedance discontinuity.

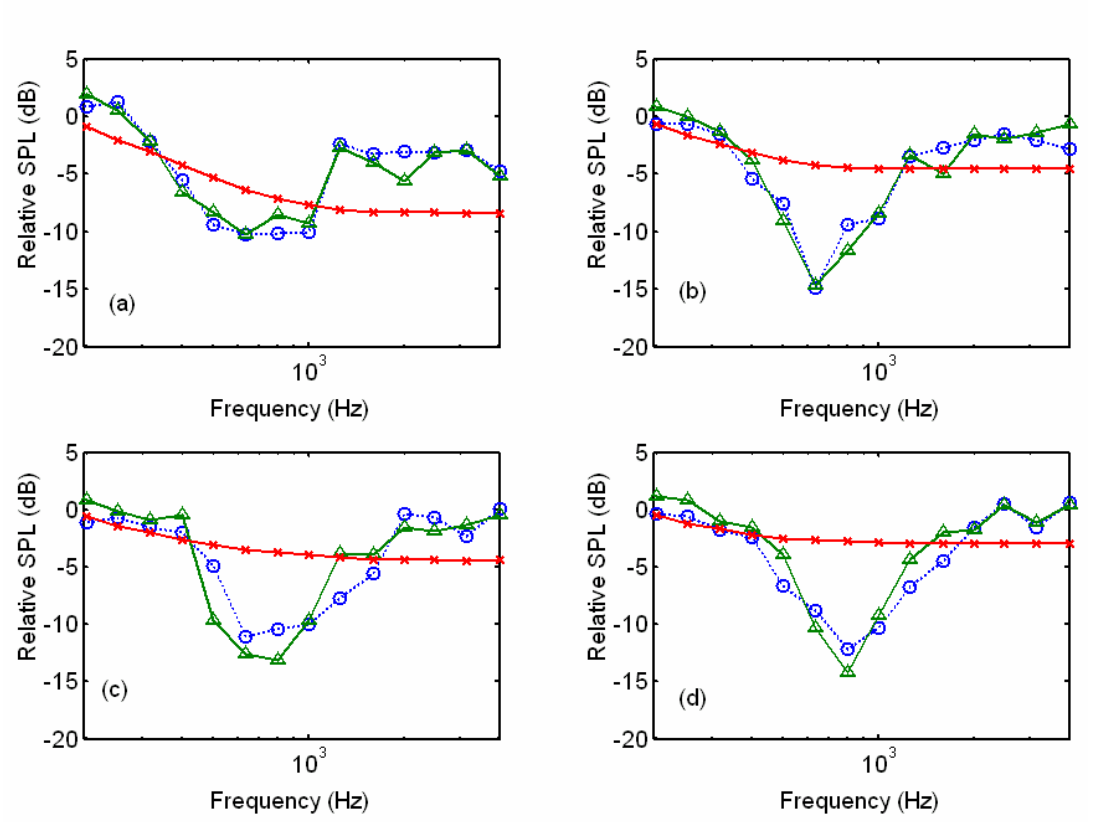

FIG. 3.11: Comparison of measured and predicted relative SPL in model corridor in anechoic chamber. Source height = 0.13 m, receiver height = 0.67 m, impedance discontinuity at 1.8 m.

Measurement: ; Coherent prediction: ; Incoherent prediction: .

Source-receiver distance: (a) 2 m, (b) 2.5 m, (c) 3 m, (d) 3.5 m.

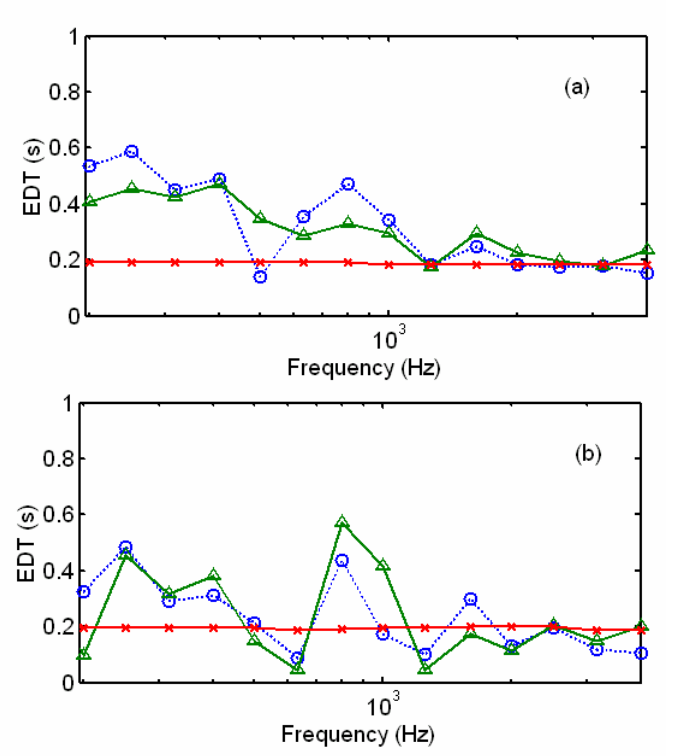

FIG. 3.12: Measured and predicted EDT spectra in model corridor in anechoic chamber. Change of impedance at y = 1.8 m.

Measurement: ; Coherent prediction: ; Incoherent prediction: .

(a) Source at (0.2, 0, 0.13), receiver at (0.2, 2, 0.67);

(b) Source at (0.2, 0, 0.13), receiver at (0.4, 2.5, 0.67).

FIG. 3.13: The loud speaker placed inside the model tunnel with a single impedance discontinuity.

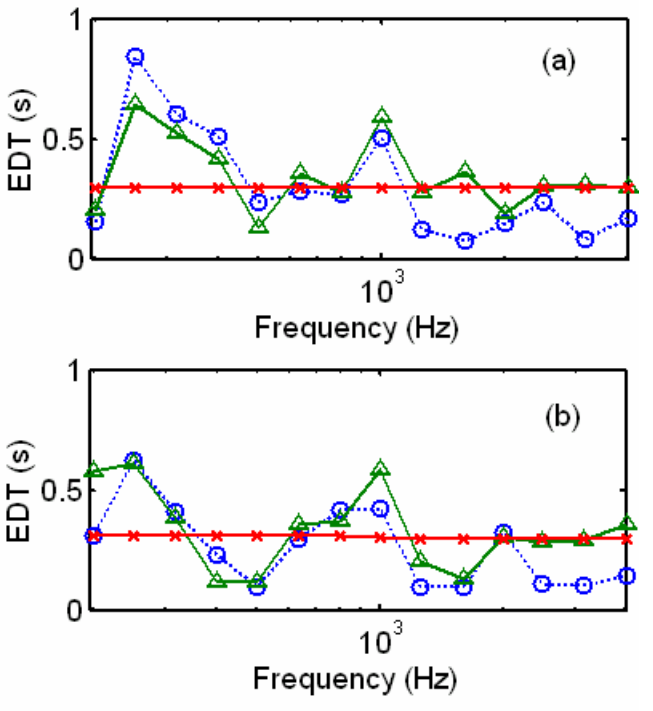

FIG. 3.14: Measured and predicted EDT spectra in model tunnel.

Measurement: ; Coherent prediction: ; Incoherent prediction: .

(a) Source at (0.58, 0, 0.2), receiver at (0.58, 16, 0.5), y_D=10 m;

(b) Source at (0.2, 0, 0.2), receiver at (0.2, 10, 0.5), y_D=7 m.

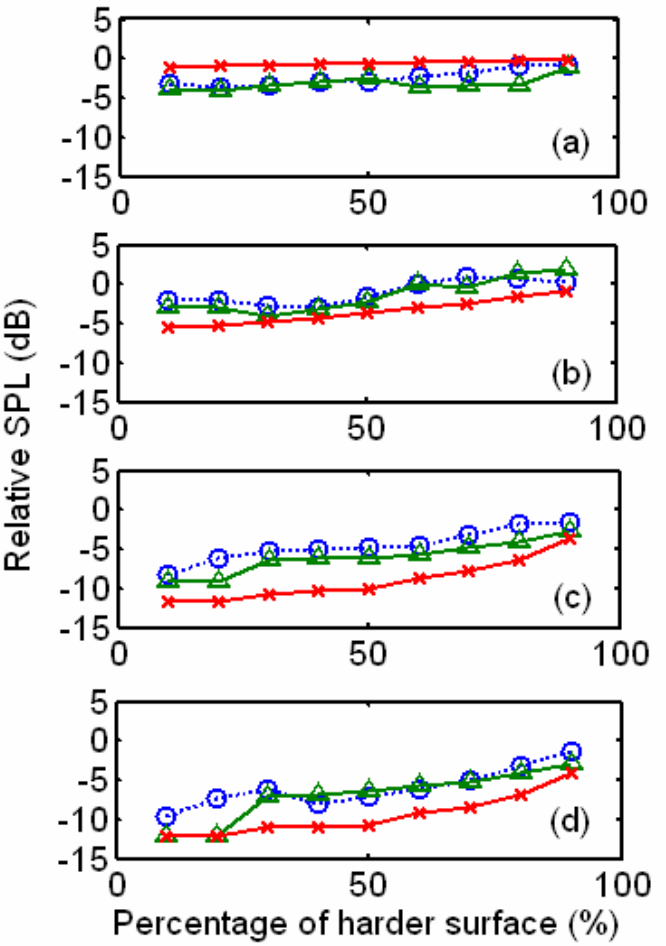

FIG. 3.15: Comparison of measured and predicted relative SPL at different percentage of harder surface on the ground.

Source at (0.2, 0, 0.2), receiver at (0.2, 10, 0.5).

Measurement: ; Coherent prediction: ; Incoherent prediction:

(a) 200 Hz;

(b) 400 Hz;

(c) 1250 Hz;

(d) 1600 Hz.

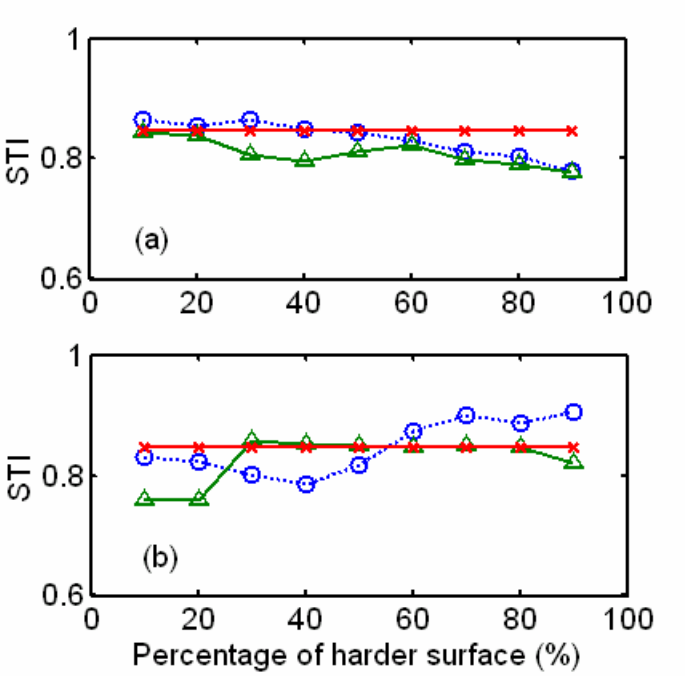

FIG. 3.16: Comparison of measured and predicted STI at different percentage of fiberglass coverage. Source at (0.58, 0, 0.2), receiver at (0.58, 10, 0.5). Measurement: ; Coherent prediction: ; Incoherent prediction:

(a) 500 Hz;

(b) 2000 Hz.

Chapter 4

Optimal positioning of sound absorption material in a long enclosure

4.1 Introduction

A theoretical model for the prediction of sound field in a long enclosure with an impedance discontinuity was described in Chapter 3. It was shown that the diffraction effect was not important and could be ignored in the computation. In this way, the calculation procedure would be greatly simplified, but the phase information was still included.

Noise abatement is another main objective of this research. One of the popular means of noise attenuation is the installation of sound absorption materials. It is generally agreed that when the area of the sound absorption material increases, the amount of noise attenuation also increases. However, when the area of the absorption material remains the same, its location and the pattern in an enclosure will have an effect on the sound absorption efficiency. In this chapter, the reduction of noise in a long enclosure by the sound absorption materials will be studied first, with the help of the proposed theoretical model. The improvement of speech intelligibility by the installation of sound absorption materials will be examined in the second part of this chapter.

4.2 Strategic positioning of sound absorption materials

Kang studied the sound attenuation in long enclosures by computer simulation with the incoherent model [1]. He suggested that the absorbers should be evenly arranged in a section in order to obtain a higher attenuation. In his analysis, the sound absorption materials were located on the entire length of the long enclosure. There was no change of impedance on the four boundaries. He also highlighted that the angle dependence of absorption coefficients, which was not included in his prediction model, was an important factor. In this section, the coherent model will be used to study the effect of the location of sound absorption materials on their performance in a long enclosure. The angle dependent absorption coefficient and the boundaries with mixed impedance will be considered.

4.2.1 Effect of the pattern of sound absorption material on noise reduction

First the effect of the pattern of the sound absorption material will be investigated. A fixed amount of sound absorption material is placed on the lower horizontal plane in an imaginary long enclosure. A layer of 3-cm thick fiberglass is chosen to represent the sound absorption material. The impedance of the fiberglass has been characterized in Chapter 2 (Fig. 2.16(a)). The spherical wave reflection coefficient is computed with the one-parameter model with a hard-back layer [2]. The effective flow resistivity is 40 kPa s m^{-2}. Results are presented in terms of noise reduction. It is the difference between the predicted sound pressure level with (SPL_W) and without ($SPL_{W/O}$) the lining of fiberglass:

$$NR = SPL_W - SPL_{W/O}. \tag{4.1}$$

The width and the height of the long enclosure are 6 m and 4 m respectively. The

source and receiver are placed inside the enclosure and separated by 50 m. The fiberglass covers 40% of the ground area between the source and the receiver. There are five different locations of the fiberglass, as shown in Fig. 4.1. The fiberglass is divided into two strips in Figs. 4.1(c) and 4.1(e). The other three boundaries are modeled as perfectly hard.

The sound pressure levels predicted in the five scenarios with reference to that for completely hard ground are shown in Fig. 4.2. The performance of the fiberglass in cases A and B are identical. The curves of the noise reduction obtained are exactly the same. The five cases show similar results below 400 Hz. Case C yields an extra reduction of 1 dB at 50 – 80 Hz, and a sudden drop of sound pressure level at 500 Hz. Results of cases C and D are similar above the frequency band of 630 Hz. However, it is obvious that the other three cases give an extra reduction of 2 to 3 dB at this frequency range.

The noise reduction expressed in A-weighted SPL for cases A to E are -10.8 dB(A), -10.8 dB(A), -8.1 dB(A), -10.7 dB(A) and -8.1 dB(A) respectively. It is seen from this preliminary analysis that the fiberglass achieves higher noise reduction efficiency when it is placed in a continuous length, instead of dividing into two sheets. Moreover, the exact location of a certain amount of absorption material in the enclosure is not important. Further analysis can be made by placing absorptive materials at the junction of two boundaries.

4.2.2 Effect of the amount of sound absorption material on noise reduction

It is generally believed that an increase in the area of sound absorption material will cause a higher level of noise reduction in a room. However, Boulanger *et al.* [3]

examined the propagation of sound over mixed impedance ground and got a different result. They found that the frequency of the first dip of the excess attenuation was predicted to be highest at approximately 70% hard surface cover rather than the expected 100%. In this section, the effect of the amount of sound absorption material on noise reduction in a long enclosure will be studied with the predictions from the coherent model.

Three different cases will be explored in this section. The geometry of the imaginary long enclosure in Case 1 is identical to the one shown in Fig. 3.9. The ground of the long enclosure is partly covered with fiberglass (see Fig. 4.1(a)). In the second case, the ceiling of the long enclosure is also lined with sound absorption material. In the third case, only the ground and the left vertical wall are covered with sound absorption material. The cross-section of the long enclosure in the three scenarios is shown in Fig. 4.3. The distance between the source and receiver is 50 m.

The noise reduction spectra for Case 1 are plotted in Fig. 4.4. For the ease of comparison, not all the spectra from 10 % to 100 % of fiberglass coverage are shown in Fig. 4.4. The results obtained from the different cases are similar below frequency bands of 160 Hz. Above that frequency range, the noise reduction effect is very significant when the fiberglass coverage changes from 10 % to 20 %. There is almost a double of the reduction in SPL. Between 30 % to 50 % coverage, the predicted results are similar. Further reduction is obtained at 60 % coverage. It is interesting to find that between 800 Hz and 4000 Hz the noise reduction at 70 % coverage of fiberglass is close to that at 100 % coverage. This is due to the interference effects of the direct and reflected waves. When the fiberglass coverage is increased to 80 %, the result is similar to that at 60 %.

Different results are yielded when the fiberglass is lined on the ground and the

ceiling in Case 2. Fig. 4.5 shows the corresponding noise reduction spectra. Maximum noise reduction is found at 100 % fiberglass coverage, whereas the performance of 60 % and 70 % fiberglass coverage are similar now. Dips are found at 80 % and 100 % coverage between 250 Hz and 1000 Hz. There is no significant extra noise reduction observed when compared to Case 1. It shows that extra lining of fiberglass on the ceiling does not have a significant effect on the noise reduction. The noise reduction caused by the lining of fiberglass on the horizontal planes has almost reached the maximum observable value.

In the last case the fiberglass is modeled to be placed on the ground and the left vertical wall. The predicted noise spectra for the different percentages of fiberglass coverage are shown in Fig. 4.6. The trend of the curves is similar to that in Fig. 4.4, but the amount of noise reduction has been greatly increased. Noise reductions for frequencies above 1250 Hz at 70 % and 100 % fiberglass coverage are similar. The performance of fiberglass coverage of 60 % is also marginally better than that of 80 % in this frequency range.

A comparison of the noise reduction of the three cases, expressed in A-weighted SPL, is given in Fig. 4.7. The amount of noise reduction is directly proportional to the amount of fiberglass lining in Case 2. However, noise reduction at 70 % fiberglass coverage is found to be similar to that at 100 % coverage in Case 1 and Case 3. Furthermore, the noise reduction at 60 % fiberglass coverage is marginally higher than that at 80 % in these two cases. This is an example to demonstrate that when a sufficiently large amount of sound absorption material is used, extra insertion of such materials will not necessarily lead to an observable increase in noise reduction. On the other hand, when the fiberglass is to be lined on two boundary surfaces to increase the noise reduction, it is recommended to place them on planes perpendicular to each

other. It is surprising to find that the performance of the fiberglass is generally worse in Case 2 than in Case 1. This is due to interference effects, which will not be observed in the incoherent model. When the fiberglass is placed on perpendicular surfaces, as in Case 3, the noise reduction obtained is almost double of that in Case 1.

The performance of the installation of other kinds of sound absorption material can also be studied with the coherent model. An example of the lining of carpet will be discussed here. The impedance of the carpet is characterized by Attenborough's two-parameter model [4]. The effective flow resistivity and the change of porosity with depth are 200 kPa s m^{-2} and 50 m^{-1} respectively. The left vertical wall and the ground are covered with carpet (but the question of feasibility will not be discussed here). The coverage ranges from 10 % to 100 % of the area between the source and the receiver as before. The predicted noise reduction spectra are shown in Fig. 4.8(a). As the percentage of fiberglass coverage increases, the amount of noise being reduced is increased correspondingly. It gives a more regular pattern than the results shown in Fig. 4.6, in which the surfaces were covered with fiberglass. The noise reduction in A-weighted SPL is shown in Fig. 4.8(b).

It has been shown in this section that an optimization of the pattern and the amount of the sound absorption material can be carried out with the coherent prediction model. In the above examples, a layer of 3-cm thick fiberglass was chosen as the absorptive material. The results show that it has little effect on low-frequency sound. The fact is that low-frequency sound contributes little to the A-weighted sound pressure level and the computation of STI. In general, a suitable kind of sound absorption material can be chosen by comparing the noise reduction spectra and the A-weighted SPL. For example, if there is a need to reduce noise in the low-frequency region effectively, a much thicker layer of fiberglass can be applied.

4.3 Improvement on speech intelligibility

4.3.1 Effect of noise on the prediction of STI

As described in Chapter 2, the coherent model provides a better alternative for the prediction model of reverberation time and speech transmission index, which are the governing factors for speech intelligibility in an enclosure. A design target of speech intelligibility in terms of reverberation time and STI in long enclosures, such as train stations and long corridors, can be achieved by different methods with the help of the proposed coherent model.

In the previous experimental validation of the coherent model, the signal-to-noise ratio is generally over 20 dB. The term in square brackets of Eq. (2.16) approaches 1. It means the effect of interfering noise on the prediction of STI is negligible. Therefore, Eq. (2.17) has been used in the previous calculations. The overall STI is the weighted average of the values at the seven frequency bands from 125 Hz to 8000 Hz. However, the signal-to-noise ratio is not always high in reality. Either the source is not powerful enough, or the noise level is overwhelming when compared to the source. When the signal-to-noise ratio is small, it becomes an significant factor and must be included in the prediction model.

The effect of noise on the prediction of STI will be discussed with an example. When noise is excluded from the model, the coherent prediction of STI in the corridor in Section 2.3.3 is 0.7 at a source-receiver distance of 10 m. If the signal-to-noise ratio is small, Eq. (2.16) should be used to predict STI at the seven octave bands instead. In fact, the S/N ratios do not always share the same values at the seven octave bands. For example, the noise produced by people talking and that by a running train in an underground train station belong to different frequency bands, and they have different noise levels as well.

The determination of STI under the condition which the S/N ratios are different at the seven octave bands will be described here. The background noise level is taken in a building corridor. The main source of the noise comes from the air-conditioning system, which is typical in offices and classrooms. When the signal level is tuned down, the S/N ratios from 125 to 8000 Hz in octave bands are -7.8 dB, 3.4 dB, 9.7 dB, 16.4 dB, 15.7 dB, 17.3 dB and 18.9 dB respectively. The octave band STI can be found from the first seven curves in Fig. 4.9 according to the S/N ratios. They are represented by crosses in the figure. The seven values are then weighted and averaged to give a final STI, which is 0.59 in this case.

If the S/N ratios at the seven octave bands are the same, the curve of the overall STI versus S/N ratio can be plotted, as shown in Fig. 4.9. It increases with the S/N ratio. When the S/N ratio is high, e.g. over 20 dB, the STI value becomes steady. On the other hand, when the S/N ratio equals to zero, the overall STI is just above 0.4, indicating poor speech intelligibility. One can easily identify the expected speech intelligibility at different noise conditions from the curves in Fig. 4.9. This provides essential information for considering possible acoustic treatments with respect to real-life conditions. It is also demonstrated that an accurate prediction of STI at the octave bands is crucial when the S/N ratios at the seven frequency bands are not the same in reality.

4.3.2 Improvement of STI and EDT

It is known that the early decay of a long enclosure governs the STI. In this section, the improvement of the arrangement of absorption material on STI and EDT will be studied. The three cases in the previous section will be investigated.

For Case 1 and 2 in Fig. 4.3, the improvement in the speech intelligibility is not

obvious. When the fiberglass is placed on areas of the perpendicular surfaces in Case 3, there is a significant improvement in both the STI and EDT. The reduction in EDT for different percentage of fiberglass coverage is shown in Fig. 4.10(a). The performance of 80 % coverage is close to that of 100 %. The maximum reduction of EDT is over 2 s at 800 Hz. The amount of reduction in EDT varies for different frequency bands, particularly favorable to the high frequency region. Fig. 4.10(b) demonstrates the reduction of EDT by covering parts of the two boundary surfaces with carpet. The maximum reduction in EDT is 1.2 s at 2500 Hz with the surfaces totally covered with carpet. When the requirement of EDT in a long enclosure is known, the amount of absorption material can be determined from these graphs accordingly.

The improvement of STI by the installation of absorption material is shown in Fig. 4.11. The surfaces of the left vertical wall and the ground are lined with fiberglass and carpet in Fig. 4.11(a) and Fig. 4.11(b) respectively. It is found that the lining of these sound absorption materials favors the high frequency region. There is only a slight increase of STI at 125 Hz in both figures. Between 500 Hz and 4000 Hz, the change in STI increases with the fiberglass coverage in Fig. 4.11(a). The improvement is over 0.5 at 2000 Hz and 4000 Hz when the fiberglass coverage reaches 40 %. This change will bring a significant improvement in the overall value of STI. It is illustrated in Fig. 4.11(b) that the improvement in STI is directly proportional to the increase in the coverage of fiberglass. The performance of the fiberglass is significantly higher than that of the carpet. However, the choice of absorption material depends not only on its performance, but also on its cost and the feasibility of installation in different enclosures.

4.4 Conclusions

An example of the practical usage of the coherent prediction scheme has been demonstrated in this chapter. The efficiency of the installation of sound absorption material is investigated with the coherent model. The absorption material is found to be most effective when it is placed in a continuous length, instead of dividing into sections. It is interesting to find that an increase in the amount of the absorption material does not always result in a higher level of noise reduction, when the percentage of surface covered is relatively large. In the cases studied in this chapter, the fiberglass and the carpet are chosen as examples of sound absorption materials. Further analysis can be made by comparing the performance of other absorbers.

The coherent model can assist the strategic lining of sound absorption material in a long enclosure to achieve different acoustic purposes. The choice of sound absorption materials can be made by comparing their performance on noise reduction and/or improvement on speech intelligibility, depending on the function of the enclosure. As a result, the performance and cost-effectiveness of the acoustic treatment will be greatly enhanced with the help of the coherent prediction model.

References

1. J. Kang, “Sound attenuation in long enclosures,” Building and environment, **3**, 245-253 (1996).
2. K. M. Li, T. Waters-Fuller and K. Attenborough, “Sound propagation from a point source over extended-reaction ground,” J. Acoust. Soc. Am. **104**, 679-685 (1998).
3. P. Boulanger, T. Waters-Fuller, K. Attenborough and K. M. Li, “Models and measurements of sound propagation from a point source over mixed impedance ground,” J. Acoust. Soc. Am. **102**, 1432-1442 (1997).
4. K. Attenborough, “Ground parameter information for propagation modeling,” J. Acoust. Soc. Am. **92**, 418-427 (1992).

Figures

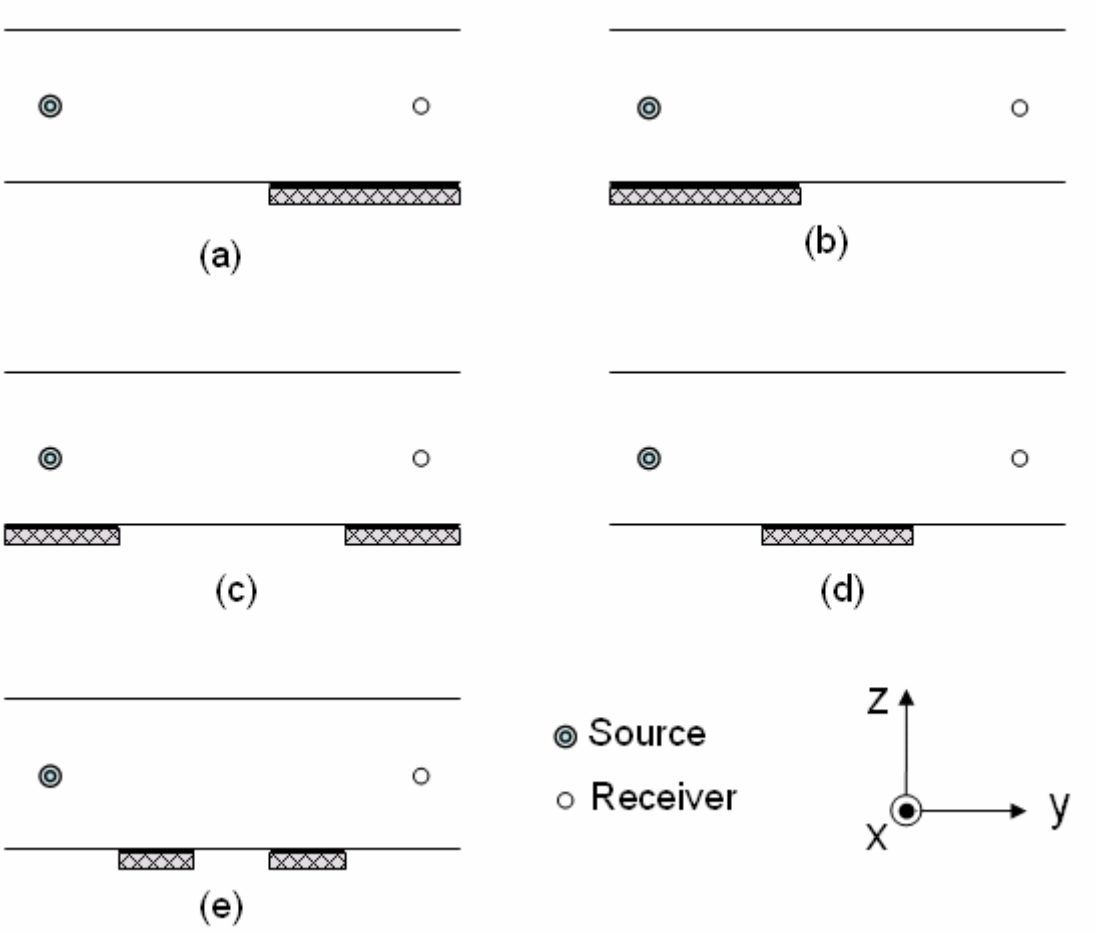

FIG. 4.1: Different geometries in long enclosure for five cases:

(a) Case A

(b) Caes B

(c) Case C

(d) Case D

(e) Case E

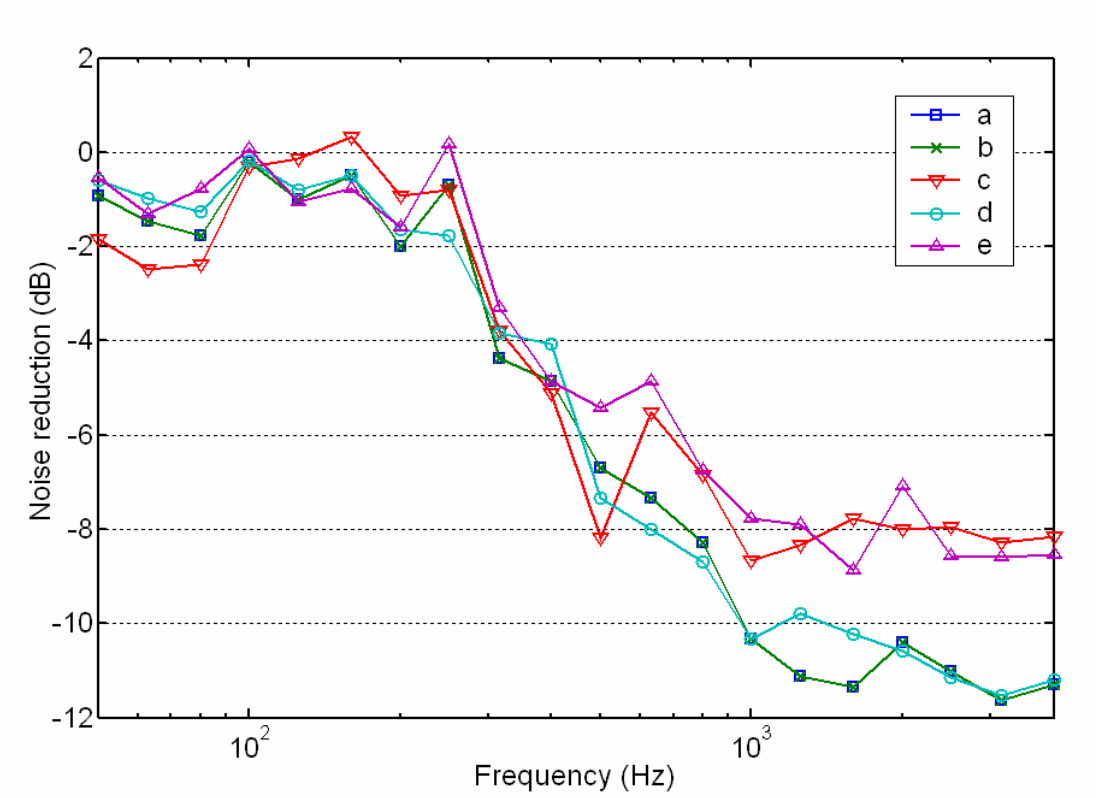

FIG. 4.2: Plot of relative SPL in a long enclosure with five different patterns of sound absorption material.

(a) Case A

(b) Caes B

(c) Case C

(d) Case D

(e) Case E

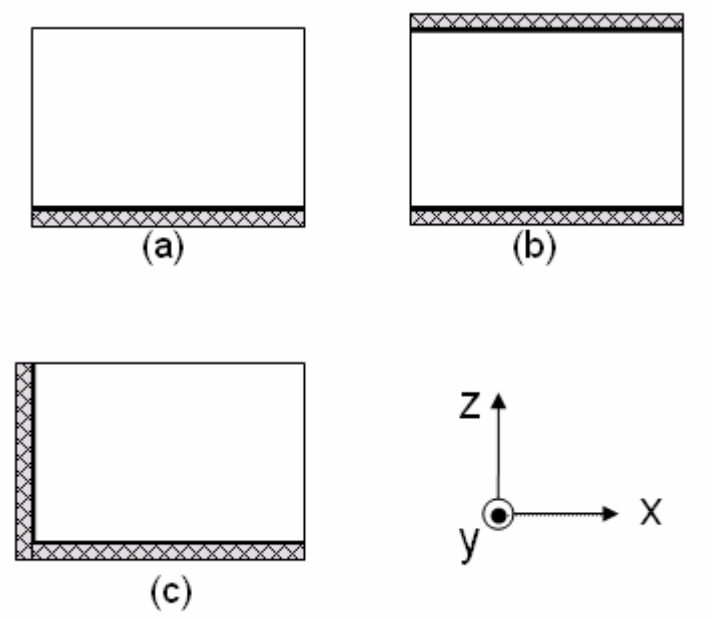

FIG. 4.3: Cross-sectional view of the long enclosure for the three cases.

(a) Case 1

(b) Case 2

(c) Case 3

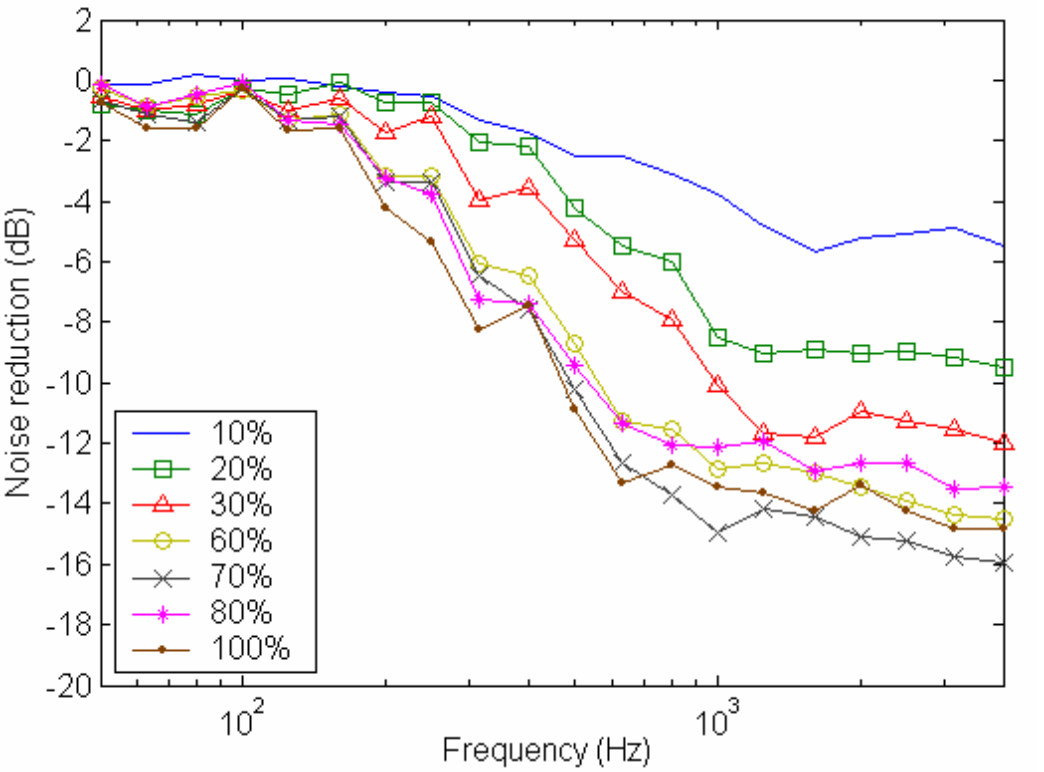

FIG. 4.4: Plot of noise reduction spectra in a long enclosure with the ground covered with different percentage of fibreglass (Case 1).

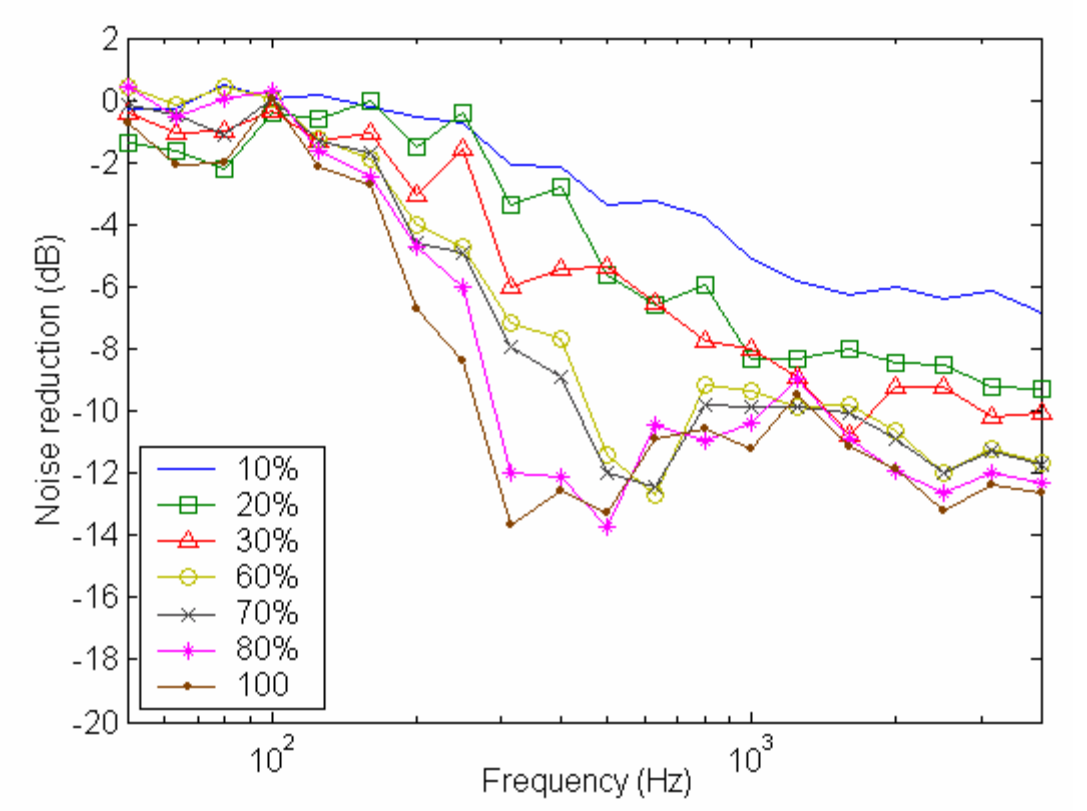

FIG. 4.5: Plot of noise reduction spectra in a long enclosure with the ground and ceiling covered with different percentage of fibreglass (Case 2).

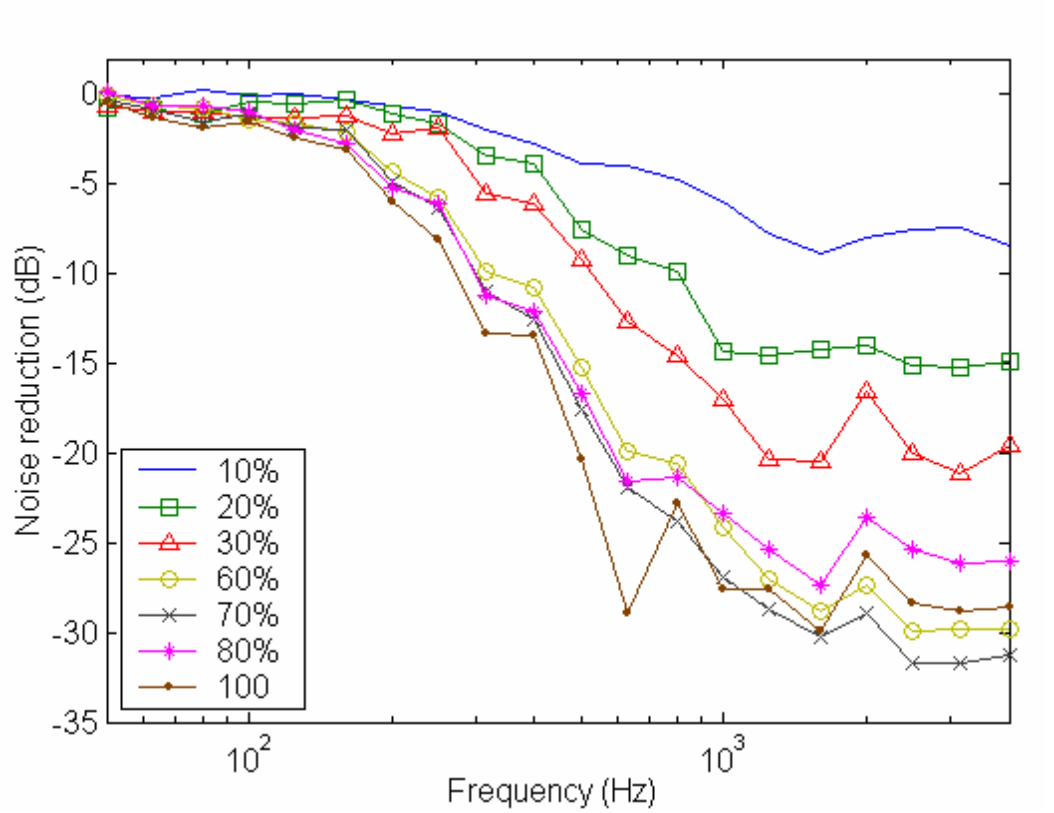

FIG. 4.6: Plot of noise reduction spectra in a long enclosure with the ground and the left vertical wall covered with different percentage of fibreglass (Case 3).

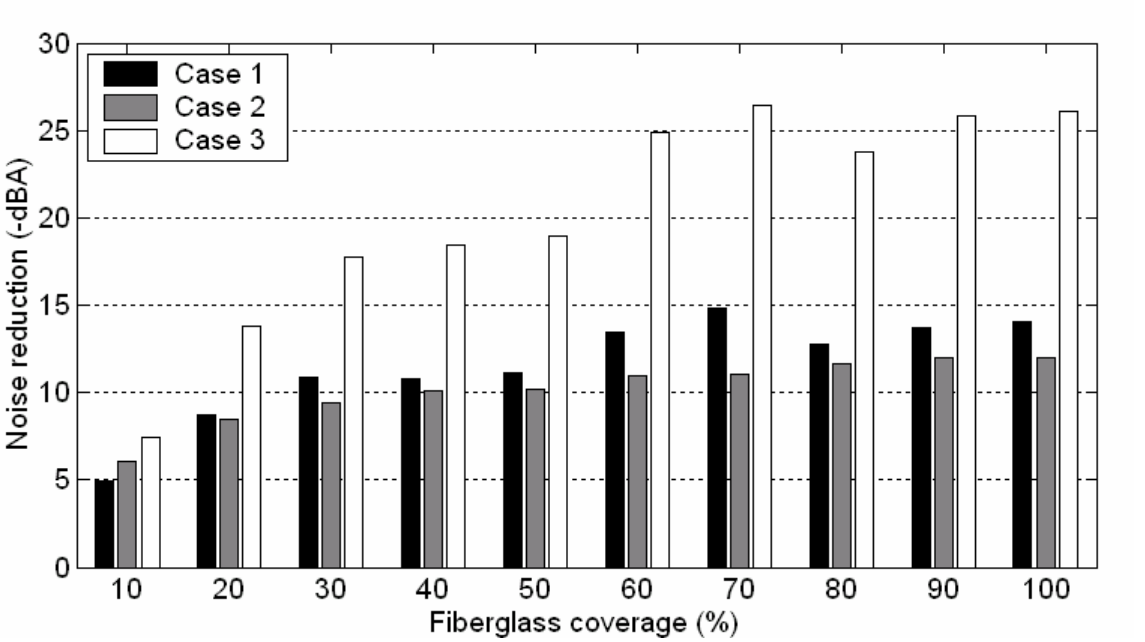

FIG. 4.7: Noise reduction in A-weighted SPL.

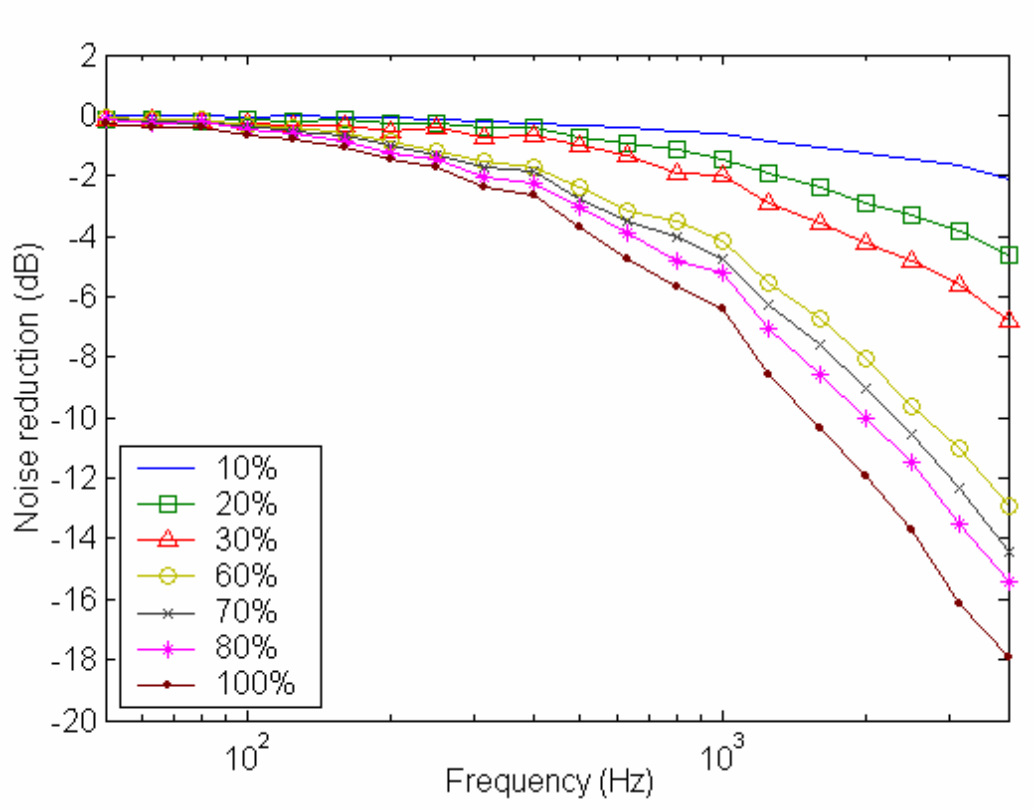

(a)

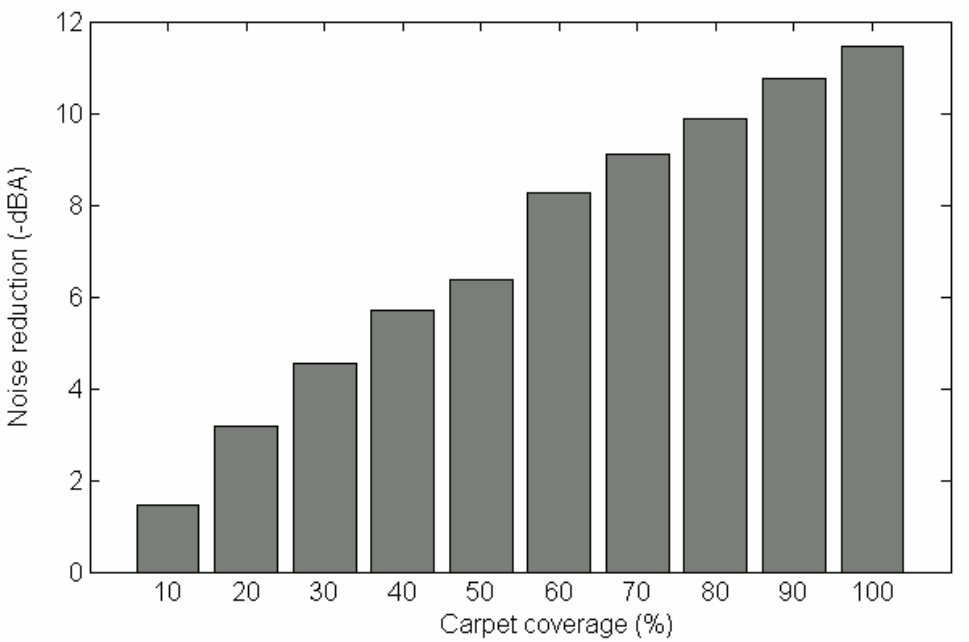

(b)

FIG. 4.8: Noise reduction in a long enclosure with the ground and the left vertical wall covered with different percentage of carpet (Case 4).

(a) Noise reduction spectra;

(b) Plot of noise reduction in A-weighted SPL.

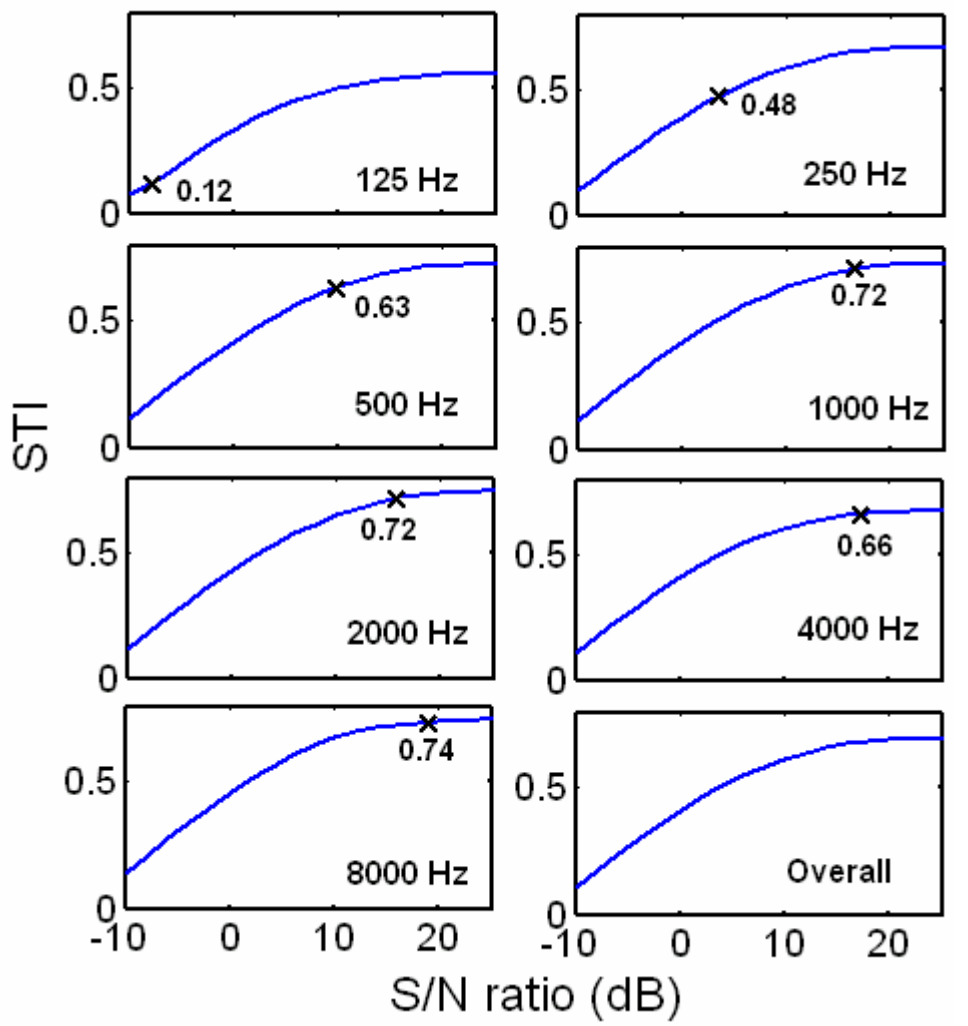

FIG. 4.9: Plot of STI against S/N ratio: source-receiver distance = 10 m.

Cross (x): STI value at each octave band determined by the corresponding S/N ratio.

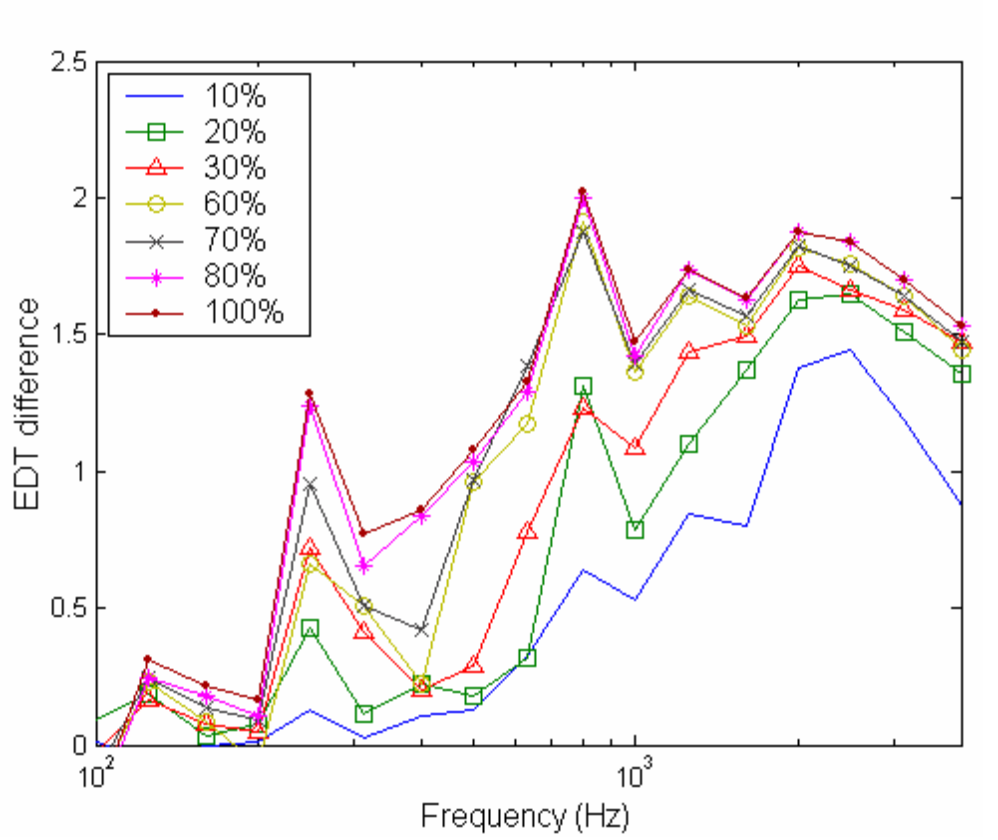

(a)

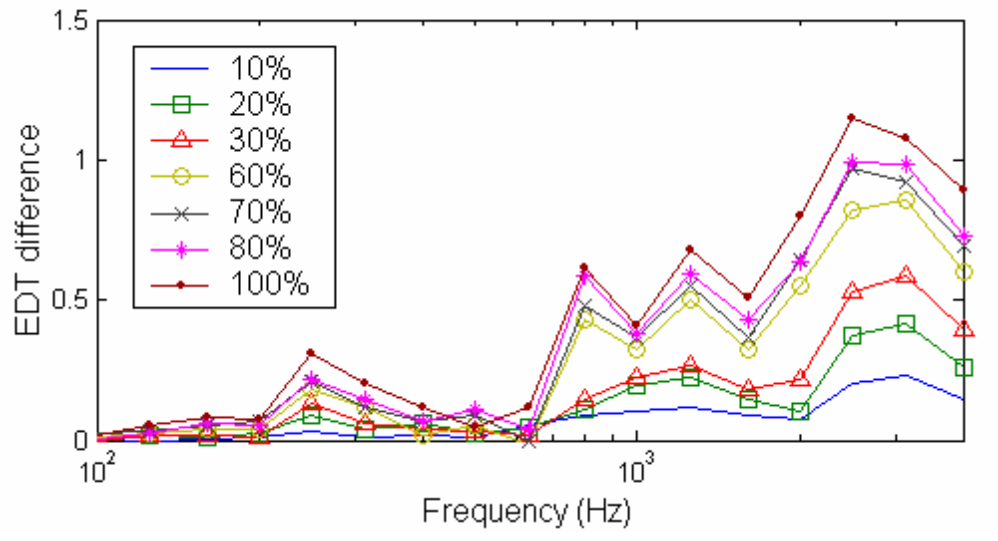

(b)

FIG. 4.10: Improvement in EDT at different fibreglass coverage.

(a) Coverage of fibreglass on two surfaces;

(b) Coverage of carpet on two surfaces.

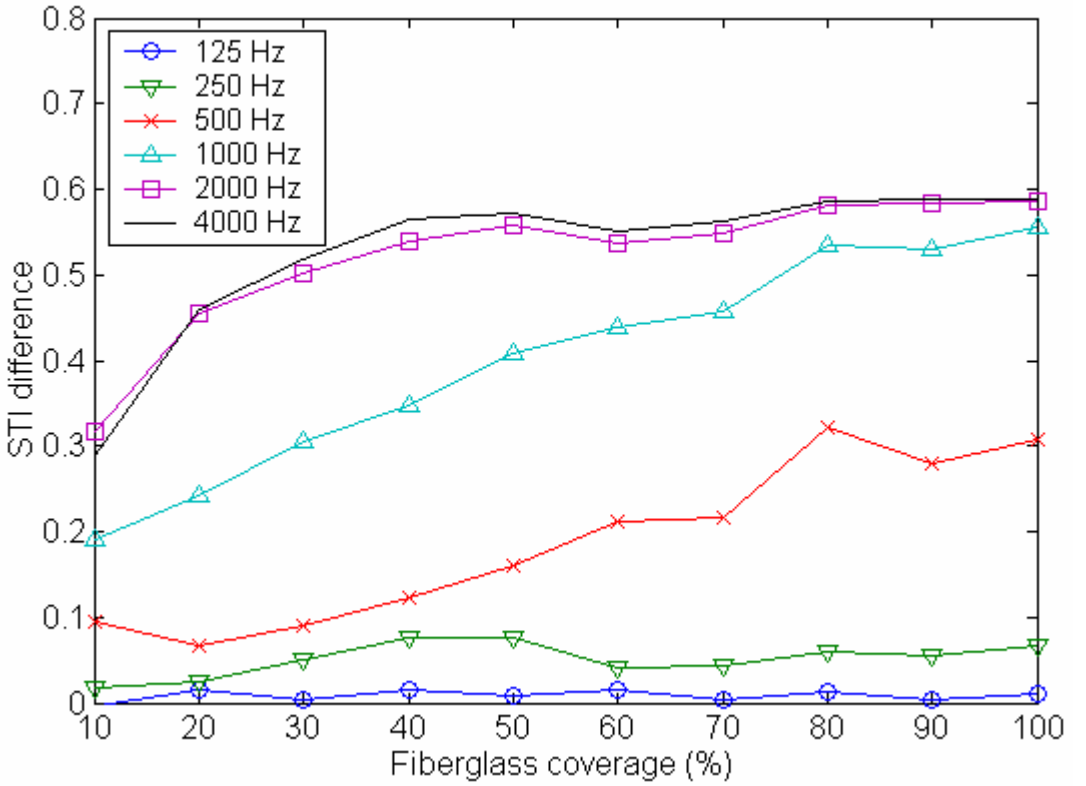

(a)

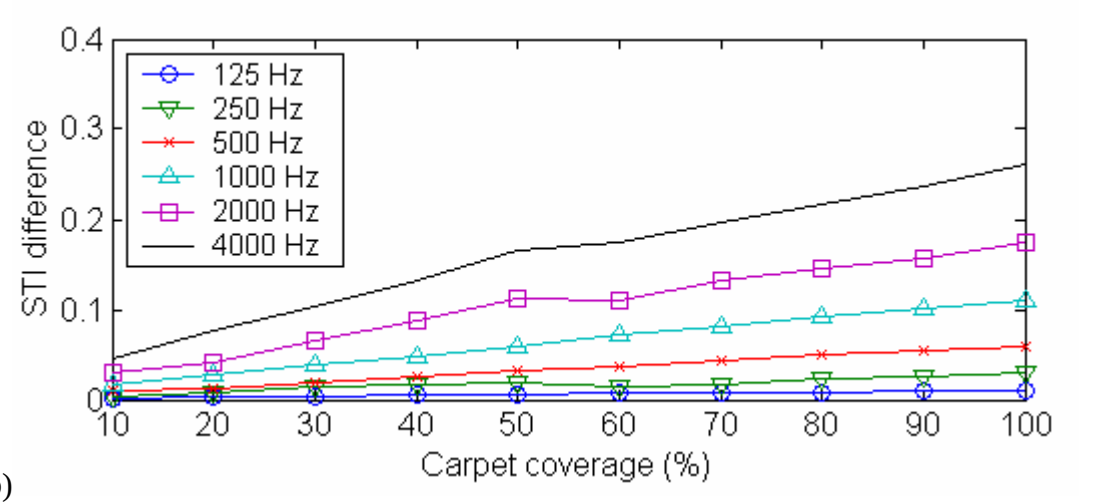

(b)

FIG. 4.11: Improvement in STI with lining of sound absorption material on two boundaries.

(a) Coverage of fibreglass on two surfaces;

(b) Coverage of carpet on two surfaces.

Chapter 5

Concluding Remarks

5.1 Conclusions

The contents of this research are summarized in this chapter. The study of noise reduction in long enclosures, such as tunnels, underground stations and long corridors, begins with the examination of sound characteristics in these spaces. It is known that the sound field in a long room is not diffuse, and that the classic theory of room acoustics is not applicable.

In the first part of the thesis, the coherent model, or the complex image model, has been extended to predict the reverberation time and the speech transmission index in a long enclosure. The numerical model is based on an image-source method, and geometrically reflecting boundaries are considered. An approximate analytical solution is used to predict the frequency response of the sound field. This method is different from the previous energy-based models in which the interference effects between the direct and reflected waves are included. Furthermore, the angle-dependence of reflection coefficients of the boundaries and the change of phase upon reflection are incorporated in the coherent model. Due to relatively long distance of sound propagation, the effect of atmospheric absorption is also considered. The impulse response is generated by applying the inverse Fourier transform on the frequency response. The decay curve is obtained by a reverse-time integration of the impulse response. The reverberation time is determined from the decay curve.

Subsequent calculations are performed on the impulse response to deduce the speech transmission index accordingly.

Experiments have been carried out in three sites to validate the coherent model in the prediction of reverberation time and speech transmission index. The first one is the western harbour tunnel. The boundaries of this tunnel are perfectly hard. The second one is a corridor in the department of mechanical engineering in the Hong Kong Polytechnic University. The ceiling and the ground are impedance boundaries, and the vertical walls are rigid. The third one is a model tunnel made with hard plywood. It is set up in the anechoic chamber. The lower horizontal ground is covered with fibreglass. The source and receiver are placed at different positions in the experimental sites. The measured data are compared with the predictions from the coherent and incoherent models. Results suggest that the coherent model can give more accurate approximations. Interference effects are observed and predicted.

Since the impulse response is obtained by inverse Fourier transform of the predicted sound field, the number of data in the single frequency increases from low to high frequency bands, which means the computational time will also increase. The advantage of the coherent model can also be observed better in narrow band analysis, as the number of frequencies included in each band increases with the width of the band, and the interference effects might be averaged out and become less significant. Considering the computational time and the significance of the interference effects, the coherent model is therefore preferable in narrow band analysis, and in low frequency regions. It has also been demonstrated that the spherical wave reflection coefficient should not be replaced by the plane wave reflection coefficient, especially in cases of long source-receiver distance and enclosures with relatively soft boundaries, and in low frequency ranges.

The lining of sound absorption materials on boundary surfaces is a common practice of noise reduction. However, it will not be economical, nor can it achieve maximum efficiency, if the sound absorption materials are installed on the entire length of an enclosure. It is necessary to optimize the pattern, the amount, and the location of the absorption materials. Therefore, the coherent model is modified to consider the existence of impedance discontinuity on the boundary surfaces in the second part of this thesis. A single change of impedance in a two-dimensional duct is focused as the fundamental study of the problem. The diffraction term described in the De Jong model is incorporated into the coherent model to account for the diffraction at the impedance discontinuity. Analysis is made to examine the impact of diffraction on the computation. The diffraction effect at the impedance discontinuity is shown to be insignificant, and it is ignored in the formulation. Results obtained from the modified theoretical model are compared with those from another numerical model which is based on an integral method. Only slight discrepancies are found.

Investigation is then moved on to a rectangular long enclosure with the assumption that the diffraction effect is not important. A set of equations are developed on the basis of the coherent model to predict the noise reduction and acoustic indices (EDT and STI) in a long enclosure with impedance discontinuities. The formulation is similar to that introduced in Chapter 2, except for the determination of the spherical wave reflection coefficients corresponding to the regions of different impedance values. It is necessary to find out the number of times an image reflects from the surface regions. In order to validate the numerical model, two model tunnels of different sizes are set up: one in the anechoic chamber and the other in a remote area. Experiments are conducted in the scale models by varying the position of the change of impedance on the lower horizontal plane. The coherent

model produces results in excellent agreement with experimental data collected, even when the diffraction at the impedance discontinuity is ignored. The accuracy of the coherent model is shown to be greater than that of the incoherent model, because the mutual interference between the source and the receiver has been included.

The verified coherent model is then used as a tool to investigate the optimal positioning of sound absorption material in a long enclosure. Several cases in an imaginary long enclosure are presented as examples to show how to determine the location with the numerical model. First, a fixed amount of fibreglass is lined on five different positions of the ground of the enclosure. The fibreglass is separated as two portions in two cases. The levels of noise reduction in these five cases are compared. It is found that when the amount of absorption material is fixed, a continuous lining can give a better performance rather than cutting them into two pieces. Next, the boundaries of the long enclosure are lined with different amount of sound absorption materials. The fibreglass and the carpet are chosen as examples of sound absorption materials. It is surprising to find that an increase in the amount of absorption material does not necessarily mean a higher degree of noise reduction. Moreover, perpendicular boundaries are preferred to parallel planes when the absorption material can be installed on two surfaces.

Finally, the installation of sound absorption material for the improvement of speech intelligibility is investigated. The effect of noise on the prediction of STI is clarified. The improvement of speech intelligibility in terms of STI and EDT by the insertion of fibreglass and carpet in a long enclosure is studied. The coherent model serves as a helpful tool in the strategic lining of sound absorption material in a long enclosure to achieve noise reduction and other acoustic purposes. The choice of sound absorption materials can be made by comparing their performance on noise reduction

and/or improvement on speech intelligibility. As a result, the performance and cost-effectiveness of the acoustic treatment can be greatly enhanced with the predictions from the coherent numerical model.

5.2 Recommendations for future work

Based on the research study described in this thesis, the following areas are recommended for further exploration:

1. In this research, the prediction scheme is focused on a single point source. It provides a fundamental basis for the operation of multiple sources, which involve a summation of the sound field from separate point sources. Multiple sources are commonly found in underground stations and road tunnels. The study and improvement of speech intelligibility of such public address systems is essential. In addition to the investigation of single and multiple point sources, line sources and dipole sources can also be considered.

2. The theory is based on the assumption of an omni-directional point source. The directivity of source has been ignored in the present study. The theoretical model will be more comprehensive if the directivity effect of source is included.

3. Simple patterns of the positioning of sound absorption material are presented in this thesis. Further investigation on more complicated patterns, or a combination of different types of materials, can be considered to obtain a higher degree of noise reduction. It is also recommended to improve the performance of duct silencers with the coherent model. The acoustics of ducts without air flow can be modelled by the numerical model.

4. Sound propagation in a long enclosure with flat inhomogeneous surfaces has been discussed in this thesis. It will be useful to extend the theory to the sound propagation at a tunnel mouth. An impedance discontinuity occurs when the boundaries change from hard to totally absorptive.

5. The propagation of sound in an L-shape or T-shape corridor is another interesting area of research. The L-shape or T-shape branch is a common feature at either end of a long corridor in buildings.

6. A special example of a long enclosure is the train, which is usually made up of several compartments. It contains scattering objects like the seats and handrails. When a train is passing through a tunnel, the situation becomes one long enclosure being surrounded by another. Noise reduction in such enclosure is a complicated yet practical problem. The speech intelligibility in a train compartment with different percentage of occupancy can also be investigated.